Computer Simulation of High Fluence Ion Beam Surface Modification Processes

by

Mukundhan Rangaswamy

dissertation submitted to the Faculty of the

Virginia Polytechnic Institute and State University

in partial fulfillment of the requirements for the degree of

Doctor of Philosophy

in

Materials Engineering Science

APPROVED:

Diana Farkas, Chairperson

Charles R. Houska

Kenneth S. Grabowski

Charles W. Smith

Jack L. Lytton

February 24, 1989

Blacksburg, Virginia

Computer Simulation of High Fluence Ion Beam Surface Modification Processes

by

Mukundhan Rangaswamy

Diana Farkas, Chairperson

Materials Engineering Science

(ABSTRACT)

Various processes that participate in ion beam surface modification are studied using phenomenological, analytical and first principle models.

The processes that are modelled phenomenologically include preferential sputtering, radiation-damage induced migration and second phase precipitation. The models are based on numerical solutions of the transport equation and include the processes of ion collection, sputtering, lattice dilation or accomodation and diffusion as well.

The model for preferential sputtering takes into account the depletion of the preferentially sputtered element at the surface and the atomic transport process that results from the concentration gradients caused by the depletion. Results are presented for the case of Ta implantation into Fe. In the radiation-damage induced migration the flux of the solute atoms is coupled to the concentration gradient of the of the continously introduced defects. Examples of implantation of Sn into Fe and N into Fe are modeled to demonstrate the influence of radiation-damage induced migration. The precipitation of second phases during irradiation is modelled using thermodynamic considerations but with solubility values under irradiation obtained from experiment. In the model the solute atoms in excess of the solubility limit are assumed to precipitate out. Calculations are presented for the case of N implantation into Nb.

Using first principle calculation for binary collisions in solids a computer simulation code was developed to study the collisional mixing occurring during high fluence ion implantation. It is based on the Monte Carlo code TRIM, and is capable of updating the target composition as the implantation process proceeds to high fluences. The physical basis for the dynamic simulation as well as a detailed analysis on the statistics required for obtaining the profiles with a given accuracy are presented. vectorized results in a high computational efficiency. The predicted collisional broadening of the implantation profiles is presented for Ar bombardment into a Sn-Fe target as well as Ti implantation into C-Fe. The results are compared to those of the diffusion approximation.

A semi-empirical model based on an analytical evaluation of ion mixing at low temperatures was developed taking into account collisional mixing and thermal spike effects, as well as the thermal spike shape. The ion beam mixing parameter for the thermal spike is derived as being proportional to different powers of the damage parameter, i.e. the damage energy scaled by the cohesive energy of the matrix, dependent on the thermal spike shape and point defect density in the thermal spike regions. Three different regions of ion beam induced mixing were recognized according to different density levels of the damage parameter.

An experiment was conducted to determine the effect of chemical or thermodynamic factors in the migration of C in the presence of Fe and Ti atoms. A marker layer of C in a Fe-Ti matrix was ion beam mixed using Ar. The large mixing effect is tentatively attributed to a favorable heat of mixing values.

For my Parents

Acknowledgements

The author would like to thank his committee chairperson, Dr. Diana Farkas, for her invaluable guidance during the course of this study. The author would also like to acknowledge the assistance and cooperation of Dr. C.R. Houska, Dr. J.L. Lytton and Prof. C.W. Smith in the production of this dissertation. The author is extremely grateful to Dr. K.S. Grabowski and Dr. I.L. Singer of Naval Research Laboratory, for providing the experimental facilities and copious amounts of their time towards discussing the experimental details and results. The author also expresses his thanks Dr. B. Sartwell and Dr. D. Krause of NRL for their patience and guidance in Auger analysis/Ion implantation and Magnetron sputtering respectively. The contributions of co-workers to the research are gratefully acknowledged: Prof. E. J. Savino and Dr. R. Pasianot of CNEA, Argentina, (solute-defect coupling and the TRAL code), H. Sobel (N implantation into Fe), and G-S.Chen (thermal spike model). A warm and sincere thanks is also extended to the secretarial staff of the department of Materials Engineering for their cooperation and help. And finally but most importantly the author thanks his wife for all the help, cooperation and encouragements she provided in this work.

Financial support by the Office of Naval Research under contract number N000K1-85-K-0110, NR 653-044, and by the Naval Research Laboratory under contract number N00014-86-M-023 is gratefully acknowledged.

Table of Contents

List of Illustrations

List of Tables

Chapter 1

Introduction

Ion implantation, the process of embedding ions accelerated through high voltages, has been widely applied to control modification of surface sensitive properties. High fluence ion implantation into metals and alloys has proved successful for selectively changing the surface chemistry and microstructure of materials (within about 1 μm of the surface) without changes in bulk chemistry. Super-alloys with a large concentration of the implanted species can be formed at the surface which cannot be produced by other means. It is possible to alter the composition to a significant extent within limits set by the sputtering of atoms which accompanies the implantation. Defects caused by the energetic ion bombardment can interact both with the host matrix and the implanted atoms to stabilize particular atomic configurations, such as substitutional site occupancy of over-sized impurity atoms; leading at times to the formation of an amorphous layer.

Published literature concerning ion implantation on metallurgical surfaces has demonstrated several beneficial effects on mechanical properties and corrosion resistance.

There are different processes that operate during the implantation process that determine the final concentration distribution. Some of these processes are ion collection, sputtering of atoms, lattice dilation to accommodate the implanted ions, cascade-collision mixing, radiation enhanced diffusion, thermal spikes, radiation induced segregation, second phase precipitation, and chemical or thermodynamic factors. An overview of the processes has been discussed by Averback [1].

1.1 Processes in Ion Beam Surface Modification

1.1.1 Ion Collection

An energetic ion entering a thick target will, through collisions with the target nuclei and electrons, lose its energy and finally come to rest. The total distance that the ion travels in coming to rest is called its range; the projection of this distance onto the direction of incidence is called the projected range R_p Because the number of collisions and the energy transferred per collision (and thus also the scattering angle per collision) are random variables, all ions of a given type with given initial conditions will not have the same range. Rather, the ions will form a distribution that must be characterized by quoting a mean ion range, a standard deviation in ion range, and perhaps higher moments of the distribution function. The projected range must also be described statistically.

If the target is amorphous, the range distribution will depend primarily on the energy, mass, and nuclear charge of the incoming ions, and the mass, nuclear charge, and atomic density of the target. Implanting along non-low-index directions in a crystalline target, or implanting into polycrystalline targets yields ion distributions that are adequately characterized by the range statistics for amorphous targets. For many purposes, it is sufficient to represent the distribution in projected range by a gaussian profile described by the projected range R_p and the standard deviation of the distribution or straggling ΔR_p. Estimates of the values of R_p and ΔR_p can be obtained using different theories on range distributions such as the statistical amorphous theory of Lindhard, Scharff and Schiott (LSS) [2] or the Monte-Carlo simulation code (TRIM) [3].

1.1.2 Sputtering

As the ions impinge on the target, there is an ejection of surface atoms which is dependent on the energy deposited at and immediately below the surface. This removal of surface atoms, causes the surface to recede.

Schulz and Wittmaak [4] presented a zero order approximation of ion collection during sputtering. In their model, the effects of diffusion, lattice dilation, range shortening and recoil implantation were not considered. Fig. 1.1 illustrates the effect of sputtering during ion implantation. Shown in the figure are two sets of profiles for different ratios range X_p to straggling σ. Within each set the concentration profiles shown are for increasing dose or fluence Φ. As the implantation proceeds, i.e. as Φ increases, the peak concentration increases and the surface recedes more and more with the peak of the distribution approaching the surface, till a steady state

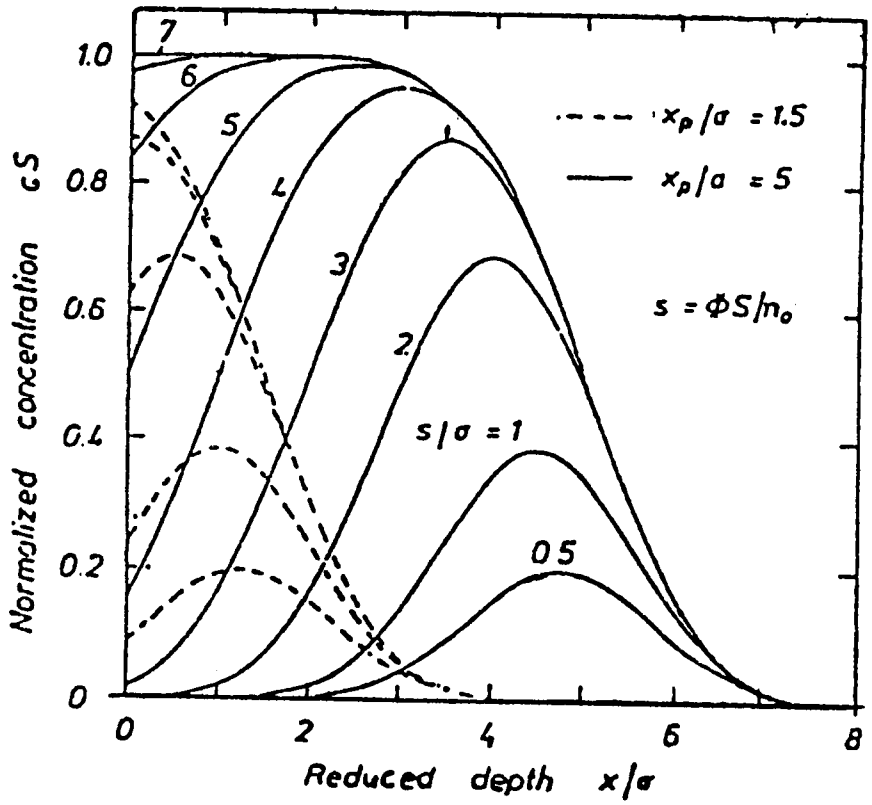

Figure 1.1. Illustration of the sputtering effect [4].

concentration is achieved. At the steady state concentration of the implanted species, the sputter rate of the implanted species equals the dose rate or flux of the implanted ions. At this level, the concentration at the surface in atom fraction reaches the value of the inverse of the sputter yield of beam atom on beam atom. The sputtering yield is determined here as the number of atoms of a particular species sputtered per incoming ion. For a larger ratio of range to straggling the profiles are deeper in the target than for a lower value of the ratio.

The recession rate of the surface will change with the concentration of the target species at the surface when different atoms sputter at different rates per incoming ion, i.e. when preferential sputtering of one of the species occurs. The effect of preferential sputtering leads to a varying total sputter yield and changes the concentration in the sub-surface region when diffusion accompanies the sputtering. In chapter 2 a model for preferential sputtering is described and example calculations are provided.

1.1.3 Effect of Lattice Dilation

The ion distribution profiles given by LSS theory and the Monte-Carlo simulation do not take into account the expansion resulting from adding ions to the work piece. While this is of negligible consequence at low fluences, the expansion effect is extremely important at higher fluences. The lattice dilation effect causes the gaussian profiles describing ions implanted early in the process to broaden and penetrate further into the material.

1.1.4 Ion mixing processes

Ion mixing processes include collision-cascade mixing, radiation enhanced diffusion and thermal spike effects.

1.1.4.1 Collision-Cascade Mixing

The ion on entering the target is slowed down continuously as it interacts inelastically with the electrons in the target. It also collides with the target atom nuclei elastically and transfers energy in discrete quantities with each collision [5]. In this elastic collision, a cascade-action takes place when several atoms around the collision point are knocked off their lattice sites. The displaced atoms quickly return to lattice sites, but in a random fashion accompanied by mixing of atoms within the cascade. This mixing process can be compared to a diffusion process with an effective diffusion coefficient.

Myers [6] has obtained an expression which at least gives an insight into the order of magnitude of this diffusion coefficient. He considers the production of vacancy-interstitial pairs. The creation of a vacancy-interstitial pair moves at least one target atom with respect to the host lattice. If the distribution of momentum transfers is assumed isotropic, the resulting migration is essentially a random-walk process. Adapting the standard expression for thermally activated diffusion in a cubic lattice to characterize the diffusion coefficient for collision-cascade-mixing gives:

$$D^{*} = \frac{1}{6}\lambda^{2}P \qquad [1.1]$$

where λ is the root-mean square separation for a vacancy-interstitial pair and P the number of displacements per target atom per unit time is given by [7]:

$$P(x) = \frac{0.8}{2NE_d} \frac{dE}{dx} \phi \qquad [1.2]$$

where ϕ is the ion flux, N is the atomic density at the solid, E_d is the effective threshold displacement energy, typically ~30 eV, and (dE/dx) is the ion energy deposited per unit depth into atomic processes; E being in eV and dx in nanometers.

The expression for D^* assumes the number of atoms moved by each atomic collision is one. Since a quantitative estimate of λ is not available, and since most of the displaced atoms are ejected from their lattice sites with an energy not much greater than the threshold value, λ is probably several times the nearest-neighbor distance. Values of 1 nm and several nanometers have been used. The main aspect of D^* is that it is flux dependent and not time or temperature dependent. The parameter Dt/Φ, the ion beam mixing parameter, which is widely used as a measure of cascade-collision mixing can be obtained from the effective diffusivity value calculated above by dividing the diffusivity value by the flux.

1.1.4.2 Radiation Enhanced Diffusion

Ion bombardment may greatly accelerate the diffusion of substitutional atoms at lower temperatures [6]. The increased vacancy concentration due to the irradiation causes a proportional increase in diffusion by the vacancy mechanism. In addition, substitutional atoms are ejected into interstitial sites from which they diffuse rapidly. These two transport processes comprise what is known as "Radiation enhanced diffusion". The major difference between this and cascade-collision mixing is that

enhanced diffusion is dependent on thermally activated defect migration. The overall atomic diffusivity under conditions of enhanced diffusion is governed by the production rate of mobile vacancies and interstitials, by the migration rate of these defects and by the probabilities of their annihilation by recombination, agglomeration, or assimilation into immobile sinks.

In general, the combination of cascade-mixing and radiation-enhanced diffusion produces a net effective diffusivity of the diffusion-like process, which is several orders greater in magnitude than the corresponding thermally activated diffusivity at low temperatures.

1.1.4.3 Influence of Temperature on Diffusion in Ion Implantation

The effect of temperature on the diffusion behavior during irradiation has been discussed widely [6,8]. At different temperatures some of the various competing mechanisms dominate. Figure 1.2 illustrates the effect of temperature on the diffusion coefficient during implantation. At lower temperatures, the temperature independent intermixing dominates diffusion up to the temperature at which the slower defects become highly mobile. At somewhat higher temperatures, in the radiation enhanced region, the excess defect concentrations of vacancies and interstitials enhances diffusion but is limited by recombination. At higher temperatures, yet in the same region, sink annihilation of defects gains importance and the diffusion coefficient becomes almost independent of temperature in the limit of predominant annihilation of defects at fixed sinks. At very high temperatures the thermal vacancy concentrations get very high and thermal diffusion dominates.

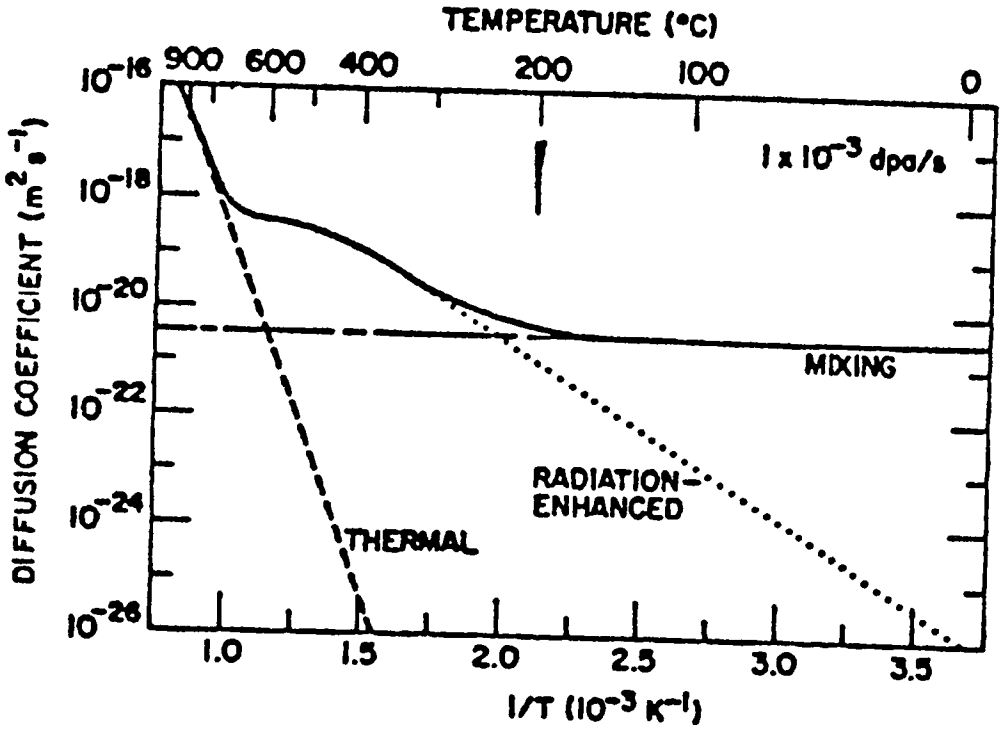

Figure 1.2. The steady state diffusion coefficient during irradiation as a function of inverse temperature.

1.1.4.4 Thermal Spike Effect

High density collisional cascades generate displaced atoms in a very localized volume. While these atoms cannot displace other atoms further, they can impart some of their energy to neighboring atoms through a many-body interaction. Thus most of their neighbor atoms are thermalized or energetically equalized in accordance to the Maxwell-Boltzmann distribution, and this results in a liquid-like thermal spike region in which the average characteristic energy of each atom is around 1 eV. This corresponds to an equivalent temperature of the order of 10^4 K. The thermal spike dimension is several tens of angstroms, i.e., approximately ten lattice constants. The thermal spike will quench in about 10^{-11} s [9]. The effect of thermal spikes is dominant in the case of heavy ion irradiation. The effect of thermal spikes is to cause a larger degree of ion beam mixing compared to that predicted by binary collision theories or cascade collision mixing. A thermal spike model based on semi-empirical and analytical expressions is presented in Chapter 7.

1.1.5 Radiation Induced Segregation

When metals and alloys are irradiated with energetic ions, interactions of radiation-induced defects with impurities and elements in the target produce significant segregation and/or the formation of second phases at grain boundaries, void surfaces, or external boundaries of the solid. This phenomenon is known as radiation-induced segregation. This has been studied in detail as evidenced by Refs. [10-14].

The radiation induced segregation phenomenon has its origin in the coupling between defect fluxes and fluxes of atoms in the target. Energetic irradiation produces point defects and defect clusters with an approximately random distribution throughout the material. Those defects that are mobile and escape recombination are re-incorporated into the crystal structure at dislocations, grain boundaries and other defect sinks. Hence, irradiation induces defect fluxes from the interior of the grains to spatially discrete sinks. Since the motion of defects is caused by the motion of atoms, fluxes of atoms are associated with defect fluxes.

Any preferential association of defects with a particular element and/or preferential precipitation of a component in defect diffusion will couple a net flux of the element to the defect fluxes. The flux of an element causes a buildup or depletion of the element in the vicinity of defect sinks and, therefore, concentration gradients even in initially homogeneous phases. The concentration gradients induce back diffusion of the segregating elements, and a quasi-steady state may be set up during irradiation whenever the defect-driven element fluxes are balanced by back diffusion [11].

Radiation-induced segregation requires two conditions (1) the presence of persistent defect fluxes and (2) a preferential coupling of the segregating species to these fluxes. The defects could be either vacancies or interstitials. Solute segregation in irradiated alloys is linked to the formation of mobile defect-solute complexes and/or to inverse kirkendall effects arising from differences in the diffusion rates of the free solute and solvent atoms when migrating via a vacancy or interstitial mechanism. The presence of defects may modify the chemical potential of the diffusing species and change its diffusional behavior. Production of defect gradients accompanies any irradiation process. Simulation codes such as the Monte Carlo code TRIM [3] and EDEP1 [2] based on the LSS theory can predict damage distributions.

Chapters 3 and 4 describe a simple model for radiation-damage induced migration and the experimental results of Sn implantation into Fe and N implantation into Fe are modelled to demonstrate the effect of this phenomenon.

1.1.6 Second Phase Precipitation

Second phase precipitation can occur during implantation, either by the reaction between the implanted species such as C or N with one or more elements of the target such as Fe or Nb but also between different elements in the target under irradiation. The precipitation of one or more phases will lead to very different concentration profiles from that predicted by the range and straggling of the implanted species. It is also of interest to know the fraction of the solute atoms that will remain in solution and that which will precipitate. A major problem in modelling the precipitation of second phases is the non-thermodynamic nature of the irradiation process. This rules out use of extensive thermodynamic data that is available to determine solubilities. Such data has to be obtained from X-ray diffraction measurements of implanted samples. In Chapter 5 a model based on the numerical solution of transport equations that includes precipitation of excess solute atoms over the solubility limit, and other implantation processes is presented.

1.1.7 Chemical and Thermodynamic Factors

Chemical driving forces can influence the migration of atoms during ion bombardment. This could lead to ion mixing results different from that predicted by

cascade-collisional mixing. This effect will be important when considered with the thermal spike effect where localized high temperatures exist.

For the case of bilayer samples, Johnson et. al. [9] used a modified effective diffusion coefficient by adding the Darken term, to consider chemical interactions that were present. The expression with the Darken term is now:

$$D^{*} = D_{AB}(1 - \frac{2\Delta H_m}{kT}) \qquad [1.3]$$

where ΔH_m is the heat of mixing, and D_{AB} is the effective interdiffusion coefficient for the binary system. Using the regular solution model, ΔH_m is given by:

$$\Delta H_m = \omega c(1 - c) \qquad [1.4]$$

where ω is defined as :

$$\omega = \omega_{AB} - \frac{(\omega_{AA} + \omega_{BB})}{2} \qquad [1.5]$$

where ω_{ij} are the interaction energies between i and j atoms and c is the concentration of B atoms. For atomic species which are strongly attractive, i.e. for negative heats of mixing, the diffusion is biased towards interdiffusion leading to greater ion mixing. For positive heats of mixing, however, the atomic species tend to segregate.

An experiment to determine the magnitude of chemical or thermodynamic factors in the case of migration of C in the presence of Fe and Ti is presented in Chapter 8.

1.2 Methods Used in Analyzing Ion Implantation Processes

Ion implantation processes can be simulated or modelled using phenomenological models using semi-empirical and analytical expressions, using analytical expressions alone and by first principle calculations based on binary collision approximations.

1.2.1 Phenomenological Models and Analytical Calculations

Phenomenological methods are based on semi-empirical models of the physical processes that are being analyzed and are generally very simple to model. Phenomenological models can use simple analytical evaluations of processes along with data obtained from the experiment to explain the phenomenon being modeled. A phenomenological model for ion implantation is presented by Farkas et.al. [15] for the case Ti implantation into Fe. Their code includes phenomenological models for the processes of ion collection, lattice dilation, diffusion-like broadening and sputtering. In this work, further phenomenological models for preferential sputtering, radiation-induced segregation and second phase precipitation are presented, which are used along with the models in Ref. [15]. The model for thermal spike effects described in Chapter 7 is based on a single analytical expression for the thermal spike effect.

1.2.2 First Principle Calculations

Computer simulation has been widely used in studying ion implantation using binary collision approximations. In the case of the transport theory, the physics of slowing down and scattering of the incident ion is combined into a single transport equation. Analytical formulations [16-18] based on the transport theory have been used to calculate the range distribution moments for a variety of ion/target combinations. One advantage of using computer programs based on the transport theory is that the calculation are very quick and range moments for all energy are calculated in a single run. Monte Carlo calculations [3,19] are another type of method used. These have a number of advantages over analytical formulations based on the transport theory. It allows for more rigorous treatment of elastic scattering, explicit consideration of surfaces and interfaces, and easy determination of energy and angular distributions.

The Monte Carlo simulation involves following a large number of individual ion 'histories' in a target. Each history begins with a given energy, position and direction. The particle is assumed to change direction as a result of binary nuclear collisions and move in a straight free-flight-path between collisions. The energy is reduced as a result of nuclear and electronic (inelastic) energy losses and a history is terminated when the energy drops below a pre-specified value.

The Monte Carlo method assumes an amorphous structure and uses random numbers to select specified parameters for the collision process.

In the current work, a Monte Carlo code based on the code TRIM simulates ion implantation as a dynamic process, updating the concentration as the implantation proceeds to high fluences. The code follows individual recoils through a number of collisions and generations until their energy drops below the

pre-specified cut-off energy value or the displacement energy. Chapter 6 gives details of the simulation and results of calculations using the code TRAL for ion mixing of Sn/Fe and C/Fe bilayers by Ar and Ti ion beams respectively.

1.3 Format of this Dissertation

The chapters in this disertation (Ch. 2 to 8) are organized in the form of research papers. The publications resulting from this work and the corresponding chapters are listed below.

Chapter 2 "Calculation of Ion Implantation Profiles Under Preferential Sputtering", M. Rangaswamy, D. Farkas and K.S. Grabowski, submitted for publication to Nucl. Instr. Meth; also presented at the AIME annual Meeting New York, Feb. 1985.

Chapter 3 "The Influence of Radiation Induced Segregation on Ion Implantation Profiles" , D. Farkas, M. Rangaswamy, R. Pasianot, and E.J. Savino, Nucl. Instr. Meth. **B16** (1986) 183;

Chapter 4 "Simulation of High Fluence N Implantation into Fe", M. Rangaswamy, D. Farkas and H.L. Sobel, Nucl. Instr. Meth. **B19/20** (1987) 196.

Chapter 5 "On the Influence of Second Phase Precipitation on Ion Implantation Profiles", D. Farkas and M. Rangaswamy, accepted for publication in Nucl. Instr. Meth.

Chapter 6 "Dynamic Monte Carlo Simulation of Collisional Mixing in Heterogeneous Media", D. Farkas, R. Pasianot, M. Rangaswamy, and E. J. Savino, to be submitted to Nucl. Instr. Meth.

Chapter 7 "Thermal Spike Related Nonlinear Effects in Ion Beam Mixing at Low Temperatures", G. Chen, D. Farkas and M. Rangaswamy, in 'Processing and Characterization of Materials Using Ion Beams' edited by L.E. Rehn, G.E. Greene and F.W. Smidt (MRS 1989); presented at the Materials Research Society Symposia, Boston MA, Nov.-Dec. 1988.

Chapter 8 "Ion Mixing of C Marker Layer in Amorphous Fe-Ti Alloy", M. Rangaswamy, K.S. Grabowski, B.D. Sartwell, and D. Farkas, to be submitted to Appl. Phys Lett.

1.4 References

[1] R.S. Averback and M.A. Kirk, in 'Surface Alloying by Ion, Electron, and Laser Beams' edited by L.E. Rehn, S.T. Picraux, and H. Wiedersich (ASM, 1987) p. 91.

[2] I. Manning and G. P. Mueller, Comp. Phys. Comm., 7, 85 (1974).

[3] J. P. Biersack and L. G. Haggmark, Nucl. Inst. Meth., 174, 257 (1980).

[4] F. Schulz, K. Wittmaak and J. Maul, Radiat. Eff., 18, 211 (1973).

[5] J. F. Gibbons, W. S. Johnson and S. W. Mylorie, 'Projected Range Statistics - Semiconductors and Related Materials',2nd ed. (distributed by Halstead Press, 1975).

[6] S. M. Myers, Nucl. Instr. Methods, 168, 265 (1980).

[7] P. Sigmund, Appl. Phys. Lett., 14, 114 (1969).

[8] H. Wiedersich, Nucl. Instr. and Meth., B7/8, (1985) 1.

[9] W. L. Johnson, Y. T. Cheng, M. Van Rossum and M-A. Nicolet, Nucl. Instr. & Meth. B7/8 (1985) 657.

[10] R.A. Johnson and L.Q. Lam, Phys. Rev. B 13 (1976) 4364.

[11] H. Wiedersich, P.R. Okamoto, and N.Q. Lam, Jour. of Nucl. Mater. 83 (1979) 98.

[12] P.R. Okamoto and L.E. Rehn, Jour. of Nucl. Mater. 83 (1979) 2.

[13] L.E. Rehn, P.R. Okamoto, D.I. Potter, and H. Wiedersich, Jour. of Nucl. Mater. 74 (1978) 242.

[14] A.D. Marwick and R.C. Piller, Radiat. Eff. 47 (1980) 195.

[15] D. Farkas, I. L. Singer, and M. Rangaswamy, J. Appl. Phys. 57 1114 (1985).

[16] P. Sigmund and A. Gras-Marti, Nucl. Instr. Meth. 182/183 (1981) 25.

[17] U. Littmark and J. F. Ziegler, Phys. Rev. 23A (1981) 64.

[18] J.P. Biersack and J.F. Ziegler, 'Ion Implantation Techniques', Springer Verlag, (1982) p. 122.

[19] M.T. Robinson and I.M. Torrens, Phys. Rev B9 (1974) 5008.

Chapter 2

Calculation of Ion Implantation Profiles Under Preferential Sputtering

2.1 Introduction

A computational model for high fluence ion implantation which took into account ion collection, lattice dilation, sputtering and diffusion-like transport processes has been described by Farkas et.al. [1]. The present work is based on the above model adding to it the effect of preferential sputtering.

Originating from the different sputtering yields of the constituents of the target are two major effects: (a) a varying total sputter yield (i.e. a varying surface recession rate; and (b) changes in concentrations at the sub-surface region when diffusion accompanies preferential sputtering. Several models which include preferential sputtering have been proposed [2-11]. The numerical models [2,3,4]

consider the effect (a) mentioned above and in one case [4] the excess atoms, originating due to the different sputtering yields of the constituents, was distributed into a finite layer at the surface. The analytical models [5-9] use the diffusion approach to model preferential sputtering. In Ref. [5] the concentration of the preferentially sputtered component was arbitrarily assumed to drop to zero at the surface. Collins [6] provides a mathematical analysis of the preferential sputtering process using diffusion theory, in which the depletion of the more volatile component is accommodated through diffusion at the surface. An analytical solution is presented by Collins for the steady state case. References [7] and [8] present analytical results for the time taken to reach steady state assuming diffusion enhancement of one species alone over a limited depth, similar to the ion penetration range. Oliva et.al. [10] include the conservation of lattice sites in their analytical treatment of preferential sputtering. The numerical model of Miotello and Mazzoldi [11] includes a fitting parameter, obtained by numerical analysis of experimental data, to consider the effect of preferential sputtering.

In the present analysis, the amount of depletion of the more volatile component is determined and included as a boundary condition of the diffusion equations. The surface erosion rate varies with time and is given by the sum of the instantaneous sputtering rates for each component. The computational method is based on a numerical solution to the diffusion equation for the implanted ions with the boundary condition controlled by preferential sputtering. The effect of preferential sputtering on the retained dose is also calculated.

2.2 Theory

A constant beam of ions of flux ϕ (in units of atoms/cm^2.sec) is incident normally on a plane target surface which initially consists of only one element. This ion flux produces a binary alloy in the target. The implanted ions are labeled as element 1 and the target atoms as element 2. In the analysis carried out, element 2 is assumed to be the preferentially sputtered component. The model presented in this work considers the effect of different implantation processes such as ion collection, lattice dilation, preferential sputtering and cascade mixing (or any other diffusion-like processes) on the evolution of the ion collection profiles.

2.2.1 Surface Recession and Diffusion Effects

Let r_1 and r_2 be the instantaneous sputtering rates, in units of atoms per unit area per second, of elements 1 and 2 from the surface. The sputter rates calculated on a volume fraction basis are given by

$$r_1 = \frac{\phi S_1 N^* C_1^*}{N_{01}} \qquad [2.1]$$

and

$$r_2 = \frac{\phi S_2 N^* (1 - C_1^*)}{N_{02}} \qquad [2.2]$$

where ϕ is the ion flux in atoms/cm^2.sec; S_1 is the sputtering yield of pure 1; S_2 is the sputtering yield of pure 2; C_1^* is the instantaneous concentration (in atom fraction) of 1 at the surface during sputtering; N_{01} is the atomic density of pure 1; N_{02} is the atomic density of pure 2; and N^* is the instantaneous atomic density at the surface given by:

$$\frac{1}{N^*} = \frac{C_1^*}{N_{01}} + \frac{(1 - C_1^*)}{N_{02}} \qquad [2.3]$$

The surface recession speed V is then given by:

$$V = r_1/N_{01} + r_2/N_{02} \qquad [2.4]$$

Substituting for r_1 and r_2 from Eqs. (2.1) and (2.2) into Eq. (2.4), we can calculate the volume sputtered per unit time per unit area, V, as:

$$V = \phi N^* \left[\frac{S_1 C_1^*}{N_{01}^2} + \frac{S_2(1 - C_1^*)}{N_{02}^2} \right] \qquad [2.5]$$

Prior to sputtering this volume contained $VN^*C_1^*$ atoms of element 1 while the actual rate at which element 1 is sputtered away is given by Eq. (2.1). Thus if element 1 is the less-preferentially sputtered component, during sputtering there will be a net flux of atoms of element 1 into the surface and this is given by:

$$Z_1 = VN^*C_1^* - \phi S_1 N^* C_1^*/N_{01} \qquad [2.6]$$

This will lead to an enhanced concentration of element 1 in the surface layer. The global steady state value of the concentration of element 1 is given by the condition:

$$\phi = r_1 = \phi N^* S_1 C_1^* / N_{01} \qquad [2.7]$$

Eq. (2.7) yields:

$$C_1^*(\text{at steady state}) = \frac{N_{01}/N_{02}}{S_1 - [1 - (N_{01}/N_{02})]} \qquad [2.8]$$

In the case where $N_{01} = N_{02}$ Eq. (2.8) reduces to $C_1^* = 1/S_1$.

The increased concentration of the preferentially less sputtered component (element 1 in our case) in the sputtered layer, leads to diffusion of 1 into the sub-surface region which is at a lower concentration. The actual concentration in the surface layer depends on the magnitudes of the two competing mechanisms, preferential sputtering which increases the concentration of the preferentially less sputtered element and diffusion. Because of the implantation process there is likely to be diffusion, even at room temperature, due to collision cascade mixing, thermal spikes or radiation enhanced diffusion.

2.2.2 Method of Calculation of the Implantation Profile.

The profile of the ions implanted to high fluences is affected by four processes: (1) Ion collection, with a Gaussian distribution, (2) sputter erosion of the surface, (3) lattice dilation as a result of ion collection, and (4) diffusion-like broadening resulting from the collision cascades or radiation-enhanced diffusion.

The term "diffusion-like" is used here to denote transport processes that in a first approximation obey Fick's second law with constant diffusivities:

$$\frac{\partial C_1}{\partial t} = D_1 \frac{\partial^2 C_1}{\partial x^2} \qquad [2.9]$$

$$\frac{\partial C_2}{\partial t} = D_2 \frac{\partial^2 C_2}{\partial x^2} \qquad [2.10]$$

These equations describe thermal and radiation-enhanced diffusion, as well as cascade mixing. The non-linearity introduced in the differential equations as a result of considering different atomic densities of the diffusing constituents [6] has been dropped.

The diffusion coefficients for the two elements 1 and 2 are considered equal and constant. These originate due to the implantation process and could be due to either collision-cascade mixing, thermal spikes, or radiation enhanced diffusion or a combination of effects. Following the method in the earlier model [1], an estimate is made of the order of the diffusivities using the diffusion approximation to atomic mixing [12]. The actual diffusivities used result from comparison of of the present calculations with experimental profiles and thus are only semi-quantitative values.

As in Ref. [1] using Eqs. (2.9) and (2.10), a D_1 (equal to D_2) value was obtained which gave calculated profiles that best fit the experimental curves. The diffusion equations were solved by a finite difference technique, the Cranck-Nicholson method. A detailed description of the method used to account for the ion collection, sputter erosion, and lattice dilation is given in Ref. [1]. The enhanced concentration of the less preferentially sputtered element in the surface layer is obtained by transferring the net flux of atoms of element 1 given by Eq. (2.6) into the first bin of the finite-difference set up. A listing of the program SPUTEFF that includes the model for preferential sputtering is given in the Appendix.

2.3 Results and Discussion

To illustrate an example of preferential sputtering, results of calculations carried out for 150 keV Ta implanted into Fe are presented. The experimental results used were obtained from Ref. [13]. The range R_p and the range straggling ΔR_p were the same as that used by Grabowski et.al., obtained from the codes EDEP1 [14]. Table 2.1 gives the values of R_p and ΔR_p obtained by using the two codes EDEP1 and TRIM [15]. The similar values of R_p and ΔR_p were obtained from the two codes. The sputtering yields of Ta and Fe were obtained from the R.B.S. measurements [13] illustrated in Fig. 2.1. The sputtering yield of Fe was obtained from the initial sputter rate of Fe at which period only Fe is present, i.e. using Eq. (2.2) at $\Phi \rightarrow 0$, Φ being the fluence. The sputtering yield of Ta was obtained from the approximately steady state sputter rate of Fe using Eqs. (2.7) and (2.5) and from the condition that at steady state the sputter rate of Ta was equal to the incoming flux of Ta. Sputtering yield values of 3.6 for Ta and 6.3 for Fe were obtained, indicating a significant difference in the two sputtering yields.

In comparing experimental concentration profiles to calculated ones, the concentration of Ta was obtained by considering the atom fractions of Ta and Fe only. Though carbon and oxygen were used in fitting the RBS data, they were ignored when calculating the Ta concentration since the model calculations do not include them. Comparison of experimental and calculated profiles yielded an effective diffusion coefficient D_1 of $1 \times 10^{-15} cm^2/sec$. This was of the same order of magnitude as the value obtained from diffusion approximation to cascade mixing [12] for a flux of $24 \times 10^{12} Ta/cm^2$-sec and corresponds to an ion mixing parameter (Dt/Φ) value of 0.4167 nm^4. For the lowest fluence of $1 \times 10^{16}/cm^2$, however, a higher D_1 value of 3x

Table 2 . 1. Range R_p and Range Straggling ΔR_p for 150 keV Ta implanted into Fe, obtained using L.S.S. Theory and Monte-Carlo Simulation.

R_p	ΔR_p	
20.6 nm	7.0 nm	(L.S.S.)
20.9 nm	7.3 nm	(Monte-Carlo)

$10^{-15}cm^2/sec$ gave the best fit as shown in Fig. 2.2. This probably indicates that a higher diffusivity was in operation initially but as more and more defects were introduced the diffusivity lowered to $1x10^{-15}cm^2/sec$.

Figures 2.3, 2.4 and 2.5 compare the experimental profiles for fluences of 6, 12 and $18x10^{16}/cm^2$ with calculated results using two diffusivities i.e. $1x10^{-15}cm^2/sec$ (the best-fit value) and $3x10^{-15}cm^2/sec$. While the higher diffusivity shows a significant tail portion at depths greater than the peak range of the ions it must be understood that this is due to the assumption of constant diffusivity in the model. In reality, the diffusivity is depth dependent and should drop rapidly beyond the range R_p. Thus, while there will be a difference in the profiles obtained using the two different diffusivities, the differences will not be as great as shown here.

Figure 2.6 illustrates the effect that different diffusivities could have on the almost steady state profile for a fluence of $18x10^{16}Ta/cm^2$. At zero diffusivity the steady state is reached at a lower concentration in the surface region than for the case of $1x10^{-15}cm^2/sec$, but with higher diffusivities the surface concentration drops as diffusion reduces the concentration gradient. The higher diffusivities result in a marked increase in the amount of Ta collected by the target. The effect of different diffusivities on the retained dose for different fluences is shown in Fig. 2.7. The increase in the retained dose will not be as much as indicated if depth dependent diffusivities were used. However, it is clear from this figure that the retained dose is higher at higher diffusivities and also that the time taken to reach steady state increases with diffusivity. Though it is not clearly visible in Fig. 2.7, the lower fluence region of the retained dose curve showed a lower retained dose for higher diffusivities. This is due to the increasing concentration gradient from the surface inwards which causes diffusion of atoms from the peak concentration region to the

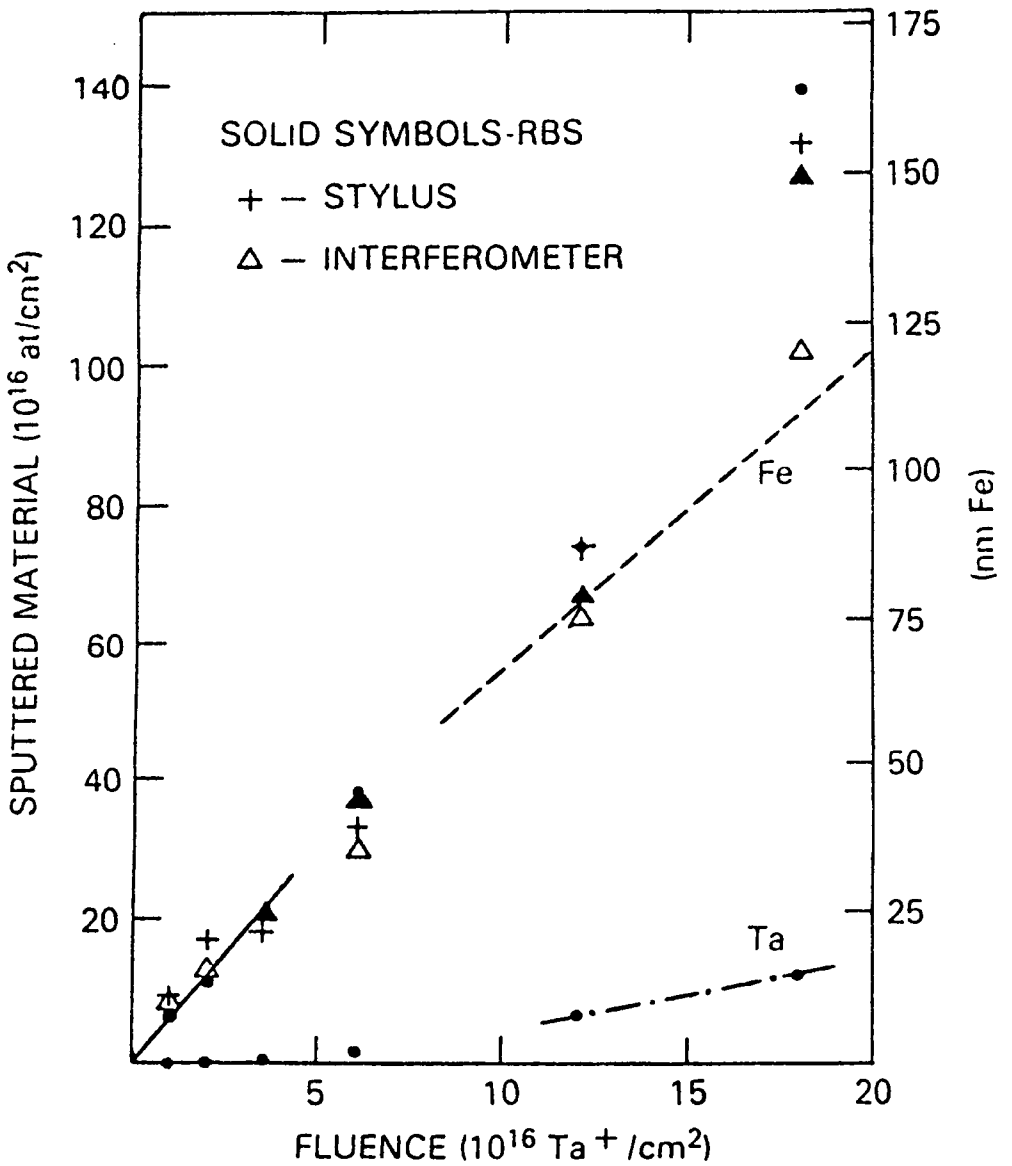

Figure 2.1. Sputter rates of Ta and Fe during 150 keV Ta implantation into Fe. The initial total (Fe+Ta) and Fe sputter rates are represented by the solid line, the steady state sputter rate of Fe by the dashed line and the steady state sputter rate of Ta with a slope of 1 by the dot-dashed line (from Ref. [13]).

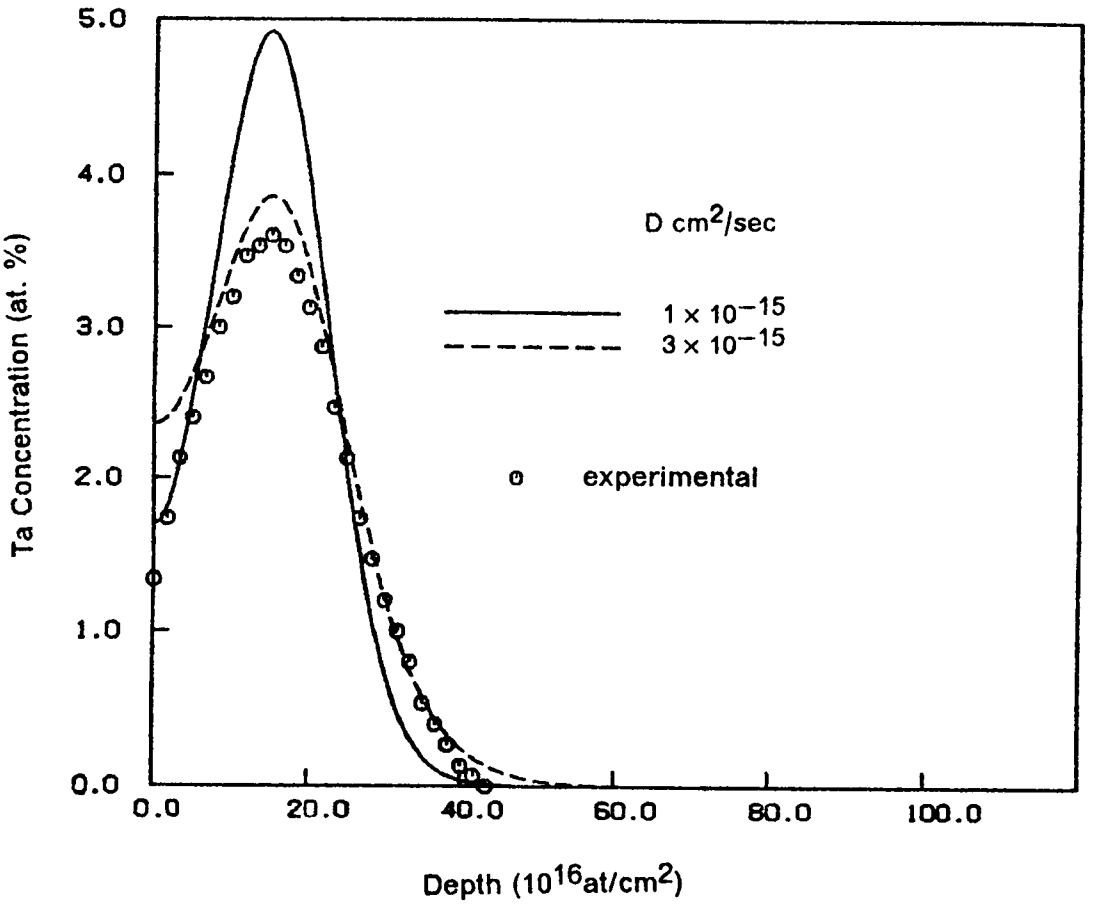

Figure 2.2. Experimental and calculated Ta concentration profiles for a fluence of 1x10^{16}/cm^2 with different diffusivities.

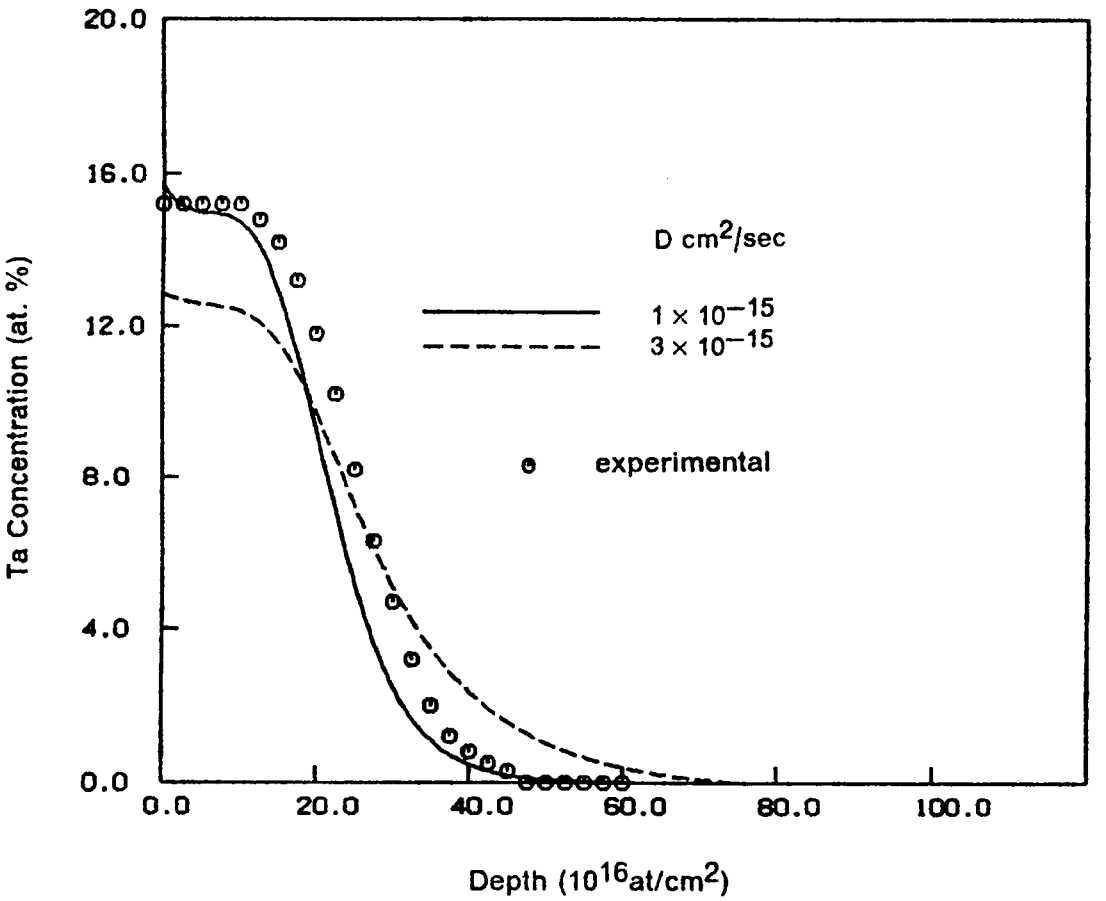

Figure 2.3. Experimental and calculated Ta concentration profiles for a fluence of 6×10^{16}/cm^2 with different diffusivities.

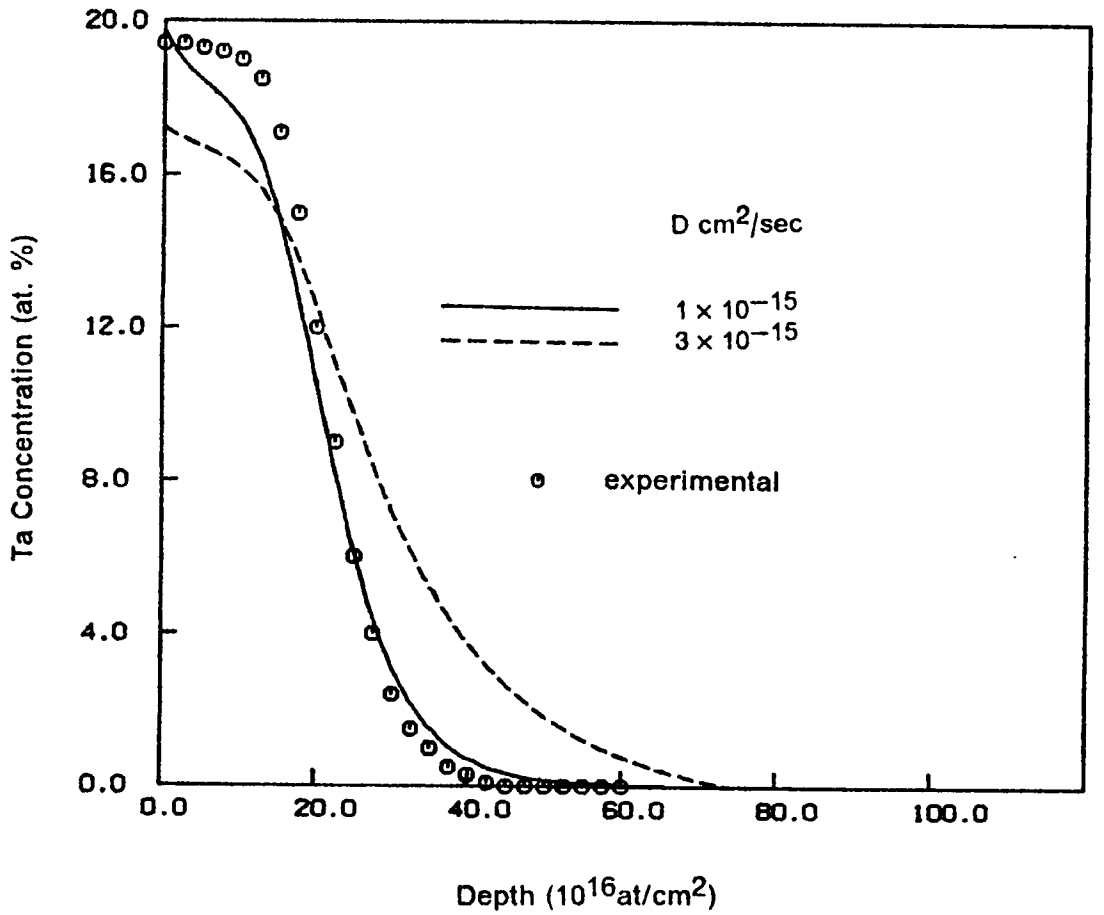

Figure 2.4. Experimental and calculated Ta concentration profiles for a fluence of 12x10^{16}/cm^2 with different diffusivities.

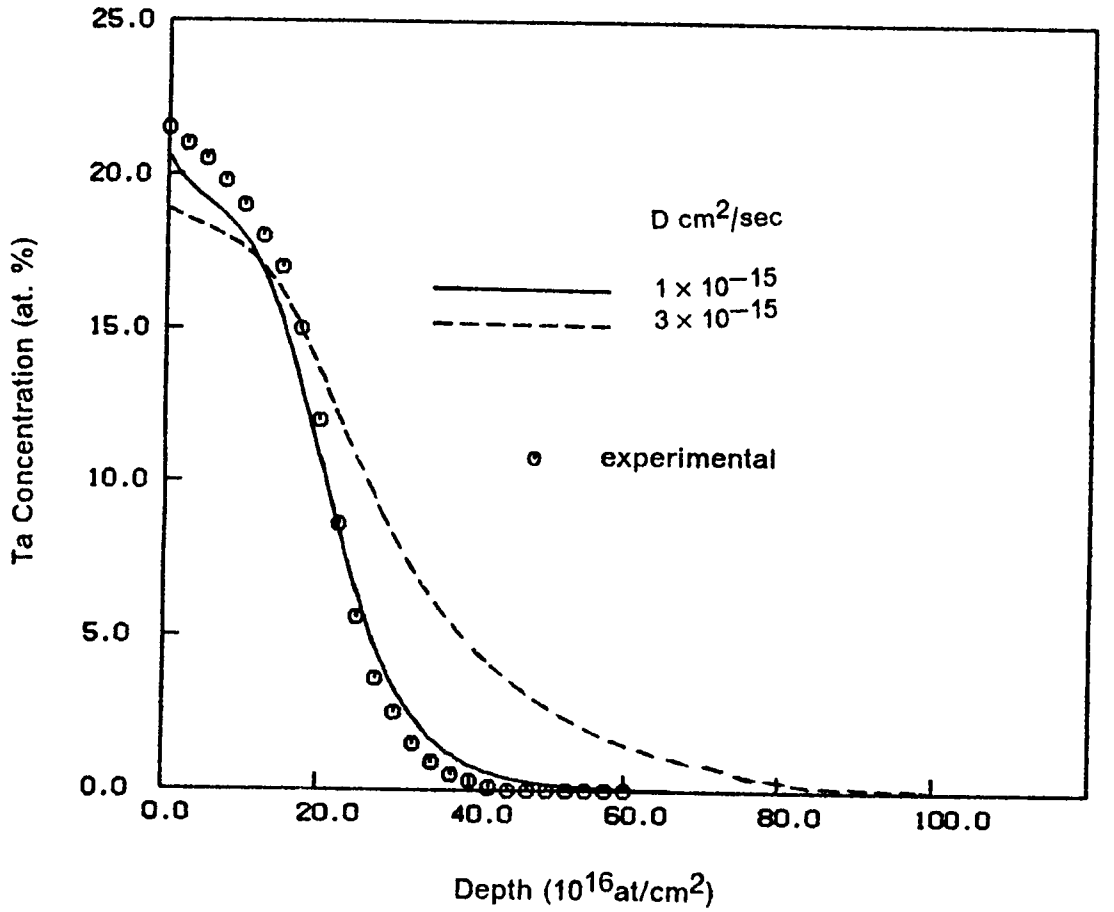

Figure 2.5. Experimental and calculated Ta concentration profiles for a fluence of $18 \times 10^{16}/cm^2$ with different diffusivities.

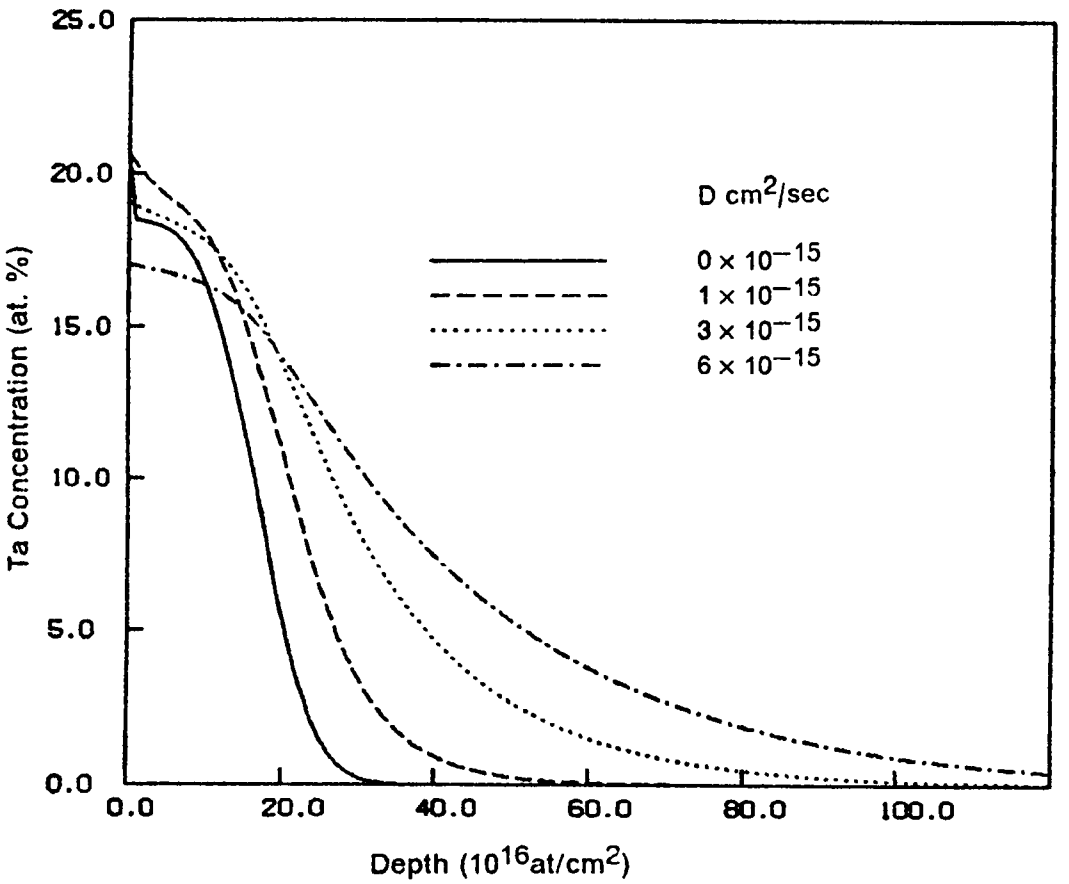

Figure 2.6. Predicted variation of the concentration profiles for the fluence of $18x10^{16}/cm^2$ with different diffusivities.

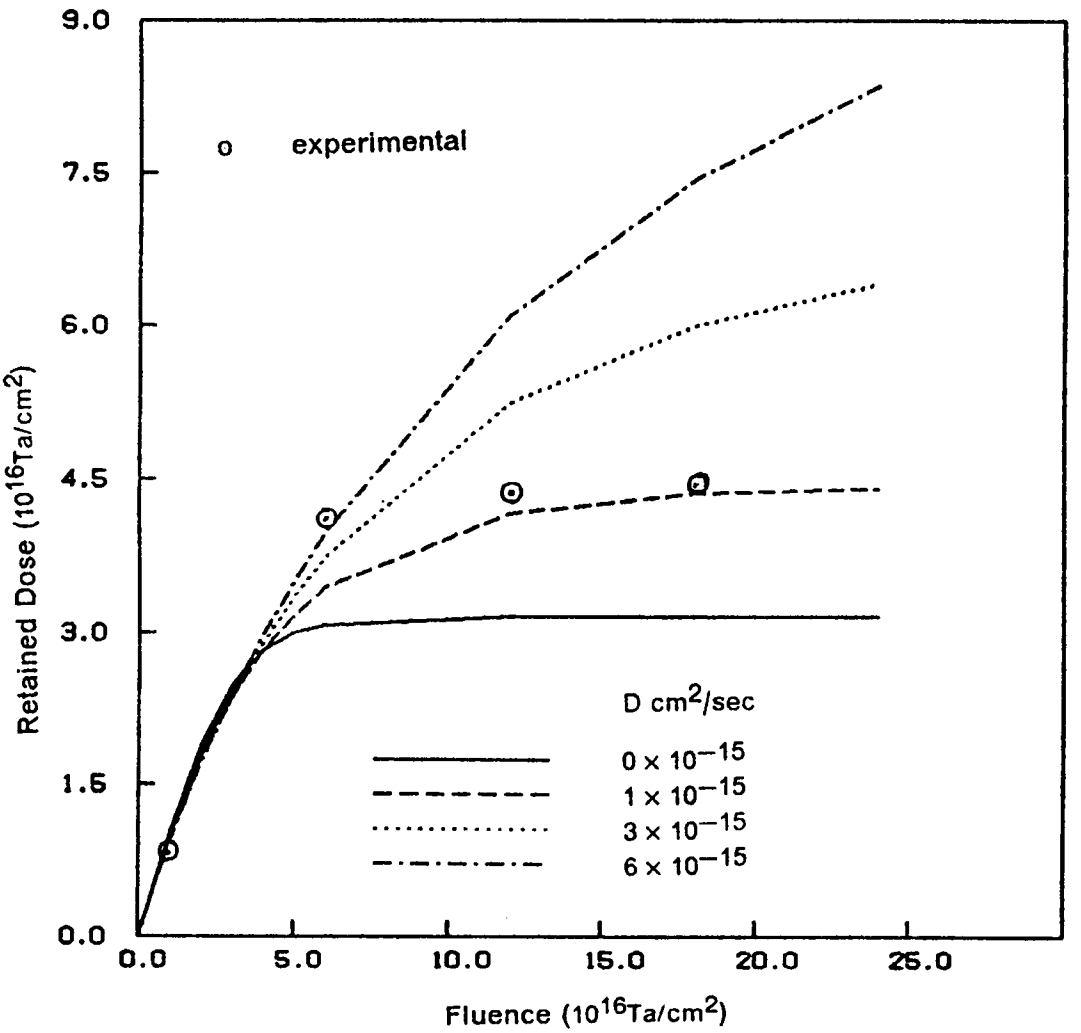

Figure 2.7. Experimental and calculated retained dose at different fluences with different diffusivities.

surface that are subsequently lost in sputtering. These results indicate that the effect of preferential sputtering accompanied by diffusion on the retained dose is significant.

2.4 Conclusions

The simple numerical model presented can simulate the effects of preferential sputtering during ion implantation. From the results obtained it is clear that preferential sputtering strongly affects the ion collection profiles and if diffusion is present the effect extends well into the target. In the case Ta implantation into Fe, the effect of preferential sputtering accompanied by diffusion causes a large increase in the retained dose. The effect on the retained dose is significant for fluences greater than $5x10^{16}cm^2/s$. Higher diffusivities increase the retained dose as well as the time taken to reach steady state. The diffusion like process is best represented by an effective diffusivity of $1x10^{-15}cm^2/s$ and this is in agreement with the predictions of a ballistic mixing model, suggesting that the diffusion-like effects observed in this case are dominantly cascade mixing.

2.5 References

[1] D. Farkas, I. L. Singer, and M. Rangaswamy, J. Appl. Phys. 57 1114 (1985).

[2] C. M. Davisson, Naval Research Lab. Memorandum Report 5409.

[3] H. Krautle, Nucl. Instrum. Methods 134 167 (1976).

[4] G. W. Reynolds, A. R. Knudson and C. R. Gosset, Nucl. Inst. Meth. 182/183 179 (1981).

[5] H. W. Pickering, J. Vac. Sci. Technol. 13 618 (1976).

[6] R. Collins, Rad. Effects 37 13 (1978).

[7] R. Webb, G. Carter and R. Collins, Rad. Effects 39 129 (1978).

[8] R. Collins, Rad. Eff. Lett. 43 111 (1979).

[9] G. Carter, R. Webb and R. Collins, Rad. Eff. Lett. 43 125 (1979).

[10] A. Oliva, R. Kelly and G. Falcone, Surf. Science 166 403 (1986).

[11] A. Miotello and P. Mazzoldi, J. Appl. Phys. 54 4235 (1983).

[12] S. M. Myers, Nucl. Instr. Methods 168 265 (1980).

[13] K. S. Grabowski, F. D. Correll and F. R. Vozzo, Nucl. Instr. Meth. B7/8 798 (1985); and K. S. Grabowski, Private Communication.

[14] I. Manning and G. P. Mueller, Comp. Phys. Comm. 7 85 (1974).

[15] J. P. Biersack, L. G. Haggmark, Nucl. Inst. Meth. 174 257 (1980).

Chapter 3

The Influence of Radiation-Damage Induced Migration on Ion Implantation Profiles

3.1 Introduction

Surface modification by ion implantation has become an important technique for producing materials with unique surface properties [1]. In recent years extensive research has been directed toward the understanding of several phenomena that affect the final implantation profiles [2,3]. Some of these phenomena are: surface recession due to sputtering, collisional mixing and matrix density modification due to the ion beam, diffusion of the implanted species, etc. In connection with this last process, it was shown in a recent work [4] that a diffusion-like transport of the implanted atoms was significant during high fluence Ti implantation into 52100 steel.

The present work is concerned with the diffusion of the implanted species and coupling of these fluxes with defects and defect fluxes developed during the ion bombardment of the substrate. This coupling is the main contribution to the radiation induced segregation phenomenon (RIS) and has been the object of extensive investigations [5,6,7,8]. The effect of defects introduced during implantation can significantly alter the chemical potential of the implanted species and influence its diffusion. This radiation-damage induced migration (RDIM) can be considered as a part of the general radiation induced segregation phenomenon. The present calculations address the problem of determining the effect of solute-defect coupling phenomena occurring simultaneously with the implantation process on the final ion collection profiles. The effect of sputtering, mixing and density modification are also included in the present study. The calculations are carried out using a numerical method, the general procedure of which is described in detail in Ref. [4]. A simple model is used that describes the coupling with only one adjustable parameter. Although the model is too simple to yield quantitative results, the objective is to determine whether the effect of RDIM on the shape of high fluence implantation profiles is significant.

3.2 The Model

The formalism considers the effects of ion collection, diffusion-like broadening resulting from cascade mixing (or any other diffusion-like processes), lattice dilation, sputtering, and radiation induced segregation on the evolution of the ion collection profiles in high fluence ion implantation. The diffusion equations are

solved by a finite difference technique, the Cranck-Nicholson method. Sputter erosion and lattice dilation are accounted for within the finite difference set up by coordinate transformations. The simple model for RDIM which is included in the numerical calculations is described below.

To set up a continuity equation that describes the mass conservation of the implanted species, a simple and phenomenological approach is taken. For the solute flux we can write:

$$-J_1 = D_{11}\frac{dC_1}{dx} + D_{12}\frac{dC_2}{dx} \qquad [3.1]$$

where D_{11} is the diffusion coefficient, essentially describing the mixing effect, and D_{12} the parameter representing the coupling between the solute and defect fluxes. Both of them are approximated as depth independent to simplify calculations. C_1 stands for solute concentration and C_2 for defect concentration (only one type of defect is taken into account). Therefore, the continuity equation reads

$$\frac{\partial C_1}{\partial t} = D_{11}\frac{\partial^2 C_1}{\partial x^2} + D_{12}\frac{\partial^2 C_2}{\partial x^2} + g_1(x) \qquad 0 \leq x < \infty, t > 0 \qquad [3.2]$$

$g_1(x)$ is the generation rate of solute species because of the implantation process and is calculated using a Monte-Carlo computer code [9]. In the same fashion, a similar equation for C_2 must be included which contains a generation term $g_2(x)$ assumed to be proportional to the damage function $g_d(x)$ (again calculated with the same Monte-Carlo code). Since the model does not include rigorous calculations involving interactions between the generated defects and their annihilation at sinks, the constant of proportionality was chosen arbitrarily so that every 100 implanted ions

introduced one defect, up to a saturation value of 10^{-3} defects. However, this assumption does not affect the purpose of the calculations except that the numerical value of coupling parameter will have no specific quantitative significance. The coefficients D_{11} and D_{12} are fitting parameters that result from comparison between numerical calculations and experimental profiles.

No assumption is made about the particular transport mechanisms that are present because of the nature of the approach. The model simply describes the effect of a coupling term between solute and damage that could be due to several physical processes. The model is too simple to properly describe a particular mechanism. For example, if the diffusion-like transport is a vacancy mechanism and the coupling is in fact radiation-induced segregation, it would be necessary to separately account for the fluxes of vacancies, interstitials and other defect complexes. This would involve several parameters that could make comparison with experiment very difficult. In the present phenomenological approach only one parameter, D_{12} is used to describe coupling effects i.e. RDIM. The parameter D_{12} essentially represents a component of the chemical potential of the diffusing solute originating from the presence of defects and in particular the gradient of the defect concentration. This is analogous to the cross-diffusion terms considered in multi-component diffusion. This parameter is varied to study the changes that occur in the high fluence profiles as the coupling effect is included.

3.3 Experiment and Calculations

A sample of Fe was implanted with Sn at 200 keV up to a dose of 5 x 10^{16} atoms/cm^2 at room temperature. A current density of 2 μA/cm^2 was used. The implanted sample was then analyzed with the X.P.S. technique using an erosion beam of Ar^+ at 10 keV.

Similar experimental results were obtained from Ref. [10] for the case of a 52100 steel sample implanted with Ti at 190 keV and then analyzed with the A.E.S. technique.

The implantations were done at room temperature, corresponding to vacancy diffusivities of less than $10^{-21}cm^2$/sec obtained from standard Fe self-diffusion data [11]. The mobility of radiation-induced vacancies may be different from that obtained from self-diffusion data since only the migration activation energy is needed, the vacancies being formed by the irradiation. The vacancy diffusivity under irradiation conditions at 300 K is about $3\times10^{-10}cm^2/s$ in pure Fe, but since the vacancies are quickly trapped by impurity atoms or annihilated by Fe self-interstitials they are essentially immobile [12,13]. It was found that the calculated implantation profiles were not affected by defect diffusivities of this order of magnitude. Therefore the equation for the defects was written as

$$\frac{\partial C_2}{\partial t} = g_2(x) \qquad [3.3]$$

i.e. a linear growth with time. Eqn. (3.2) was solved numerically using the finite-difference method described in Ref. [4]. The parameters D_{11} and D_{12} were varied to obtain a best fit with experiment.

As mentioned earlier, since the the constant of proportionality between $g_2(x)$ and the damage function $g_d(x)$ is somewhat doubtful, the magnitude of D_{12} will have no quantitative meaning. Despite this, the sign of D_{12} can be asserted as shown in the following section.

3.4 Results and Discussion

Figures 3.1 and 3.2 show the damage and probable range distributions for the case of Sn and Ti respectively, calculated using the Monte-Carlo computer code. Figures 3.3 and 3.4 show the experimental measurements and several fitting curves for the two cases. A sputtering yield of 2 was used in both the cases.

From comparison between experiment and the results of the Monte-Carlo code we conclude that some transport mechanism was present at the time of implantation. As in previous work [4], D_{11} is obtained from the comparison of calculated and experimental profiles. These comparisons yielded a value of $6\times 10^{-15}cm^2/s$ for both Sn and Ti. With a flux of $6.242\times10^{13}/cm^2$, this corresponds to an ion mixing parameter (Dt/Φ) value of 0.9612 nm^4. The magnitude of the D_{11} coefficients obtained (10^{-14}-$10^{-15}cm^2/sec$) is consistent with the cascade mixing mechanism, as described by the Kinchin-Pease relation [14-16].

The calculations in Fig. 3.3 were carried out with D_{12} values of 0, $+8\times10^{-13}cm^2/sec$ and $-8\times10^{-13}cm^2/sec$ and that in Fig. 3.4 with D_{12} values of 0, $+2\times10^{-13}cm^2/sec$ and $-2\times10^{-13}cm^2/sec$. Figure 3.3 shows that in the case of Sn the best fit, considering the trend of the experimental profile at the surface is obtained with a positive coupling coefficient; which would mean diffusion along the defect

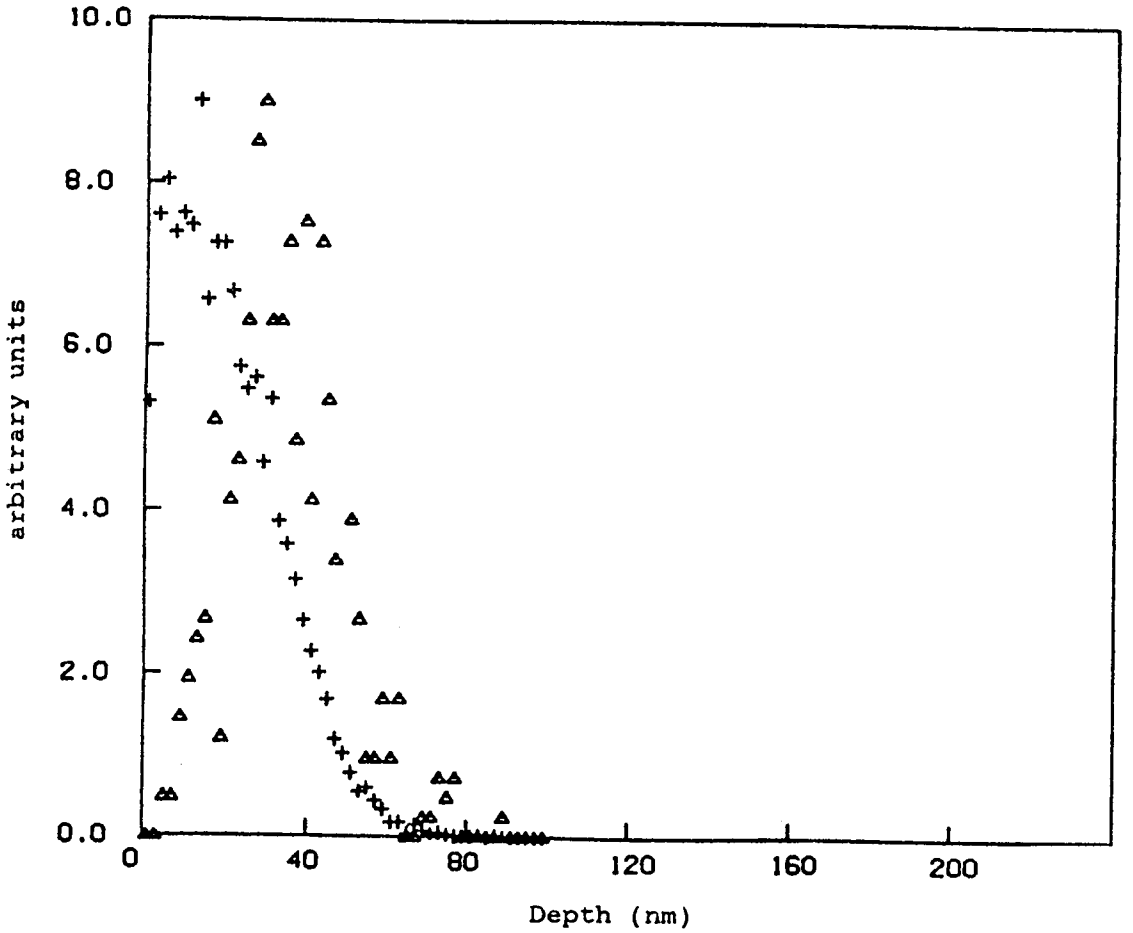

Figure 3.1. Probability distribution (Δ) and the damage profile (+), in arbitrary units, of the 200 keV Sn ion implantation into Fe, as calculated by the Monte-Carlo code TRIM.

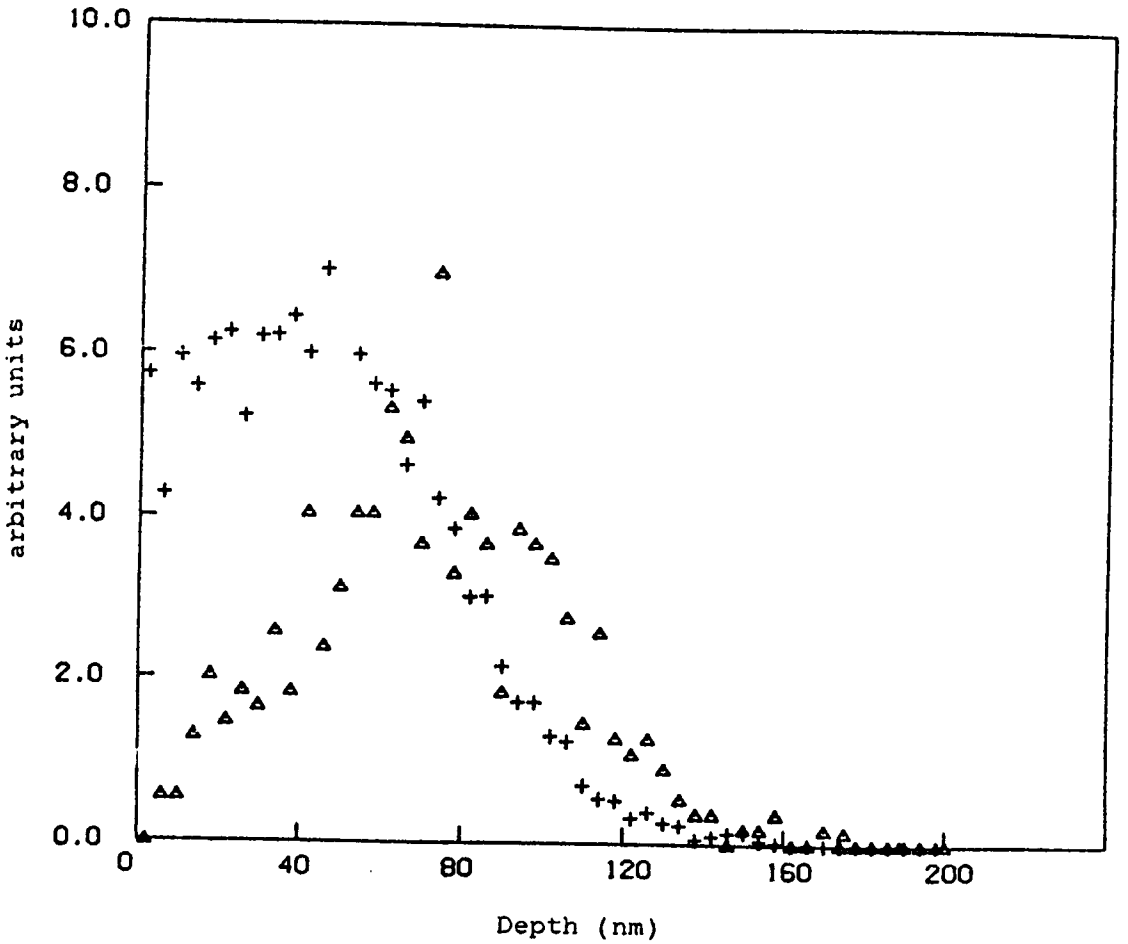

Figure 3.2. Probability distribution (Δ) and the damage profile (+), in arbitrary units, of the 190 keV Ti ion implantation into 52100 steel, as calculated by the Monte-Carlo code TRIM.

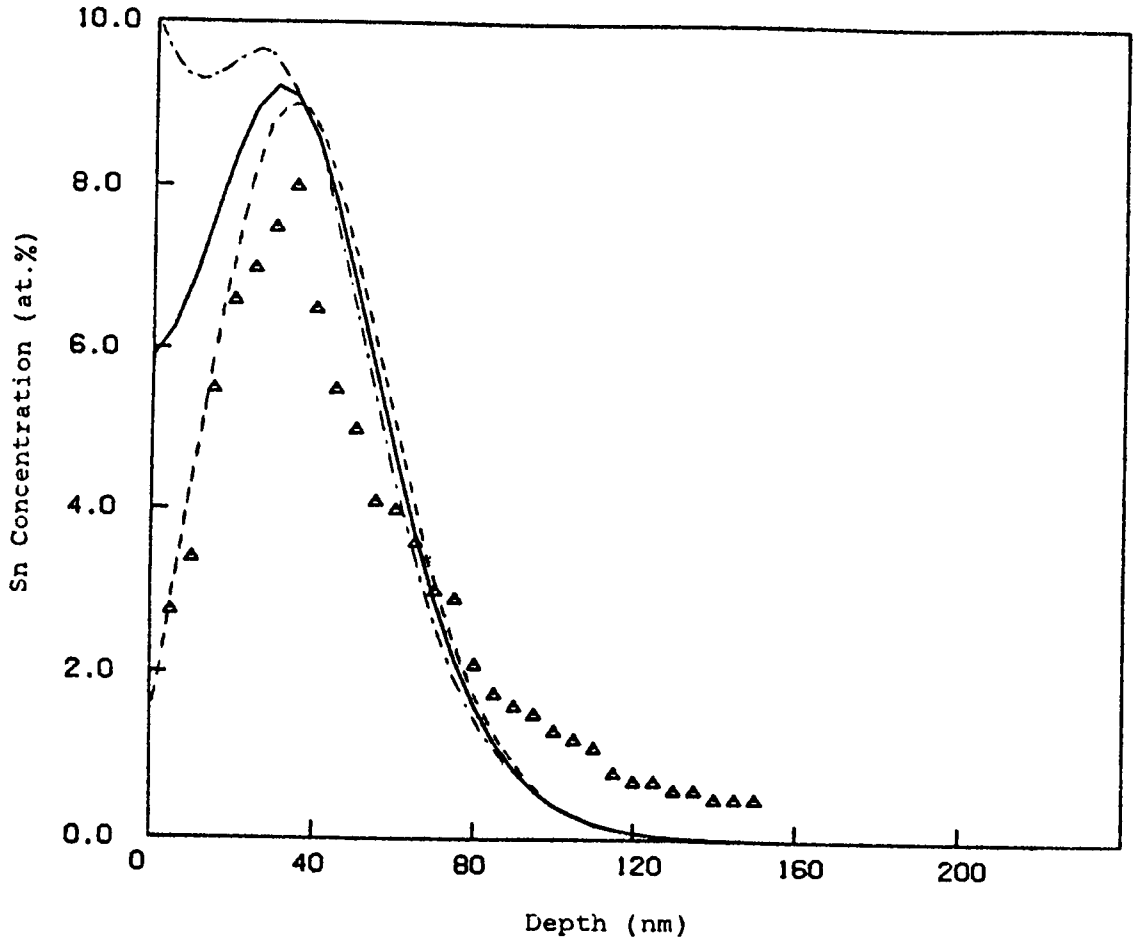

Figure 3.3. Experimental and calculated Sn profiles for 200 keV implantation of Sn into Fe upto a fluence of $5\times10^{16}Sn^{+}/cm^{2}$. (Δ : experimental; — : $D_{12}=0$; - - : $D_{12}=+8\times10^{-13}cm^{2}/s$; ··· : $D_{12}=-8\times10^{-13}cm^{2}/s$)

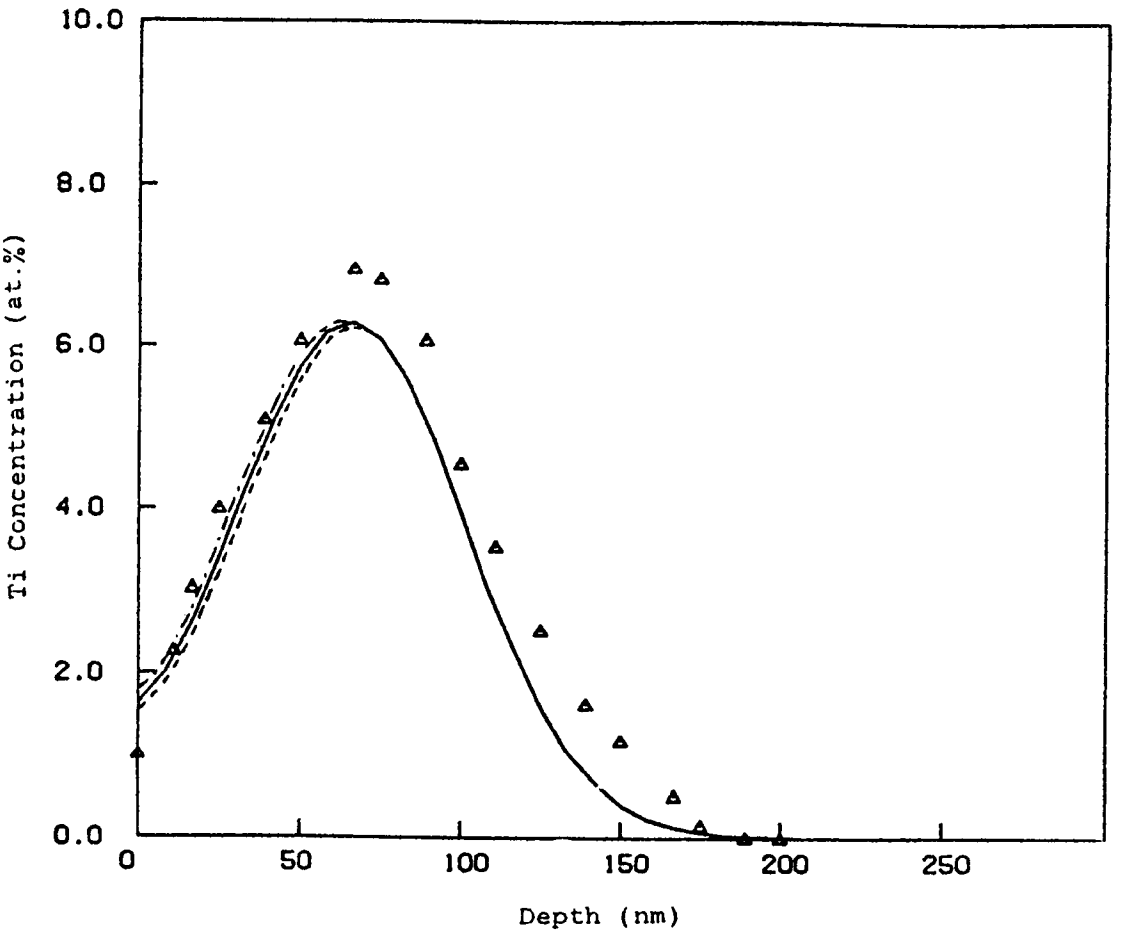

Figure 3.4. Experimental and calculated Ti profiles for 190 keV implantation of Ti into Fe upto a fluence of $5\times10^{16}Ti^{+}/cm^{2}$. (Δ : experimental; —:$D_{12}=0$; - - : $D_{12}=+2\times10^{-13}cm^{2}/s$; -·- : $D_{12}=-2\times10^{-13}cm^{2}/s$)

gradient (see Eq. (3.1), inward direction). In the case of Ti no significant difference was observed on variation of D_{12} as shown in Fig. 3.4. The difference in behavior observed in the cases of Sn and Ti could be due to the difference in the shape and position of the damage distribution with respect to the surface. The Ti damage profile is broader and the peak concentration is farther away from the surface than in the case of Sn.

An attempt can be made to try to interpret the results in terms of possible mechanisms. Because of the low temperature of implantation, the present case is obviously not one of the typical radiation-induced segregation case with migration of atoms and defects by temperature dependent diffusion. It is possible that a similar effect could be caused by migration of atoms in the cascade mixing process if this mechanism preferentially transports one of the components. This could cause a net flow of solute atoms up or down the defect gradient. Note that the defect gradient, as used in our calculations, coincides with the damage generation gradient.

The nature of defects that affect the transport of solute atom is not clear. In a general case, the sign of the D_{12} can sometimes be correlated with the mechanism. For example, if a vacancy mechanism is operative, the faster diffusing component, which in the present case would be Sn [11,17], will go up the defect gradient. The results of our calculations, however, show Sn to move down the defect gradient suggesting that the observed effect cannot be explained by a vacancy mechanism, as can be expected for low temperatures.

The present results show good agreement between experiment and the model. Despite this, the very long tail seen in the experimental profile of Sn is not explained by any of the fittings. We can only speculate on the reason for this tail; it could, for example, be due to the mixing process that takes place during the analysis technique [18,19]. The results of the present model, although semi-quantitative,

demonstrate that the phenomenon of RDIM may have a significant effect on the final ion collection profiles. This effect appears to be confined to the surface (damaged) region. A more refined model which includes space variable diffusion would have to be developed in order to further support this conclusion. It should be noted that preferential sputtering of Sn atoms during implantation could also occur and this may contribute to the shape of the Sn profiles. In the calculations carried out, the contribution of preferential sputtering has not been considered.

3.5 Conclusions

The coupling of solute flux with the defect gradient can have a significant effect on the ion collection profiles. The simple model that is proposed can account for the ion collection profiles in a semi-quantitative way. In the case of Sn, the positive sign of the solute-defect coupling coefficient suggests that a vacancy mechanism was not dominant.

3.6 References

[1] G. Dearnaley, Rad. Eff. 63 (1982) 1.

[2] F. Schulz and K. Wittmaak, Radiat. Eff. 29 (1976) 31.

[3] H. Krautle, Nucl. Instrum. Methods 134 (1976) 167.

[4] D. Farkas, I. L. Singer, and M. Rangaswamy, J. Appl. Phys. 57 (1985) 1114.

[5] A. D. Marwick and R. C. Piller, Radiation Effects 47 (1980) 195.

[6] R. A. Johnson and N. Q. Lam, Physical Review B 13 (1976) 4364.

[7] P. R. Okamoto and L. E. Rehn, J. Nucl. Mat. 83 (1979) 2.

[8] H. Wiedersich, P. R. Okamoto and N. Q. Lam, J. Nucl. Mater. 83 (1979) 98.

[9] J. P. Biersack and L. G. Haggmark, Nucl. Inst. Meth. 174 (1980) 257.

[10] I. L. Singer, J. Vac. Sci. Technology. A 1 (1983) 419.

[11] C. J. Smithells, "Metals Reference Book", 3rd edition (Butterworths, Washington, 1962), p. 594.

[12] L. De Schepper, G. Knuyt, L. M. Stals, and P. Moser, Rad. Eff. Lett. 76 (1983) 43.

[13] A. Vehanen, P. Hautojarvi, J. Johansson, J. Yli-Kauppila, and P. Moser, Phys. Rev. B. 25 (1982) 762.

[14] G. H. Kinchin and R. S. Pease, Rep. Prog. Phys. 18 (1955) 1.

[15] P. K. Haff and Z. E. Switkowski, J. App. Phy. 48 (8) (1977) 3383.

[16] H. H. Andersen, Appl. Phy. 18 (1979) 131.

[17] K. Hennesen, H. Keller and H. Viefhaus, Scripta Met. 18 (1984) 1319.

[18] P. Sigmund and A. Gras-Marti, Nucl. Inst. Meth. 168 (1980) 389.

[19] U. Littmark and W. O. Hofer, Nucl. Inst. Meth. 168 (1980) 329.

Chapter 4

Simulation of High Fluence N Implantation into Fe

4.1 Introduction

N implantation into metals to create wear-resistant surfaces [1,2,3] is one application of high fluence ion implantation into metals as a viable technique to create surfaces with unique properties. Consequently, extensive research has been directed towards understanding the processes that occur during implantation that affect the final solute profiles. Despite this work, there is a large body of literature reporting experimental data of N implanted metals that is not understood [4-7].

This chapter is concerned with modeling experimental profiles of N implanted into iron using a phenomenological approach. The model accounts for ion-collection, lattice dilation, sputtering, and diffusion-like broadening resulting from cascade mixing or any other diffusion-like processes. The model also includes the coupling of the solute flux with the radiation induced defects (i.e. radiation-damage

induced migration) using a numerical approach [8,9]. The objective of the present work is to model experimental data [6,7] in order to evaluate the importance of these processes at high fluence under varying temperatures and fluences.

4.2 Theoretical considerations

The concentration profiles of N implanted into metals are affected by several processes; these are:

- ion collection that follows a gaussian type curve,
- diffusion-like broadening resulting from cascade mixing (or any other diffusion-like processes),
- lattice dilation occurring from the large percentage of interstitial atoms placed in the matrix,
- sputtering,
- radiation-damage induced migration, and
- precipitation of nitrides simultaneously with the diffusion process.

The diffusion equations are solved by a finite difference technique, the Cranck-Nicholson method. Sputter erosion and lattice dilation are accounted for within the finite difference set up by coordinate transformations [10,11]. Also, at each time step the N that exceeds a certain solubility limit is precipitated as a nitride and removed from the diffusion process. The model used for considering the precipitation of nitrides is described in Chapter 5. The details of the numerical procedure are reported in Refs. [8,9,11] and in Chapter 3.

4.3 Coupling of Solute and Defect Fluxes

The simple model for radiation-damage induced migration which is included in the numerical calculation uses a phenomenological approach. The continuity equation, described in detail in Chapter 3 and in Ref. [11], reads

$$\frac{\partial C_1}{\partial t} = D_{11}\frac{\partial^2 C_1}{\partial x^2} + D_{12}\frac{\partial^2 C_2}{\partial x^2} + g_1(x) \qquad 0 \leq x < \infty, t > 0 \qquad [4.1]$$

where D_{11} is the N diffusion coefficient, essentially describing the mixing effect, D_{12} is the parameter representing the coupling between the solute and defect fluxes, C_1 is the N concentration and C_2 is the defect concentration (only one type defect is taken into account), and g_1 (x) is the generation rate of solute species because of the implantation process and is calculated using the Monte-Carlo computer code TRIM [12]. In the same fashion, a similar equation for C_2 must be included which contains a generation term $g_2(x)$ assumed to be proportional to the damage function $g_d(x)$ (again calculated with the same Monte-Carlo code). Since the model does not include rigorous calculations involving interactions between the generated defects and their annihilation at sinks, the constant of proportionality was chosen arbitrarily as in the previous chapter. This means that the value of coupling parameter D_{12} will have no specific quantitative significance similar to the case considered in the previous chapter. The coefficients D_{11} and D_{12} are fitting parameters that result from comparison between numerical calculations and experimental profiles.

Again no assumption is made about the particular transport mechanisms that are present because of the nature of the approach, since the model is too simple to properly describe a particular mechanism. In a rigorous treatment it would be

necessary to separately account for the fluxes of vacancies, interstitials and other defect complexes. The effect of newly formed precipitates and their effect on defect migration will also have to be considered. This would involve several parameters that could make comparison with experiment very difficult. In the present phenomenological approach only one parameter, D_{12} is used to describe coupling effects. The parameters D_{11} and D_{12} are varied to study the changes that occur in the high fluence profiles as the temperature increases.

4.4 Results and Discussion

The formalism was applied to the simulation of several experimental profiles available in the literature. These were N implanted into Fe up to a fluence of 10^{17}/ cm^2 at 40 keV with a flux of $6.249 \times 10^{13}/cm^2$ of Moncoffre et al [6], who carried out the implantation at 20, 100, 150, and 200 °C, and that of Singer [7], who carried it out at room temperature at 40 keV up to fluences of $20 \times 10^{16}/cm^2$. Some of these profiles, especially the higher temperature ones, can only be explained by including the effect of radiation-damage induced migration. The simple model for radiation-damage induced migration discussed above can reproduce the two peak structure observed in these profiles.

The first series of calculations was performed without including the precipitation of nitrides in order to study the effect of radiation induced segregation. The range and straggling were obtained from calculations carried out using the Monte-Carlo code TRIM in each case. The code was also used to obtain the values for range and straggling of the damage profiles. The values are listed in Table 4.1.

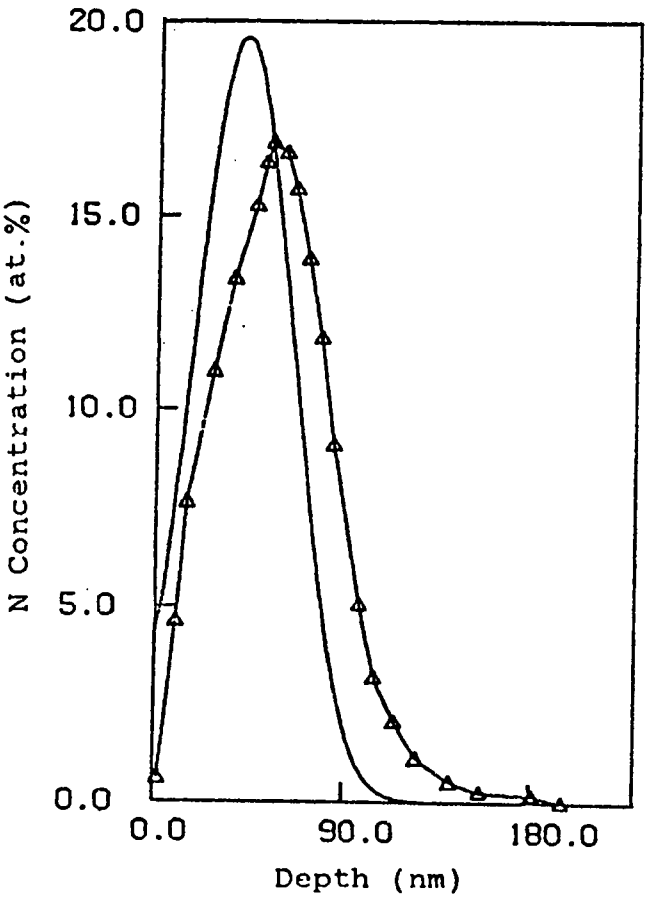

Figure 4.1. Calculated (——) and experimental [6] (—Δ—) profiles of 40 keV N in Fe for a fluence of $10^{17}/cm^2$ at 20°C. [$D_{11} = 1\times10^{-16}cm^2/s$, $D_{12} = 5\times10^{-15}cm^2/s$].

It was found that the set of experimental profiles obtained at different temperatures and fluences for 40 keV could be fit by using a nearly constant ratio of D_{11}/D_{12}, that varied in only 25% among the different temperatures and doses. The best fit value of both coefficients increased with temperature, as expected for a thermally activated diffusion process. Figures 4.I to 4.4 show some of the calculated profiles using the best fit values, together with the experimental ones at different temperatures.

The best fit values obtained are consistent with an interstitial diffusion mechanism, that is $D_{11}/D_{12} > 0$, where the interstitial species segregates down the defect gradient. Also, the obtained values of D_{11} allow the calculation of the activation energy for the diffusion process. Figure 4.5 shows the Arrhenius plot of the obtained data, giving an activation energy of 32 kJ. This value is lower than that of thermal diffusion of N into Fe measured by several authors [13,14] to be around 75 kJ. The values of diffusivities obtained for room temperature are similar to those of N diffusion in Fe under no irradiation. At higher temperatures the values obtained are lower than the diffusion coefficient for unirradiated material. This is probably due to the formation of complexes binding the nitrogen to other defects introduced by the irradiation. These complexes are expected to have a much lower mobility. Alternatively, this may be interpreted as a trapping effect on the nitrogen by the defects that result from the implantation process.

A second series of calculations included the effect of precipitate formation. If the solubility limit was taken from thermodynamic values it was found that nearly all the nitrogen is predicted to precipitate and the resulting profiles are similar to those calculated for very low diffusivities, disagreeing with the experimental ones. It can be concluded from this that the precipitation process does not occur according to thermodynamic equilibrium. Furthermore, the results indicate that the effect of

Table 4. 1. Range R_p and Range Straggling ΔR_p for N implanted into Fe, obtained using TRIM

Energy (keV)	R_p (nm)	ΔR_p (nm)	
40	46.0 nm	21.9 nm	(Nitrogen)
40	33.6 nm	20.0 nm	(Damage)

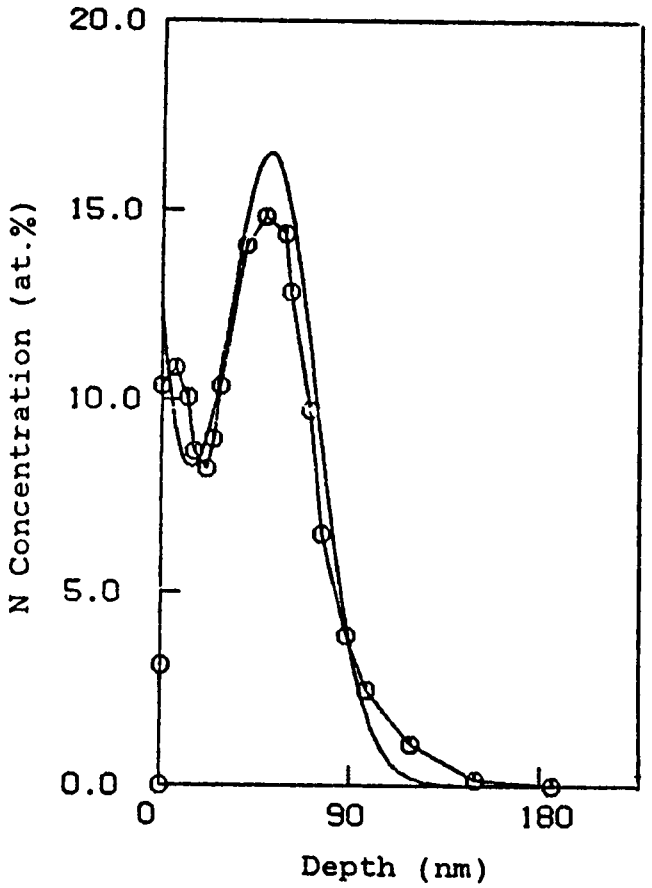

Figure 4.2. Calculated (——) and experimental [6] (—O—) profiles of 40 keV N in Fe for a fluence of $10^{17}/cm^2$ at 100°C. [$D_{11} = 1\times10^{-15}cm^2/s$, $D_{12} = 1.5\times10^{-13}cm^2/s$].

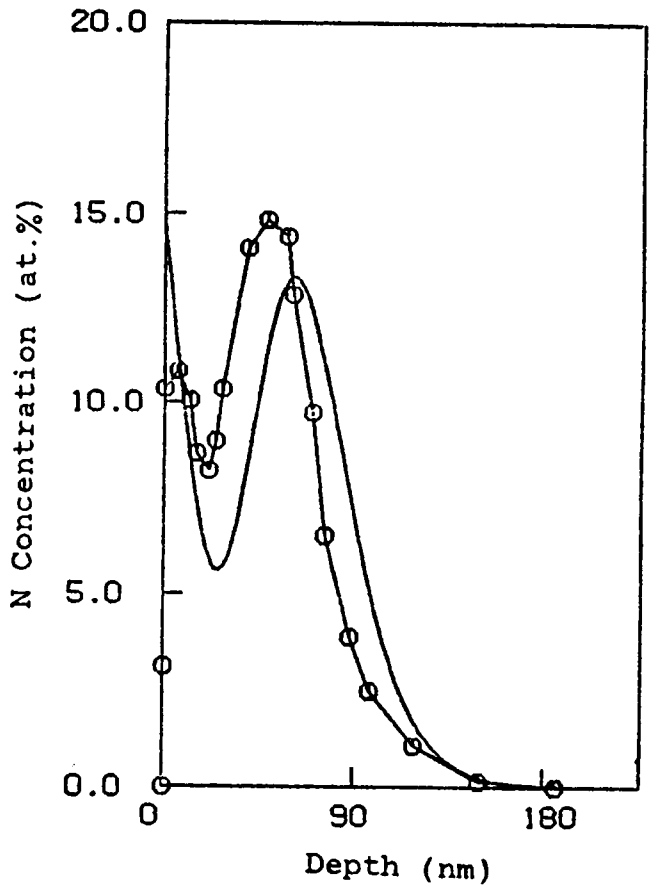

Figure 4.3. Calculated (——) and experimental [6] (—O—) profiles of 40 keV N in Fe for a fluence of $10^{17}/cm^2$ at 150°C. [$D_{11} = 5\times10^{-15}cm^2/s$, $D_{12} = 5\times10^{-13}cm^2/s$].

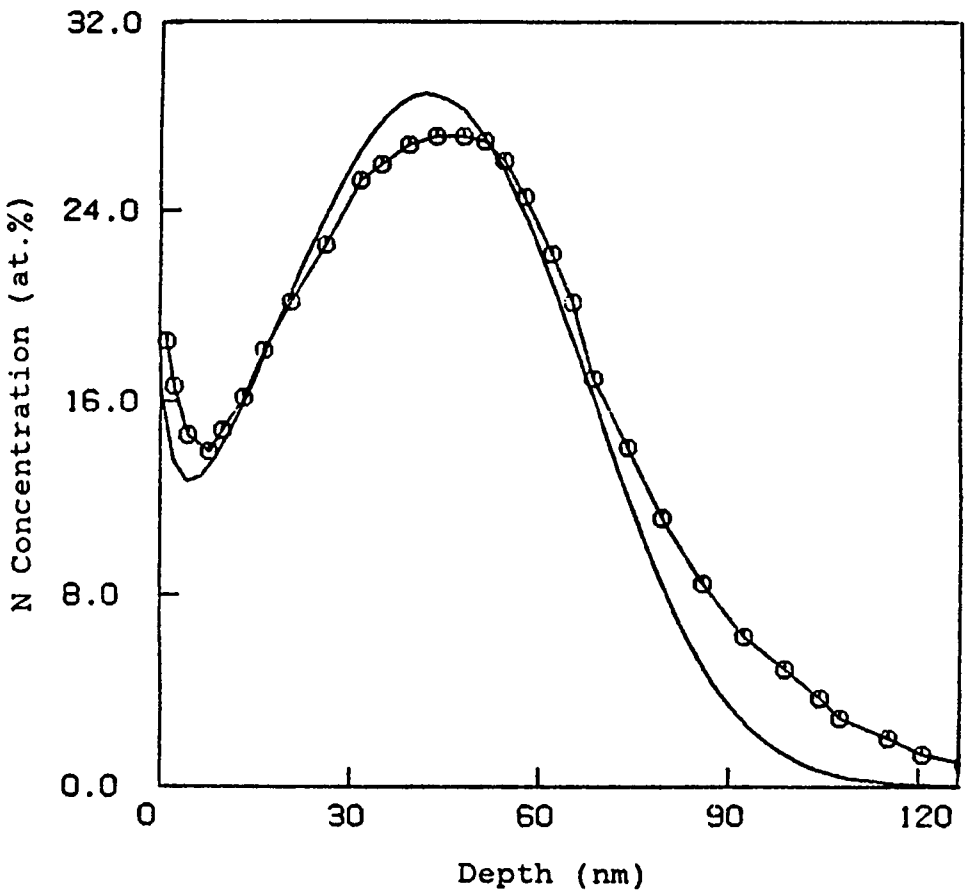

Figure 4.4. Calculated (——) and experimental [7] (—O—) profiles of 40 keV N in Fe for a fluence of $2\times10^{17}/cm^2$ at room temperature. [D_{11} = $1\times10^{-16}cm^2/s$, D_{12} = 4×10^{-14} cm^2/s]

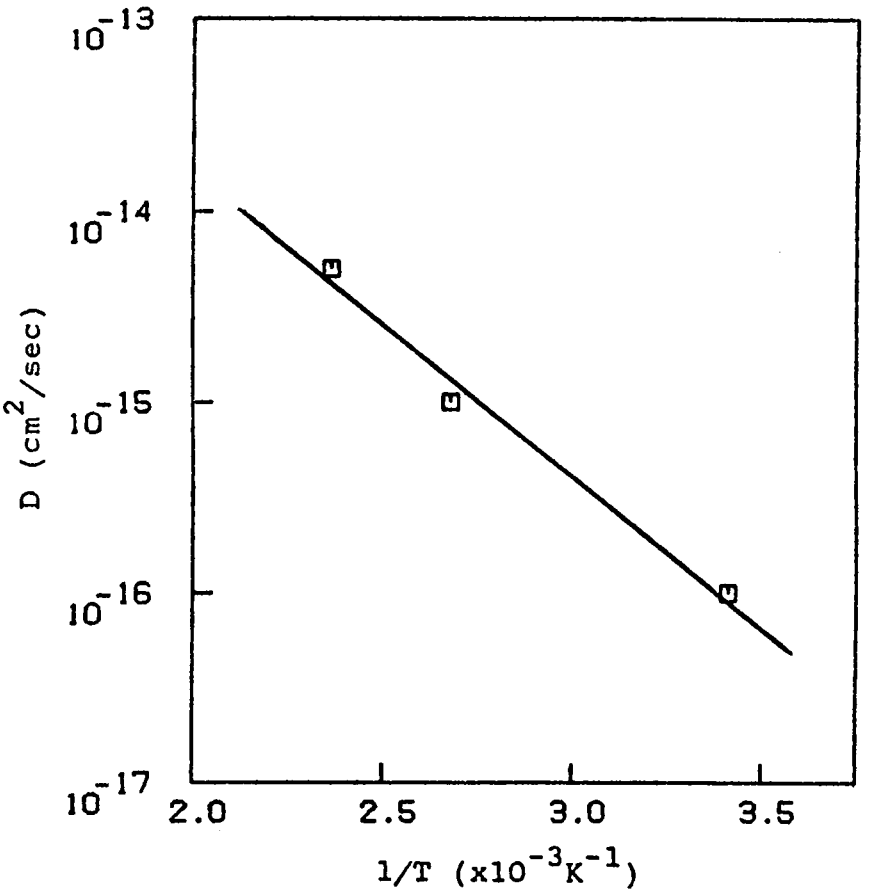

Figure 4.5. Arrhenius plot of the diffusivity D_{11} from Figs. 4.1-4.3.

precipitation on the final profiles is not as marked as that of radiation-damage induced migration.

4.5 Conclusions

The calculations show that the process of radiation-damage induced migration is important in the case of N implantation into Fe, and that it can explain the formation of the two peak structure through interstitial diffusion of N down the defect gradient. While the value of the room temperature diffusion coefficient D_{11} of N in Fe during irradiation is similar to that without irradiation conditions, the higher temperature diffusivities under irradiation are lower than that for no irradiation. The activition energy under irradiation is, however, much lower than the thermal activation energy for the diffusion of N in Fe. The precipitation of nitrides during implantation does not follow equilibrium thermodynamics and any effect of precipitation on the final concentration profiles appears to be insignificant.

4.6 References

[1] G. Dearnaley and N.E.W. Hartley, Thin Film Solids 54 (1978) 215.

[2] H. Dimigen, K. Kobs, R. Leutenecker, H. Ryssel, and P. Eichinger, Mat. Sci. Eng. 69 (1985) 181.

[3] Ion Implantation, edited by J. K. Hirvonen (Academic Press, New York, 1980).

[4] T. Barnavon, J. Tousset, S. Fayeulle, P. Guiraldenq, D. Treheux, and M. Robelet, Radiat. Eff. 77 (1983) 249.

[5] K. Hohmuth and B. Rauschenbach, Mat. Sci. Eng. 69 (1985) 489.

[6] N. Moncoffre, G. Hollinger, H. Jaffrezic, G. Marest, and J. Tousset, Nucl. Instr. Methods B7/87 (1985) 177.

[7] I. L. Singer, Vacuum 34 (1984) 853.

[8] D. Farkas, R. Pasianot, M. Rangaswamy, and E.J. Savino, Nucl. Instr. Methods B16 (1986) 183.

[9] D. Farkas and K. Ohla, Oxidation of Metals 19 (1983) 99.

[10] J. Cranck, The Mathematics of Diffusion, 2nd ed., (Clarendon, Oxford, 1975), p.4.

[11] D. Farkas, I.L. Singer, and M. Rangaswamy, J. Appl. Phys. 57 (1985) 1114.

[12] J. P. Biersack and L.G. Haggmark, Nucl. Instr. Methods 174 (1980) 257.

[13] M. A. Krishtal, Diffusion Processes in Iron Alloys, NBS TT 70-50031, (1970).

[14] C. J. Smithells, Metals Reference Book, 3rd edition (Butterworths, Washington, 1962), p.594.

Chapter 5

On the Influence of Second Phase Precipitation on Ion Implantation Profiles

5.1 Introduction

Second phase precipitation may occur during ion implantation in a number of cases of great practical importance. For example, when elements such as C and N are implanted into metals to obtain excellent wear resistant properties, the formation of carbides or nitrides has been reported extensively in the literature [1-3]. In most cases the implanted atoms form precipitates with the host metal atoms. It is difficult to predict what phases may precipitate out since the precipitation occurs under severe irradiation conditions. Metastable phases may form and existing phases may dissolve [4]. Precipitation of phases can significantly affect the migration of atoms when they get trapped as a precipitate. Precipitation from an ion implanted

supersaturated state on subsequent annealing has been analyzed and modeled by Myers [5] for the case of Sb implanted into Fe-Ti-C alloys. Kant et. al. [6] have studied the effect of implant temperature flux and fluence on precipitate size and number density. The purpose of the present work is to study the influence of such precipitation processes on the implantation profiles that are obtained at relatively high fluences. Furthermore, it is of interest to be able to predict the fraction of the implanted species that will remain in solution and the fraction that will precipitate as a second phase.

Such a model has been developed previously for precipitation processes that occur during thermal diffusion [7]. On the other hand, numerical models for the calculation of ion implantation profiles have also been developed accounting for various processes, such as ion collection, sputtering, lattice dilation, and radiation induced segregation [8-10]. We present here a model that follows similar reasoning as these previous models as applied to the case of second phase precipitation. The model is entirely phenomenological and requires information on the precipitation process, namely maximum solubility limits of the implanted species in the target. The solubility limits cannot be obtained from thermodynamic data alone, since the precipitation occurs during irradiation. Data on solubilities during implantation are becoming available through X ray measurements (see for example Ref. [11]). Using these data we present the predictions of the model for the case of N implanted into Nb.

5.2 *Description of the Model*

5.2.1 Thermodynamic Representation of Nitride Precipitation

The process of internal precipitation of a compound M_aN_b can be described by the reaction:

$$aM + bN = M_aN_b \qquad [5.1]$$

where M is the nitride forming element. The solubility limit C_{max} denotes the nitrogen content in 'equilibrium' with the nitride phase and is given by:

$$C_{max} = \left[e^{\frac{-\Delta G^0}{RT}} \right]^{-1/b} [\gamma_N]^{-1} [\gamma_M]^{-a/b} [C_M]^{-a/b} \qquad [5.2]$$

where ΔG^0 is the standard free energy of formation of the nitrides and γ_N, γ_M are the activity coefficients of N and the target element M respectively. If more than one compound is formed this calculation can be carried out for each nitride type, and the one that gives the lower value of C_{max} is the stable nitride.

The calculation of nitride stability requires data on the free energies of formation of nitrides, and the activities of N and the target elements. In the present analyses, as standard thermodynamic data can not be used directly, solubility data obtained from experiments under irradiation have been used.

5.2.2 The Numerical Procedure

The basis for the numerical model used here is the finite difference solution of the diffusion equations. The possibility of including second phase precipitation in such a solution was first explored by Goldstein and Moren [7] for the carburization process. The idea is based on the fact that the finite difference solutions are carried out over a space time grid and at each time step it is possible to see whether the concentration of a given species is higher than the solubility limit and precipitate the excess by removing it from the diffusion process. In the case of carburization the transport process is a true diffusion process and the solubility limit can be assumed to be that given by the thermodynamics of the system. In the present case the transport process can be true diffusion, radiation enhanced diffusion, collision cascade mixing, etc. These processes can be termed diffusion-like, in the sense that they produce atomic transport that can be approximated by the diffusion equation and an apparent or effective diffusion coefficient. Also, the solubility limit used can not be that of thermodynamic equilibrium, since the implantation process is highly non-equilibrium in nature. We define here an effective solubility limit resulting from the chemistry of the system and the irradiation process. These solubility limits under irradiation have to be measured separately by methods such as X-ray analysis.

For the case considered here other processes have to be accounted for, as follows:

1. The ion collection process, with a gaussian distribution given by separate codes such as TRIM [12] or EDEP1 [13].
2. Lattice dilation
3. Surface recession due to sputtering

These effects have been taken into account in the framework of a finite difference solution of the diffusion equation in previous work [8], basically by introducing the corresponding changes in the composition profile at each time step of the finite difference calculation. The detailed description of the numerical technique can be found in Ref. [8].

The numerical code used in the present work allows for three elements. Either or all three can be implanted elements. It allows for the precipitation of three different phases formed by each of the elements with the target and of different stochiometry.

At each time step of the finite difference solution the maximum solubility limits are defined for each of the possible second phases and the code compares these values with the current concentration in each bin. The excess implanted element over the solubility limit is precipitated as a second phase. The precipitated amount is now assumed to be immobile and is not included in the next step of the finite difference calculation. This is equivalent to removing it from the diffusion process. An appropriate amount of the reactive target element is also removed from the diffusion process. When the final dose is reached the profiles of the implanted element in solution and that precipitated as a second phase are added to obtain the total implantation profile.

The formalism used in the present model uses the following simplifying assumptions for precipitation:

1. The kinetics of precipitation of nitrides is much faster than the diffusion process.
2. No mixing of nitrides are considered, since their energies of formation are not known.
3. No dissolution of nitrides is allowed after they are formed.

These assumptions still allow the precipitation of different nitrides at the same depth. A listing of the program RISTRAN used in the calculations here is included in the Appendix.

5.3 *Results*

We present here the predictions of the described code for the case of N implantation into Nb targets. Linker [11] carried out detailed X ray measurements for this case that were interpreted by Rao and co-workers [14]. These measurements and analysis indicate that 70 keV N implanted into Nb with a dose rate of $3x10^{13}/cm^2/s$, results in a solubility of N into Nb of around 20 atomic %. Concentrations higher than that result in the precipitation of NbN.

Fig. 5.1 shows the implantation profiles of nitrogen with and without precipitation of second phases for three different fluences. The profile for the highest fluence of $27x10^{16}/cm^2$ is the only one that is changed due to second phase precipitation. For higher doses the effect on the shape of the profile will be more pronounced. The precipitated area is located in the central region of the composition profile corresponding to the nitrogen peak. The results in these figures were obtained using an effective diffusion coefficient of $5x10^{-16}cm^2/s$ which for the dose rate of $3x10^{13}/cm^2/s$ is the value predicted by a simple Kinchin and Pease model [15] for collision cascade mixing. The efficiency of mixing parameter Dt/Φ is given by D/ϕ, where D is the diffusivity and ϕ is the dose rate or flux value, and for the above values is 0.1667 nm^4. The effect of varying the value of the apparent diffusivity on the total retained nitrogen profile and the precipitate profile is shown in Figs. 5.2 and 5.3

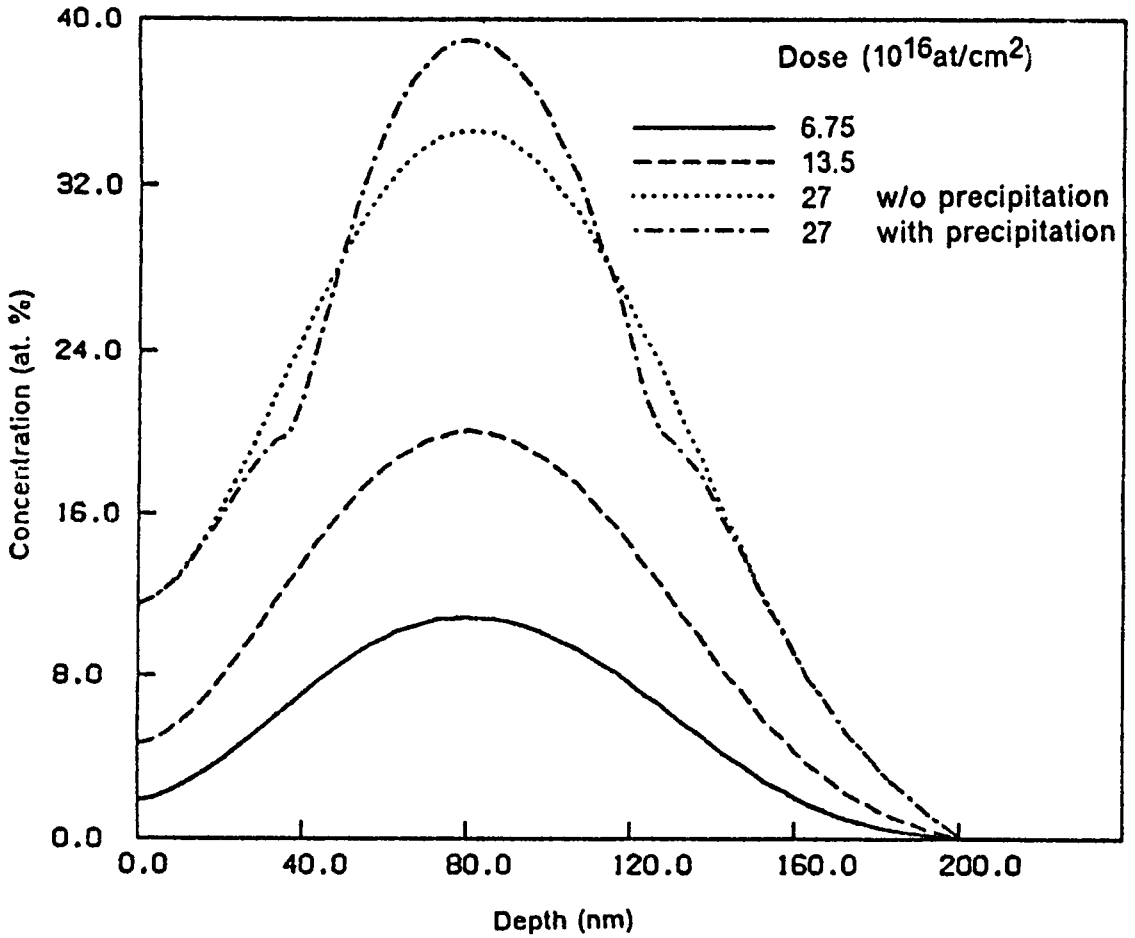

Figure 5.1. Calculated N concentration profiles for 70 keV N implantation into Nb at different fluences with and without precipitation of second phases.

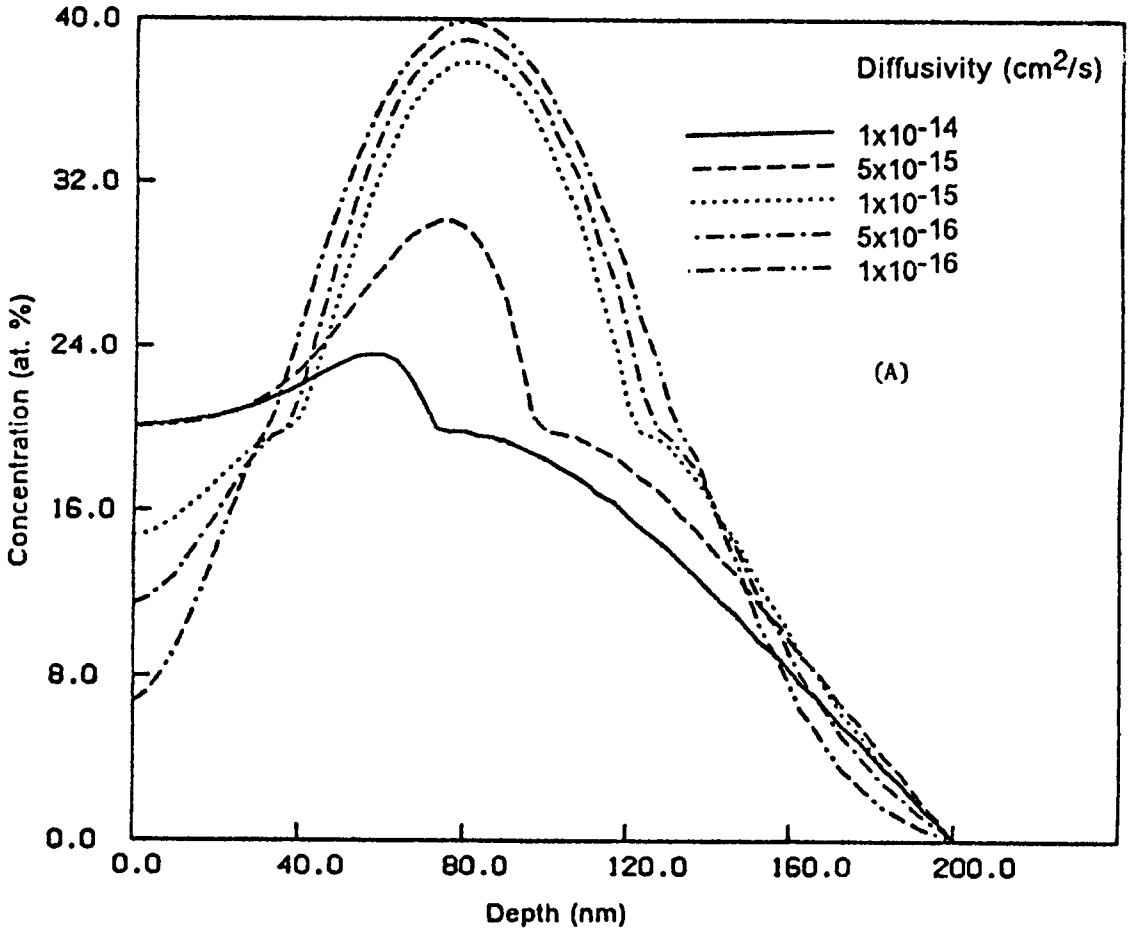

Figure 5.2. Effect of varying diffusivities on the total retained nitrogen profile

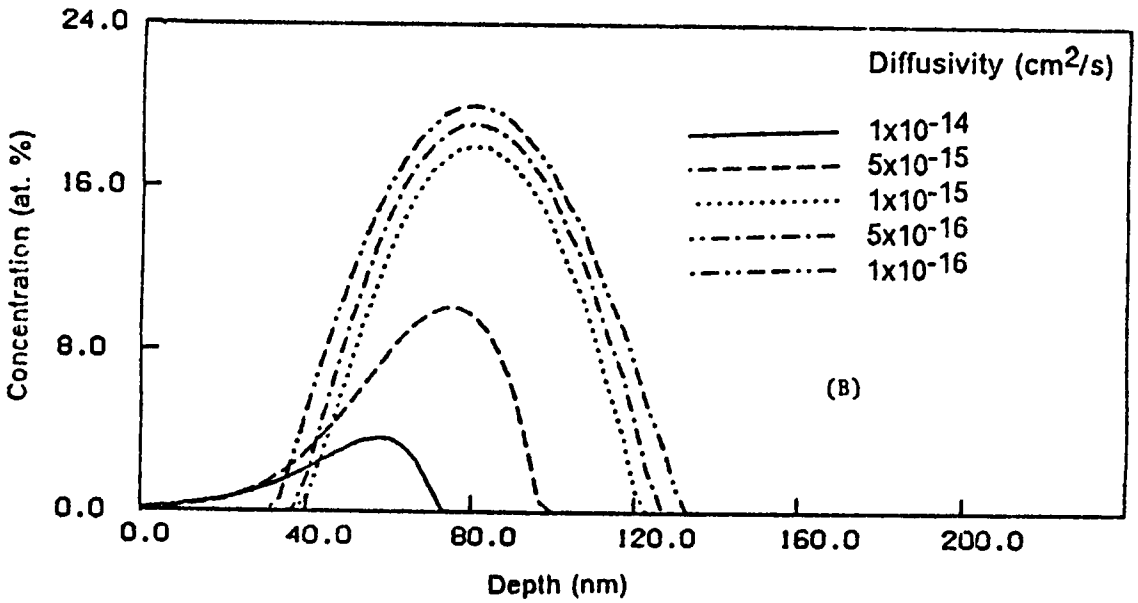

Figure 5.3. Effect of varying diffusivities on the precipitated nitrogen profile.

respectively for the highest fluence case. Note that apparent diffusivities are usually higher than the predictions of cascade mixing alone, due to the presence of radiation enhanced diffusion.

5.4 Discussion

The basic observation that can be made from the present results is that for high doses the precipitated phases can have an effect on the actual shape of the implantation profiles. This is particularly so for the deeper region of the profile. Second phase precipitation however does not affect the total retained dose of the implanted species very much since the precipitated region is away from the surface and the loss due to sputtering is not modified. The effects become more significant if the implanted species are highly mobile during the implantation process.

For relatively low doses, where the amount of precipitate is negligible or none at all which in the present case is below $14 \times 10^{16} N/cm^2$, the effects on the profile shape are not significant. The precipitated amount can be calculated using the present formalism if the solubility limits under irradiation are known.

5.5 References

[1] I. L. Singer, Vacuum 34 (1984) 853.

[2] S. Fayeulle, D. Treheux, C. Esnouf, and N. Moncoffre, Rad. Effects 83 (1984) 279.

[3] C. A. dos Santos, I. J. R. Baumvol, E. A. Garcia, and M. Behar, J. Phys. D:Appl. Phys. 17 (1984) 969.

[4] H. J. Frost and K. C. Russel, in "Phase Transformations During Implantation", (ed. F. V. Nolfi, Jr., Applied Science Publishers, London (1983)), p. 75.

[5] S. M. Myers, Radiation Effects 49 (1980) 95.

[6] R. A. Kant, S. M. Myers, and S. T. Picraux, J. Appl. Phys. 50 (1979) 214.

[7] J. I. Goldstein and A. E. Moren, Metall. Trans. 9a (1978) 1515.

[8] D. Farkas, I. L. Singer, and M. Rangaswamy, J. Appl. Phys. 57 (1985) 1114.

[9] D. Farkas, R. Pasianot, M. Rangaswamy, and E. J. Savino, Nucl. Instr. Meth. B16 (1986) 183.

[10] M. Rangaswamy, D. Farkas, and H. L. Sobel, Nucl. Instr. Meth. B19/20 (1987) 196.

[11] G. Linker, Nucl. Instr. Meth. 182/183 (1981) 501.

[12] J. P. Biersack and L.G. Haggmark, Nucl. Instr. and Meth., *174* (1980) 257.

[13] I. Manning and G. P. Mueller, Comp. Phys. Comm. 7 (1974) 85.

[14] S. I. Rao, C. R. Houska and K. S. Grabowski, Nucl. Instr. Meth. B18 (1986) 47.

[15] G. H. Kinchin and R. S. Pease, Rep. Prog. Phys. 18 (1955) 1.

Chapter 6

Dynamic Monte Carlo Simulation of Collisional Mixing in Heterogeneous Media

6.1 *Introduction*

It is well known that transport processes occurring during ion implantation to high fluences can significantly influence the final concentration profiles resulting from the process, In particular, the experimental profiles observed at high fluences are usually broader than the predictions of commonly used codes such as the Monte Carlo code TRIM [1] or those based on LSS theory [2]. In a phenomenological model it is possible to determine apparent diffusion coefficients from a best fit procedure to the actual profiles [3]. However, such a model can not separate the effects of collisional mixing from those of true diffusion or radiation enhanced diffusion. It is

therefore of great interest to develop a code that can compute the effects of collisional mixing alone, and this is the objective of the present work.

The idea of a simulation code for ion implantation profiles that can treat the compositional changes occurring in the target as the implantation proceeds has been explored previously. Moller et.al. developed the code TRIDYN [4,5], based on TRIM which through a dynamic process allows the calculation of sputtering yields in multi-component systems. The code MARLOWE [6] is capable of treating compositional changes in the target and has recently been extended dynamically in order to simulate amorphization processes induced by ion bombardment. EVOLVE [7] also includes dynamic changes of composition in the target. Most of these codes use the idea of a pseudoprojectile, basically one incoming particle for which the calculations are carried out and which is considered to have equivalent distribution and collisional effects to a large number of particles (a dose step, usually around 10^{14} particles). After the dose step the composition of the target is updated and a new pseudoprojectile is considered, until the total dose is reached. In the present work the same basic idea is used, although the pseudoprojectile distribution is calculated by a statistical process over the results for a number of particles. This fact was found to be essential in the accuracy of the calculated profiles. We present below a detailed description of the code and an analysis of the required statistics for a pseudoprojectile as well as a study of the influence of the dose step value in the results.

Finally, a comparison of the predictions of the case with experimental profiles obtained for Ar bombardment on Sn-Fe bilayer samples for different energies of the Ar beam and different thickness's of the Sn layer is presented. Also presented are calculations performed for the case of Ti implantation into Fe. This case is of particular interest because of the vacuum carburization process and because

phenomenological modeling of this case has already been carried out, yielding a collisional mixing effect which agrees in order of magnitude with the predictions of a simple Kinchin and Pease model [8]. The predicted results are compared to those predicted by diffusion approximation to ion beam mixing [9,10].

6.2 *Description of the Program*

The program is based on the code TRIM and therefore utilizes a similar treatment for each collisional process. The important parameters that are used to describe these processes are also similar, namely the displacement energy, cutoff energy, bulk and surface binding energies.

The Monte Carlo simulation involves following a large number of individual ion 'histories' in a target. Each history begins with a given energy, position and direction. The particle is assumed to change direction as a result of binary nuclear collisions and move in a straight fixed free-flight path between collisions calculated from density considerations. The direction of the ion after collision is determined by choosing random numbers between 0 and 1. The energy is reduced as a result of nuclear (elastic) and electronic (inelastic) energy losses, and the history is terminated when the energy drops below a pre-specified value. Electron energy losses are assumed to be continuous from electronic interaction as the ion travels through the target.

Energetic criteria used to determine the process that takes place are:

1. When a target particle receives an energy T greater than the displacement energy, E_d a permanent Frenkel pair is formed.

2. If a particle energy falls below the cut-off energy E_d it is assumed to have stopped.
3. When a particle hits the surface boundary and the outward component of the momentum is enough to overcome the surface binding energy, it is considered sputtered. Otherwise it is considered as reflected back into the target.

The target is assumed to be amorphous with atoms at random locations and crystalline properties are ignored. The method is applicable to a wide range of incident energies from 0.1 keV to to several MeV. The lower limit is due to the consideration of binary collisions only while the upper limit is determined by relativistic effects.

6.2.1 Basic Algorithm

The dynamic feature of the code TRAL presented here is the capability of updating the target composition as a function of depth during the bombardment process itself. The total dose is reached through a series of dose steps. The dose step effects are simulated by a number of histories I_p the effects of which are extrapolated to chosen dose step value. After each dose step the composition of the target is recalculated and the process repeated until the total dose is reached. The composition is updated by accounting the effects of collisional mixing, surface recession due to sputtering and lattice dilation due to the incoming ions. The lattice dilation is calculated assuming a certain atomic volume for each species which is maintained constant. The target is described as a number of bins and within each bin an account of the number of vacancies and interstitials introduced by the collision process is maintained. The lattice is allowed to relax at the end of each dose step.

The composition of each bin is monitored and the bin thickness changes with lattice dilation as follows:

$$\frac{\delta v(x)}{v} = \sum_i (I_i(x) - v_i(x))\Omega_i \qquad [6.1]$$

where I_i (x), v_i(x) are the concentrations of interstitials and vacancies respectively at bin 'x' and Ω_i is the atomic volume of species 'i'. The bin thickness is allowed to vary between given maximum and minimum values, which are usually one half and twice the initial thickness. The concentrations calculated at the end of a dose step cycle are the beginning ones for the new cycle.

A number of considerations were made to improve the required computing time. The most important of these is the possibility of using the vector facility of an IBM 3090 machine. It is not possible to successfully vectorize the portion of the code calculating the history of each ion since it represents a sequential process. Vectorization of the code helps in reducing computation time for certain sections of the code. The code has been developed so as to be able to compute the history of a number of ions simultaneously. A number 'p' of projectiles are launched 'simultaneously' at the target. This idea, however, is more appropriate for a true parallel processing machine. These are allowed to go 'n' steps ahead and then the 'q' (= nxp) (maximum) secondaries are treated simultaneously and '2xq' (maximum) tertiaries are generated and this continues in a tree-like fashion. At each step of this tree, atoms may come to a stop or get sputtered away. These are eliminated from further calculations. When the cascade comes to an end, a further batch of 'p' are allowed 'n' steps and the process continues till all atoms come to a stop. On vectorization of the code a factor of 2 improvement in speed was obtained.

6.2.2 Computational Accuracy

There are two main variables in the code that can be chosen as required by the desired accuracy. These are the dose step S and the number of particles I_p used to compute the statistical distribution of a pseudoprojectile. The total number of particles followed for a particular calculation (and consequently the computation time) is directly proportional to I_p and inversely proportional to S. The value of S should be small enough not to underestimate the mixing effect. This occurs for doses where there is negligible probability of successive deposition of ions at a given point, typically 10^{13}ions/cm^2 [11]. Alternatively, the problem can be analyzed using the same reasoning as for numerical solutions of the diffusion equation using a time and space grid. The numerical explicit method will be convergent if the mesh size δx and the time step δt satisfy the condition:

$$\frac{(\delta x)^2}{D\delta t} \geq \frac{1}{2} \qquad [6.2]$$

In the present case δt is S/I, where I is the current density. D can be estimated [8] as:

$$D = \frac{0.8}{2N}\left(\frac{dE}{dx}\right)\frac{I}{E_d}\frac{\lambda^2}{6} \qquad [6.3]$$

Where N is the atomic density, (dE/dx) the nuclear stopping power, E_d the displacement energy, and λ the average separation between the vacancy and interstitial in a Frenkel pair. From these equations a value for S can be derived. For the example of 300 keV Ar bombarded into a Sn-Fe target one can use (dE/dx) = 1.4x

10^{10}ev/cm (from TRIM), λ = 2 nm and E_d = 25eV. The value of S is then about 10^{15}ions/cm^2. A listing of the program TRAL is given in the Appendix.

6.3 *Results and Discussion*

6.3.1 Statistical analysis and the required dose step value

As mentioned above the two parameters that control the accuracy of the predicted profiles are S, the dose step and I_p, the number of ions considered in the statistics of a pseudoprojectile. As discussed in the previous section the dose step for which events are truly independent of one another is about 10^{13}ions/cm^2 We carried out calculations for values of the dose step starting at this value and increasing it up to 10^{15}ions/cm^2 in order to study the effects of this increase on the results. The value of I_p was also varied from one to 500 ions. The results of these calculations, for the case of 200 keV Ar^+ implanted into a target composed of 44nm of Sn deposited over Fe are shown in Figs. 6.1 and 6.2. The fluences are 10^{16} and $3x10^{15}$ions/cm^2 respectively. Figure 6.1(a) shows the results for different values of I_p using a constant dose step of 10^{15}ions/cm^2. As I_p increases, the profile approaches a smooth constant profile. Values of I_p of about 100 and above show good accuracy. However, with $I_p < 25$ a significant deviation is observed with the results being dependent on the actual value of I_p. In this case the results may also depend on the random number generator used and the seed. Similar calculations were carried out using a different seed as shown in Fig. 6.1(b). From the results illustrated in Figs. 6.1(a) and 6.1(b), it is found that for the results to be independent

of the random number seed, l_p should be at least 50. Calculations involving l_p greater than 100 have been left out from the figure as no major variation is found. Fig. 6.2 shows the effect of different dose step values. Statistics over 500 particles for each pseudoprojectile were used in these calculations. The results show that less mixing is predicted for higher dose step values. The differences between the profiles obtained for 10^{13} and 10^{15}ions/cm^2 is about 2%. This is acceptable accuracy in most cases.

In Figs. 6.3 and 6.4, the predicted ion beam mixed profiles for two different cases, namely 300 keV Ar^+ into 100nm Sn over Fe and 55 keV Ti^+ into 20nm C over Fe respectively, are shown. In both the cases the peak of the damage energy distribution is below the interface. Surface recession due to sputtering has been taken into account and the profile positions were adjusted accordingly. From the results for the Ar/Sn-Fe case it appears that the interface defined by the 50% concentration moves towards the surface as the fluence increases. This is mainly due to the difference in sizes of the Sn and Fe atoms as can be verified from Fig. 6.5, where the depth is given in terms of atoms/cm^2 to remove volume effects. Figure 6.6 illustrates the Ti/C-Fe case using the atoms/cm^2 depth scale. From Figs. 6.5 and 6.6 it can be seen that the mixing effect is larger in the lower layer than in the top. In the case of Ti/C-Fe the mixing appears to be slightly more than in the Ar/Sn-Fe case. Simulations were also carried out for the C-Fe case using Ar ions similar to the Ar/Sn-Fe case. These results are shown in Figs. 6.7 and 6.8. and demonstrate the similar trend as the Ti/C-Fe case. In all the figures the concentrations were obtained without including the implanted species. The ion-beam mixed profiles were compared with error function type profiles generated by thermal diffusion. The code used in the comparison uses an implicit finite-difference method and takes into account ion collection, sputtering and lattice dilation within the finite-difference setup

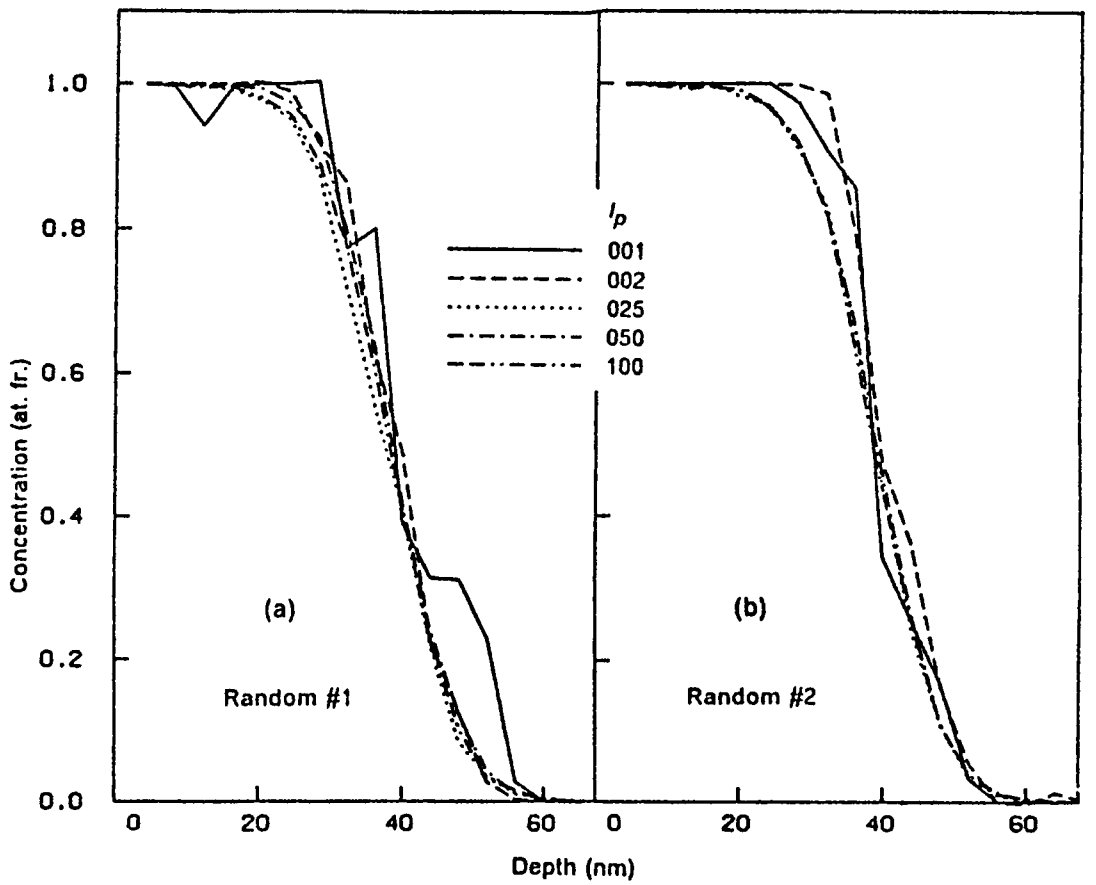

Figure 6.1. Effect of variation of the parameter I_p, the number of statistical particles, on the simulation profiles for 200 keV Ar^+ into 44nm Sn over Fe to a fluence of $10^{16}/cm^2$.

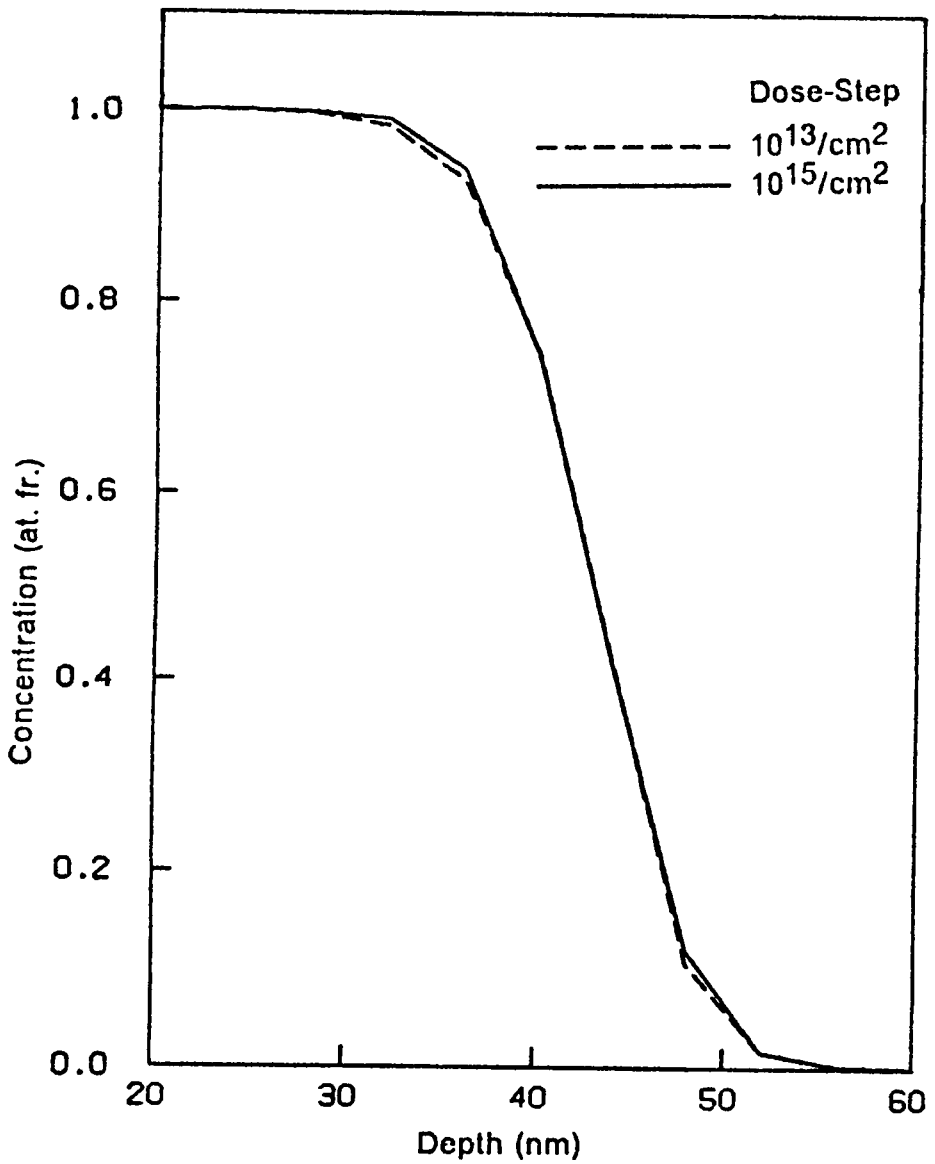

Figure 6.2. Effect of dose-step value on the ion mixing profiles for the same case as in Fig. 6.1 for a fluence of $3x10^{15}/cm^2$.

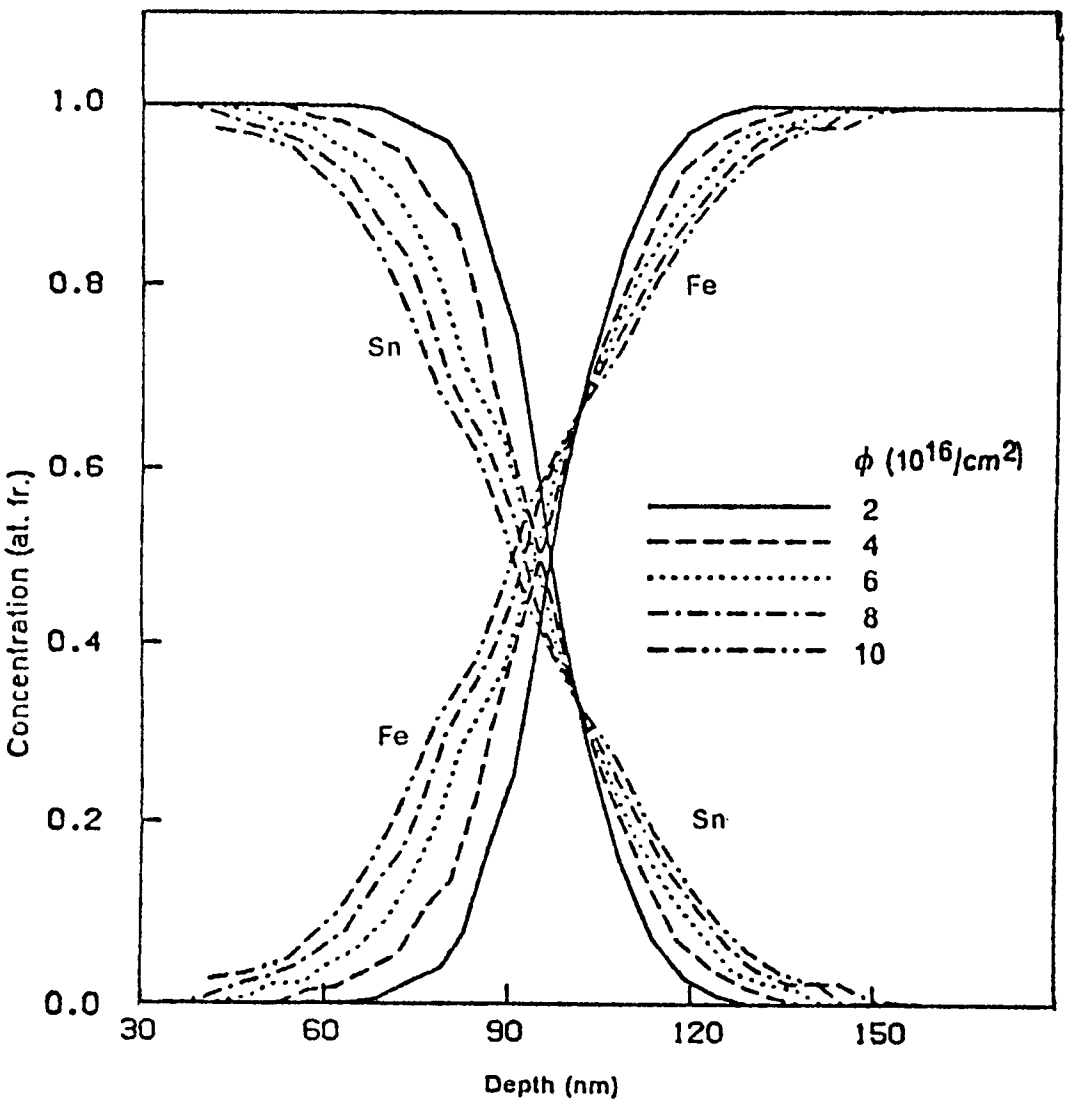

Figure 6.3. Simulation profiles for ion beam mixing of 100nm Sn over Fe by 300 keV Ar^+ for different fluences with the depth scale in nanometers.

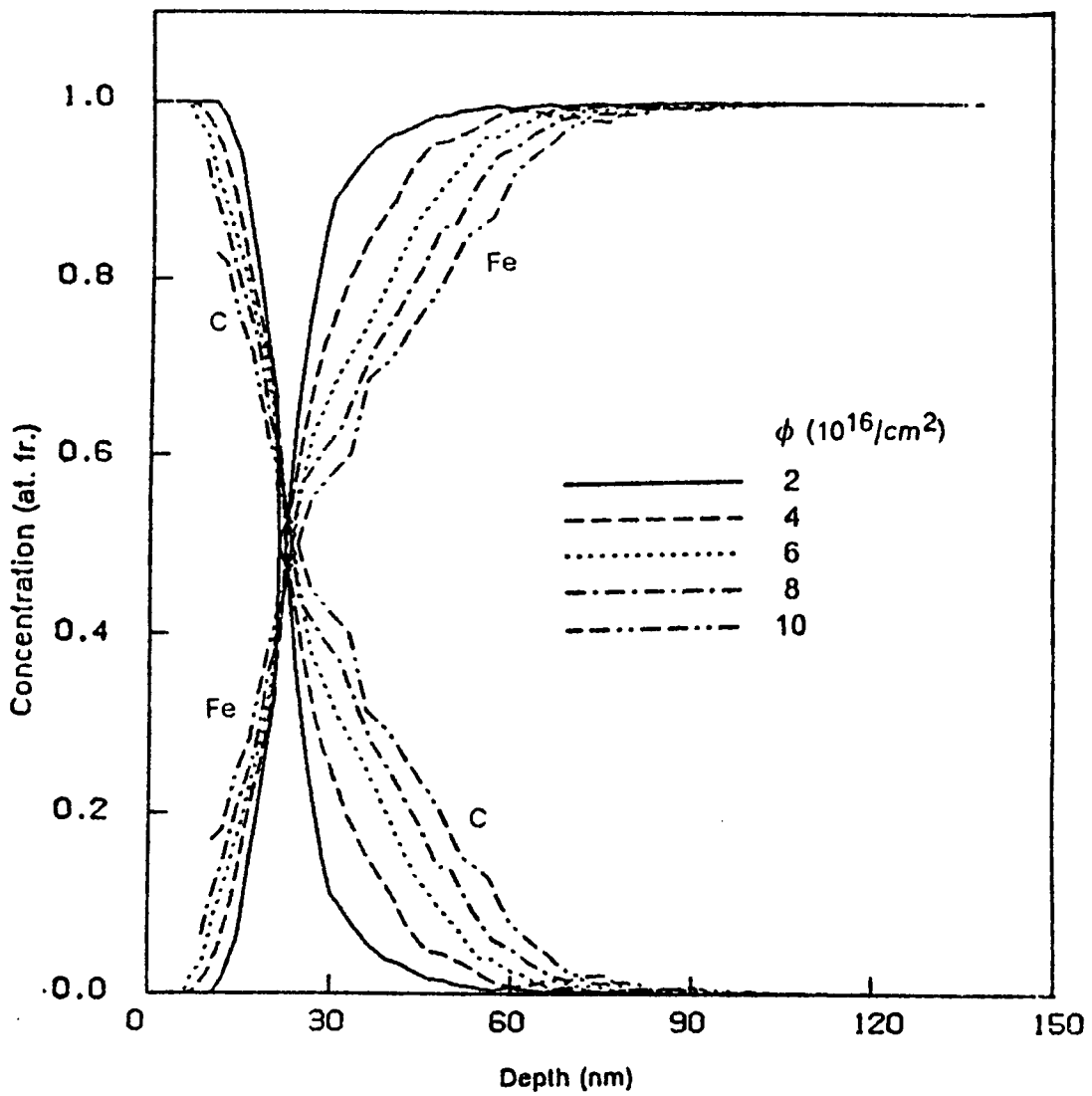

Figure 6.4. Simulation profiles for ion beam mixing of 20nm C over Fe by 55 keV Ti^+ for different fluences with the depth scale in nanometers.

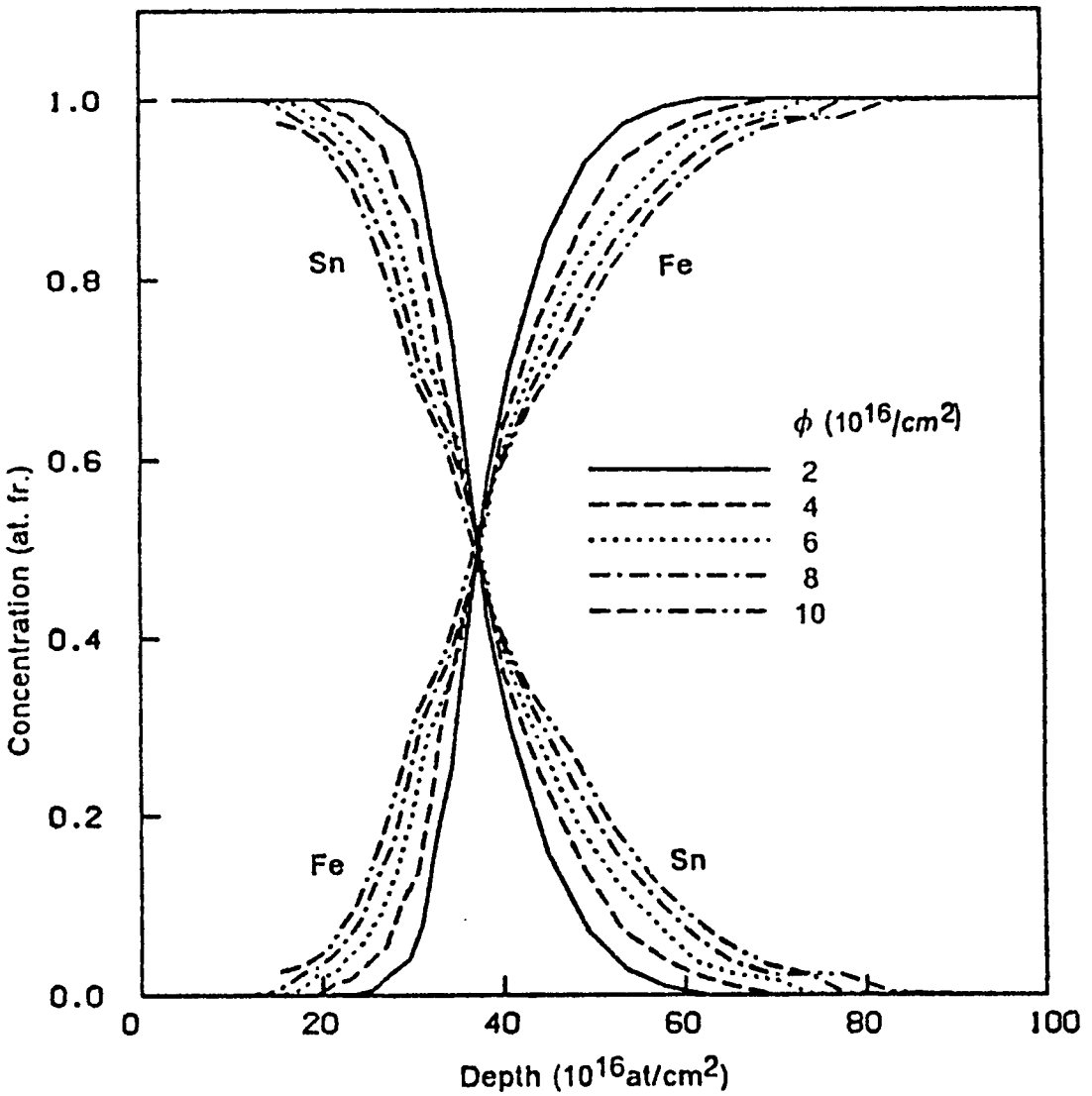

Figure 6.5. Simulation profiles for ion beam mixing of 100nm Sn over Fe by 300 keV Ar^+ for different fluences with the depth scale in atoms/cm^2.

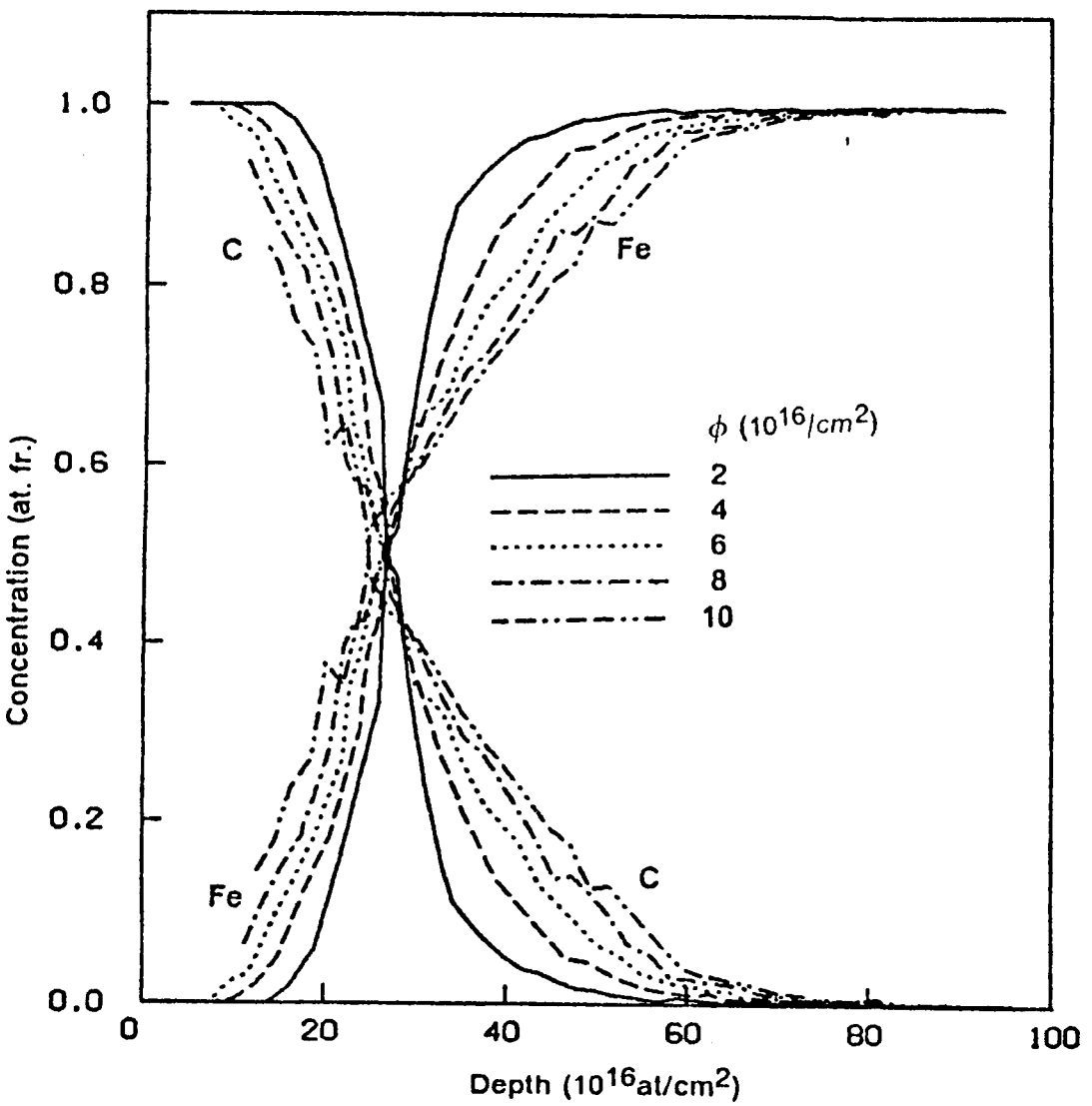

Figure 6.6. Simulation profiles for ion beam mixing of 20nm C over Fe by 55 keV Ti^+ for different fluences with the depth scale in atoms/cm^2.

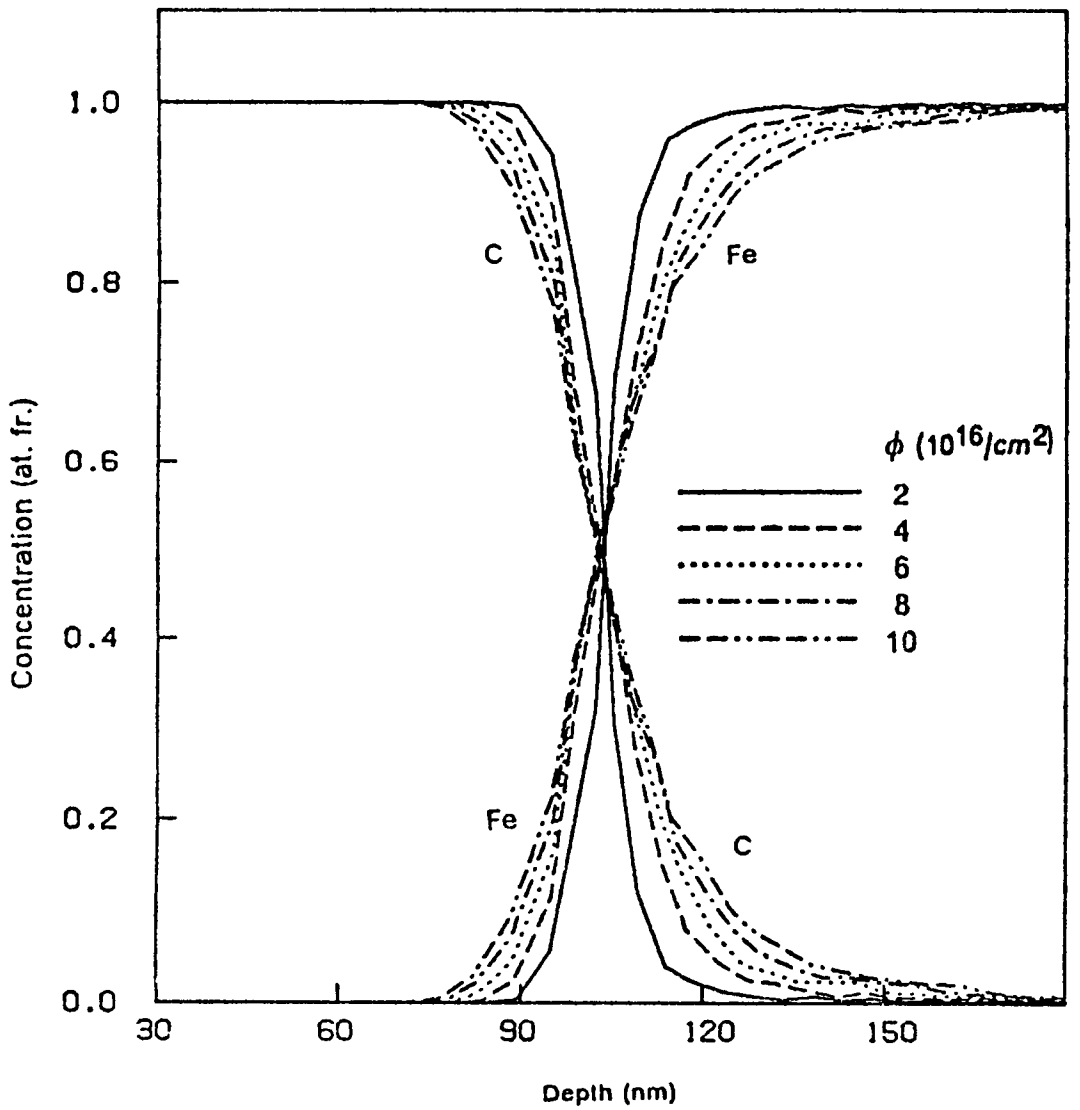

Figure 6.7. Simulation profiles for ion beam mixing of 100nm C over Fe by 300 keV Ar^+ for different fluences with the depth scale in nanometers.

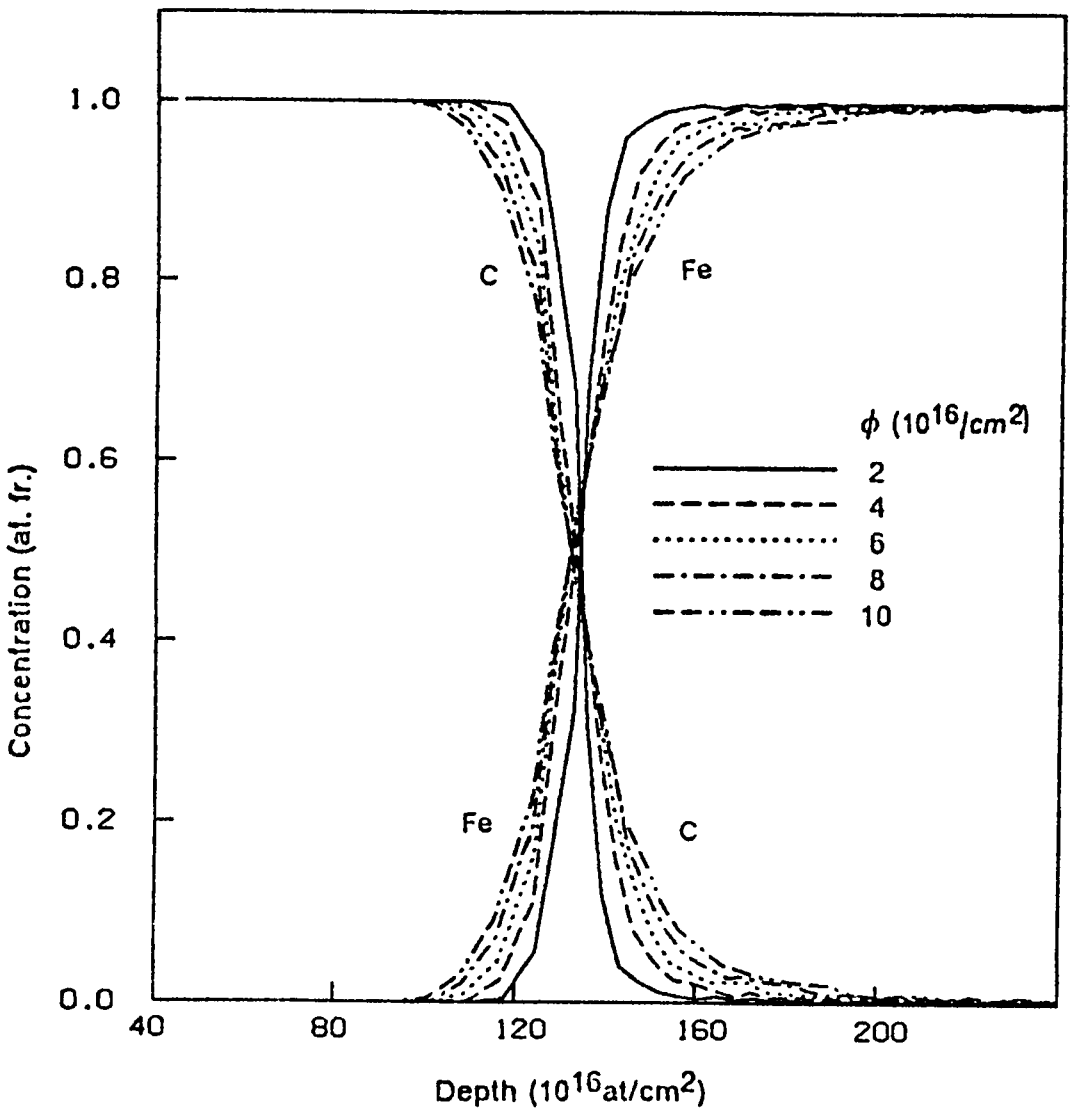

Figure 6.8. Simulation profiles for ion beam mixing of 100nm C over Fe by 300 keV Ar^+ for different fluences with the depth scale in atoms/cm^2.

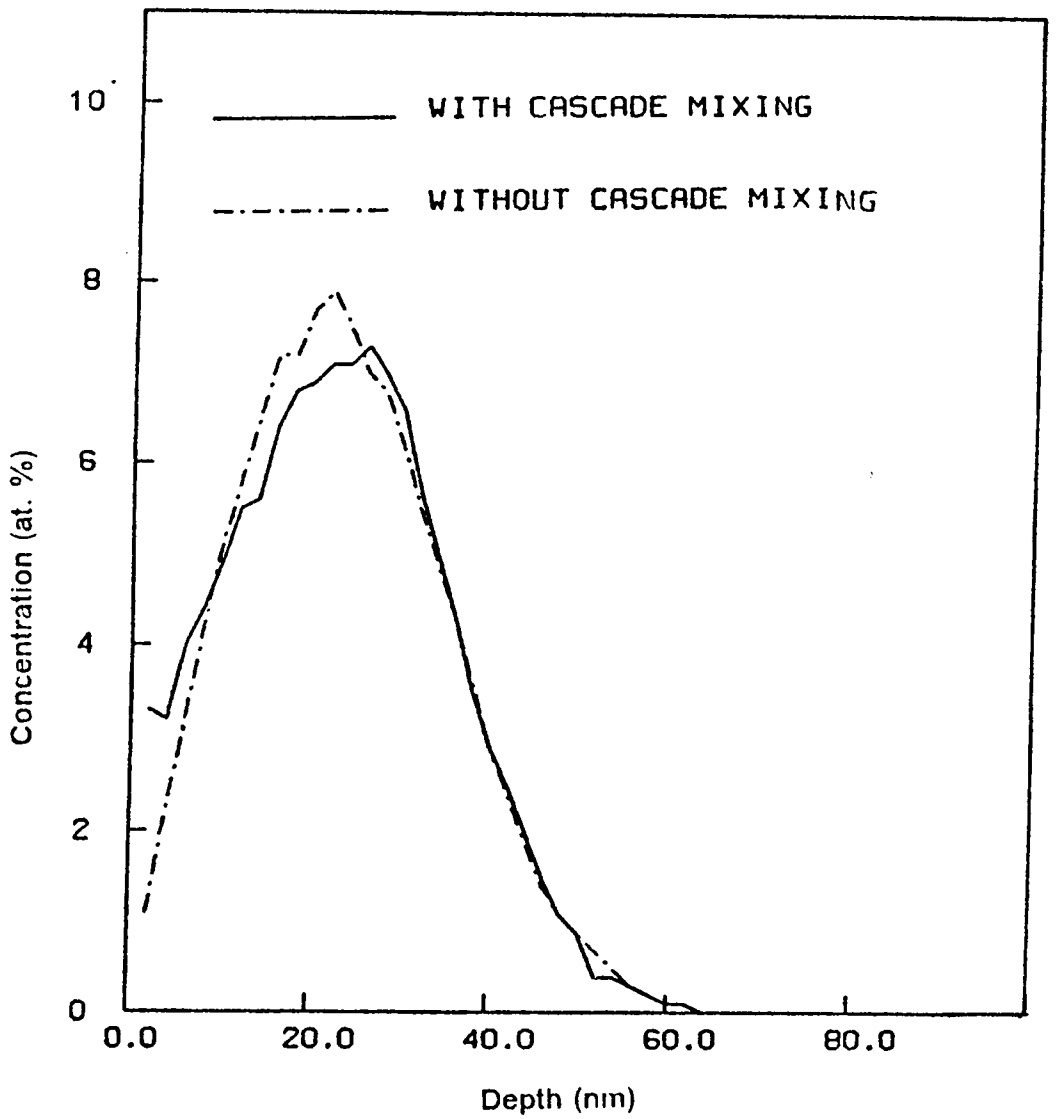

Figure 6.9. Ti concentration profiles calculated with and without cascade mixing for 55 keV Ti implantation into Fe to a fluence of $10^{16}/cm^2$.

[3]. The same sample configurations were also used in the code. A fit to the ion-beam mixed profiles was attempted using different diffusivity values. In fitting the profiles, different diffusivity values were needed for the surface and inner layers, as was expected. The inner layer required an average diffusivity that was 1.5 to 2 times larger than that required for the surface. This is about the difference in the damage energy deposition rates for the two layers. The diffusivity values used were of the order of $1-3\times10^{-15}\text{cm}^2$ using fluxes of $3\times10^{13}/\text{cm}^2$, in agreement with the values predicted for collision cascade mixing [8]. The diffusivity values correspond to ion beam mixing parameter (Dt/Φ) values of around 0.6 nm^4.

The effect of using a higher value of l_p is seen from Figs. 6.3 and 6.4, where Fig. 6.3 shows much smoother profiles. This is due to using a higher value of 200 for the Sn-Fe case while using a value of 50 for the C-Fe case. To demonstrate the broadening effect of collision-cascade mixing calculation were carried out for 55 keV Ti implantation into Fe for a fluence of $10^{16}/\text{cm}^2$ with and without the inclusion of collision-cascade mixing. The results of these calculations are presented in Fig. 6.9. The profile obtained by including collision-cascade in the calculations is broader than the one obtained by suppressing it. The broadening or ion mixing effect is dominant in the region between the surface and the peak of the profile where most of the damage is generated. The region beyond the peak is relatively unaffected by the collision-cascade process.

6.4 *References*

[1] J. P. Biersack, L. G. Haggmark, Nucl. Inst. Meth. 174 (1980) 257.

[2] I. Manning and G. P. Mueller, Comp. Phys. Comm. 7 (1974) 85.

[3] D. Farkas, I. L. Singer, and M. Rangaswamy, J. Appl. Phys. 57 (1985) 1114.

[4] W. Moller and W. Eckstein, Nucl. Instr. Meth. B2 (1984) 814.

[5] W. Moller and W. Eckstein, Nucl. Instr. Meth. B7/8 (1985) 645.

[6] M. T. Robinson and I. M. Torrens, Phys. Rev. 9 (1974) 5008.

[7] M. L. Roush, T. D. Andreadis and O. F. Goktepe, Rad. Effects 55 (1981) 119.

[8] S. M. Myers, Nucl. Instr. Methods 168 (1980) 265.

[9] R. Collins and G. Carter, Rad. Effects 54 (1981) 235.

[10] G. Carter, R. Collins and D. A. Thompson, Rad. Effects, 55 (1981) 99.

[11] J. A. Davies, in "Surface Modification and Alloying by Laser, Ion and Electron beams", eds. J. M. Poate, G. Foti and D. C. Jacobson, Plenum Press, NY, ch. 7, p. 189.

Chapter 7

Thermal Spike Related Nonlinear Effects in Ion Beam Mixing at Low Temperatures

7.1 Introduction

Ion beam induced atomic transport at low temperatures is composed of three different mechanisms which are (i) Cascade collisional mixing, (ii) Thermal spike induced short-range diffusion, and (iii) Radiation enhanced diffusion. Extensive theoretical studies have been carried out by Winterbon [1], Andersen [2], and Sigmund [3]. A Monte Carlo simulation of the process has been developed [4], based on the computer code TRIM [5]. Experimental work has been carried out in different temperature ranges, such as Nb/Si [6] and Cr/Si [7] bilayer systems. It was found that the mixing efficiency is weakly dependent on temperature below certain critical temperature points. Thus, cascade collision mixing was suggested for some time to

be the dominating mechanism in the ion beam mixing process. However, most experimental results showed much greater mixing than that predicted by cascade collisional mixing even after using adjusted values of the displacement energy [8,9]. The additional mixing observed can be understood as produced by thermal spike effects.

High density collisional cascades generate displaced atoms in a very localized volume. While these atoms cannot displace other atoms further, they can impart some of their energy to neighboring atoms through a many-body interaction. Thus most of their neighbor atoms are thermalized or energetically equalized in accordance to the Maxwell-Boltzmann distribution, and this results in a liquid-like thermal spike region in which the average characteristic energy of each atom is around 1 eV. This corresponds to an equivalent temperature of the order of 10^4 K. The thermal spike dimension is several tens of angstroms, i.e., approximately ten lattice constants. The thermal spike will quench in about 10^{-11} s [10].

Seitz and Koehler in 1956 [11], and Vineyard in 1976 [12], have developed a quantitative model for the thermal spike concept. They treated the cascade region as the initial conditions for the classical heat transfer equation and used the δ-function approximation to describe it. They assumed that basically the number of thermally activated jumps per unit volume per unit time follows an Arrhenius behavior. This model, however, does not consider the fact that a large number of point defects are created directly by the collision cascade processes. These defects may play an essential role in the subsequent thermal spike induced atomic migration process. This is seen for example in the work of Rubia et.al. [13] who used molecular-dynamics computer simulation to generate the atomic rearrangement picture of the thermal spike. The model presented here for the thermal spike includes the effects of thermal spike shape as well as the point defects generated by

the ion beam. The model allows for different damage regions, according to the energetic density of the cascade. The model is for low temperature regions where radiation enhanced diffusion is not important. After comparing the predictions of the model presented here with experimental results it is possible to establish an ion beam mixing picture with three different regions. For low damage energy densities thermal spikes are not important and cascade collision mixing is dominant. For the high density cascade regions spherical thermal spikes are expected as a consequence of collisional cascades, with the number of generated point defects following the Kinchin-Pease linear dependence [14]. For extremely high density cascade regions the thermal spike shape is expected to be cylindrical.

7.2 Theory

The basic assumption in the present work is that the jumping rate of point defects per unit volume per unit time γ is proportional to the number of defects created in the region, and for each individual point defect, their jumping rate follows the Arrehenius behavior:

$$\gamma = \alpha\sigma(x)e^{-Q/T} \qquad [7.1]$$

where α is the jumping rate constant per unit cross section, $\sigma(x)$ is the line-density of point defects at depth x, x being depth below the target surface, and Q is the atomic migration energy scaled by Boltzmann's constant.

The line-density of point defects, $\sigma(x)$, depends on the deposited energy per unit length F_D, which is a function of depth, x. $\sigma(x)$ is obtained by the Kinchin-Pease formula for the binary collision approximation as:

$$\sigma = \frac{0.42F_D}{E_d} \qquad [7.2]$$

where E_d is the displacement energy of the target atoms.

Different regions of ion beam mixing are considered according to the line-density levels of the damage energy, defined in the form of the damage parameter χ (in units of Å^{-1}), which is the damage energy scaled by the cohesive energy of the matrix ΔH_{coh}, i.e.,

$$\chi \equiv - F_D/\Delta H_{coh} \qquad [7.3]$$

and associate different thermal spike shapes with different levels of damage energy density.

7.2.1 Spherical Spike In High Density Cascade Regions

Consider a single isolated cascade with a spherical shape is of dimension λ, with λ a constant. From the Kinchin-Pease formula the line-density of displaced atoms along the direction of depth, σ_S , is obtained. In the spherical thermal spike region,

$$\sigma_S = \frac{0.42E_D}{\lambda E_d} \qquad [7.4]$$

where E_D is the total damage energy deposited by the elastic collision process. The heat transfer equation is:

$$\kappa\Delta T(R, t) = c\frac{\partial T(R, t)}{\partial t} \qquad [7.5]$$

where κ is the heat conduction coefficient and c the specific heat capacity and the initial conditions are:

$$T(R, 0_-) = 0 \qquad [7.6]$$

and

$$T(R, 0_+) = \frac{E_D}{c}\delta^3(R) \qquad [7.7]$$

where $\delta^3(R)$ is the three dimensional δ-function in spherical coordinates and R is the radial spherical coordinate. The boundary condition is

$$T(R,t)\,|_{R\to\infty} = 0. \qquad [7.8]$$

The initial bulk target temperature is simply taken to be zero since at low temperatures radiation enhanced diffusion is suppressed, and the mixing efficiency is only weakly dependent on temperature. Assuming that the heat conduction coefficient κ and specific heat capacity c are temperature-independent constants, for isotropic and chemically homogeneous media the solution to the heat transfer equation is:

$$T(R, t) = \frac{E_D c^{3/2}}{8(\pi\kappa t)^{3/2}} e^{-\frac{cR^2}{4\kappa t}} \qquad [7.9]$$

The total number of jumps induced by the thermal spike per unit length of the thermal spike in the spherical model is then:

$$\eta_S = \int_0^\infty 2\pi R dR \int_0^\infty \alpha\sigma_S e^{-Q/T(R,t)} dt \qquad [7.10]$$

Considering diffusional jumps in a circular area of radius R parallel to the surface plane and the direction of atomic jumps in this area as perpendicular to this area Eq. (7.10) yields:

$$\eta_S = \frac{0.42\alpha\lambda^{4/3}}{8\pi c^{1/3}\kappa E_d} \Gamma(\frac{4}{3}) F_D^{(2+\frac{1}{3})} Q^{-4/3} \qquad [7.11]$$

where Γ is the gamma-function.

The total number of jumps per target atom in the material after being irradiated with dose Φ is then $\eta_S\Phi/\rho$, ρ is the atomic density of the target material. The typical jumping distance r_T can be related to ρ, $< r_T^2 > = q_1\rho^{-2/3}$. Moreover, the migration energy Q may be scaled by the cohesive energy of the matrix, i.e., $Q = -q_2\Delta H_{coh}$. It is reasonable to assume that the displacement energy of the target E_d can also be scaled by ΔH_{coh}, $E_d = -q_3\Delta H_{coh}$. Then the ion mixing parameter Dt/Φ is proportional to $\eta_S < r_T^2 > /\rho$, or the mixing parameter for the spherical shaped thermal spike can be characterized by the following equation:

$$L_T^S \equiv \frac{D_T^S t}{\Phi} = \frac{B_1}{\rho^{5/3}} (-\frac{F_D}{\Delta H_{coh}})^{2+\frac{1}{3}} \qquad [7.12]$$

where B_1 is a constant and is related to c, κ, λ, q_1, q_2, and q_3. Here the subscript T is used to refer to the thermal spike related parameters, and the superscript s to refer to the spherical thermal spike model.

7.2.2 Cylindrical Spike In Extremely High Density Cascade Regions

In this case, the initial condition of the thermal spike is an energetic line described by the damage energy density $F_D\delta^2(r)$, i.e.,

$$T(r, 0_-) = 0 \qquad [7.13]$$

and

$$T(r, 0_+) = \frac{F_D}{c}\delta^2(r) \qquad [7.14]$$

where r is the radial distance from the initial energetic line, and $\delta^2(r)$ is the two dimensional delta-function. The boundary condition is

$$T(r,t)\,|_{r\to\infty} = 0. \qquad [7.15]$$

Similar to that in the case of the spherical thermal spike, the solution to the heat transfer equation is

$$T(r, t) = \frac{F_D}{4\pi\kappa t} e^{-\frac{cr^2}{4\kappa t}} \qquad [7.16]$$

Next, the total number of jumps induced in the thermal spike per unit length can be calculated and is denoted by η_c:

$$\eta_c = \int_0^\infty 2\pi r dr \int_0^\infty \frac{0.42\alpha F_D}{E_d} e^{-Q/T(r, t)} dt \qquad [7.17]$$

i.e.

$$\eta_c = \frac{0.42\alpha F_D^3}{4\pi\kappa Q^2 c E_d} \qquad [7.18]$$

The cylindrical thermal spike induced mixing parameter is

$$L_T^c \equiv \frac{D_T^c t}{\Phi} = \frac{B_2}{\rho^{5/3}} \left(- \frac{F_D}{\Delta H_{coh}} \right)^3 \qquad [7.19]$$

where D_T^c is the effective diffusion coefficient corresponding to thermal spike induced atomic migration, B_2 is a constant and is related to c, κ, λ, q_1, q_2 , and q_3. Here the superscript c is used to refer to the cylindrical thermal spike model.

7.2.3 Three Mixing Regions

The cascade collision mixing model occurs in the collision phase of a cascade. It assumes a linear cascade picture, in which two-body interactions are important and the moving atoms collide only with stationary atoms. In this way, the Kinchin-Pease formula is a good approximation in predicting the number of displaced target atoms by knock-on effect. Consequently, the effective diffusion coefficient for cascade collision mixing can be derived by an analytical way, since the collisional atomic mixing process can be considered to be near ideal random mixing. It is appropriate to conceive of the atomic diffusion as occurred in an elemental cubic volume with isotopic randomness. Thus, the effective diffusion coefficient for cascade collision mixing can be defined [15,16] as

$$D_b = (1/6) < r_b^2 > P \qquad [7.20]$$

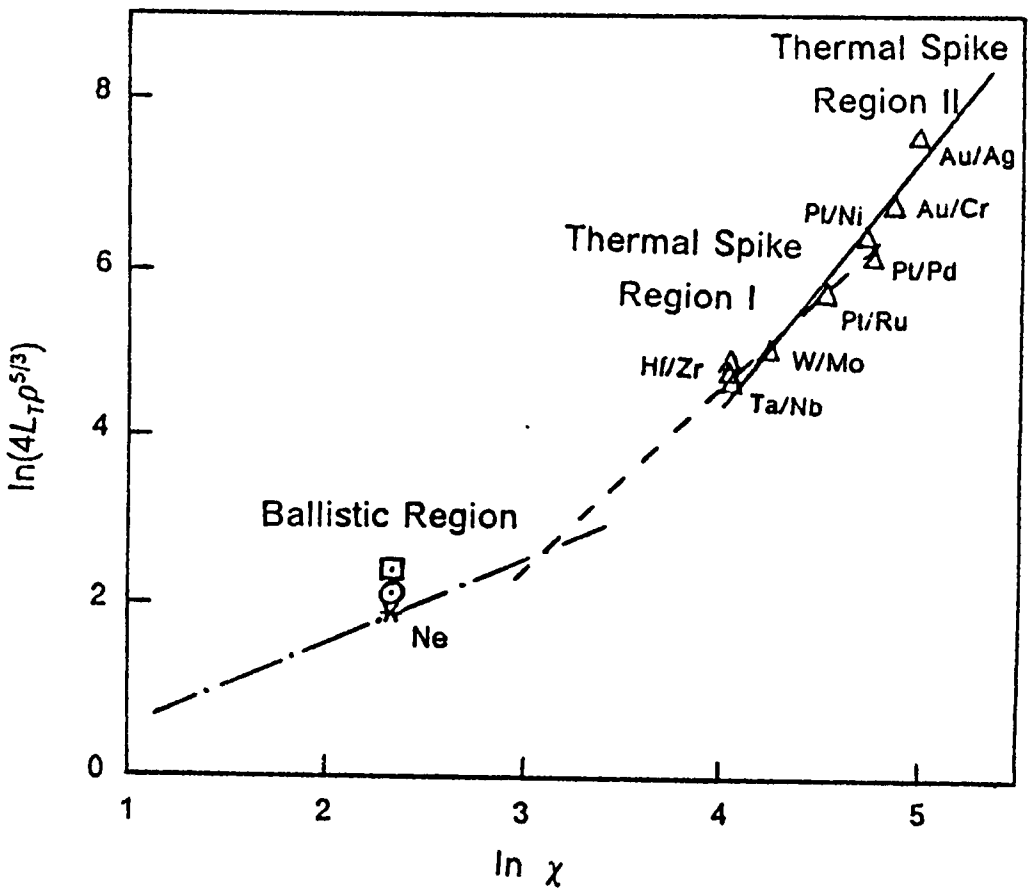

Figure 7.1. Plot of the ion beam mixing parameter as a function of the scaled deposited energy ln χ (with χ in $Å^{-1}$).

where $< r_b^2 >$ is the effective mean-square displacement of the knocked-off atoms, P is the displacement frequency of the target atom during the period of irradiation. Using the expression for D_b and the Kinchin-Pease relationship, and scaling $< r_b^2 >$ by the atomic density ρ, i.e., $< r_b^2 > = q_4 \rho^{-2/3}$, the cascade collision mixing parameter can be written as:

$$L_b = \frac{0.42}{6} B_2 \rho^{-5/3} \left(- \frac{F_D}{\Delta H_{coh}} \right) \qquad [7.21]$$

where B_2 is a constant and is related to q_3 and q_4 .

There are now three mixing regions. The first region denoted as L_b, is the cascade collision region; the second region termed as the Thermal Spike Region I, is related to the thermal spike induced ion mixing in the relatively high cascade regions; the third term is called the Thermal Spike Region II which falls into the extremely high cascade regions. In the second region the thermal spikes are expected to be spherical and in the third one cylindrical.

7.3 Comparison with Experimental Data

One of the purposes of this work is to attempt to find out how and when the thermal spike induced ion mixing is significant. The systematic experimental data from Refs. [17,18] make it possible to compare the model developed here with the available experimental data. These data are for metallic bilayer samples subjected to the irradiation of 600 keV Xe^{++} at 77 K. It has been realized that the thermal spike induced ion mixing should be much more significant than the cascade collision

Table 7. 1. Data for the bilayer system subjected to ion mixing by 600 KeV Xe used in Fig. 7.1 [17,18].

System	$-\Delta H_m$ (kj/g.at)	$-\Delta H_{coh}$ (eV/atom)	F_D (eV/Å)	ρ ($Å^{-3}$)	$4L_T$ ($10^5 Å^4$)	$\ln\chi$	$\ln(4L_T\rho^{5/3})$
Pt/Ni	7.	5.21	582.	0.0788	0.45	4.7159	6.4797
Pt/Ru	2.	6.31	570.	0.0699	0.27	4.5035	5.7691
Pt/Pd	0.	4.87	554.	0.0671	0.45	4.7341	6.2118
Hf/Zr	0.	6.34	355.	0.0440	0.26	4.0252	4.9599
W/Mo	0.	7.86	519.	0.0636	0.16	4.1901	5.0884
Ta/Nb	0.	7.84	445.	0.0556	0.14	4.0388	4.7309
Au/Ag	0.	3.38	480.	0.0588	2.37	4.9559	7.6531
Au/Cr	0.	3.96	498.	0.0712	0.78	4.8344	6.8607
Hf/Zr	0.	6.35	355.	0.0441	0.23	4.0237	4.8411

Table 7. 2. The Power Factor $(2+\mu)$ Obtained in the Different Thermal Spike Models.

	Spherical	Cylindrical
Vineyard's Model	1.67	2.0
Present Model	2.33	3.0
Least Square Fitting	2.24	> 3.0

note: The slope for the cascade collision mixing case = 1.0

mixing for these data, since the experiments belong to the energetic heavy ion bombardment ($F_D > 100$ eV/Å). Figure 7.1 gives the thermal spike induced ion mixing parameter as a function of damage energy deposited in the form of a Log-plot with $\ln(4L_T\rho^{5/3})$ representing the mixing and $\ln\chi$ the damage level. It should be noted that the data for the plot, obtained from Refs. [17,18], have negligible chemical effects. The corresponding data is listed in Table 7.1. In Fig.7.1, the least square fitting in the abscissa range of 4.0 to 4.3 is shown. The slope in this region was found to be 2.24. This compares very well with power factor $(2+\mu) = 2.33$, which follows from the spherical thermal spike model. On the other hand, for the next region, $\ln\chi \geq 4.3$, a rapid increase in ion mixing parameter obviously deviates from the trend of the region of the spherical thermal spike model. The slope of this region seems much higher than that of the previous region. The production of defects in this region is attributed to the nonlinear cascade effects, i.e., the thermal spike related defects. The slope value in this region appears more consistent with the cylindrical thermal spike model in the extremely high cascade case, i.e., $2+\mu = 3.0$. Table 7.2 lists the power factor of thermal spike models with different shapes. The slope values from the experimental data are also listed, at the relatively high cascade region and the extremely high cascade region. The cascade collision mixing model, in the low cascade regions, is listed with the slope equal to 1.0. For the cascade collision mixing data on ion mixing of metallic layers by Ne from Ref. [15] is used (circle symbol). In addition, the cascade collision mixing values calculated from the Anderson Model (square symbol) and the computer simulation code TRALL [4] (star symbol) are also included. For the cascade collision mixing with slope value of 1.0, a straight line could be constructed on the basis of these data. The difference in the slopes of the three regions can be clearly seen the figure.

7.4 Discussion and Conclusions

Ion mixing at low temperatures can be divided mainly into two phases, as mentioned in the introduction part, i.e., the cascade collision phase and the thermal spike phase. During the cascade collision phase, atoms are displaced from their lattice positions through knock-down events of binary collisions. The elastic energy transferred in each collision must be larger than the displacement energy of the target, E_d . As a result, many Frenkel pair of defects are created at the end of this phase. Low energy many-body collisions are important as the residual energy is partitioned among the atoms in the cascade volume. A significant atomic migration for the Frenkel defects could occur during this phase. The significance of these two phases at different damage levels can be understood within the framework of Fig. 7.1. Thus in a semi-empirical fashion, three distinct ion mixing regions at low temperatures dependent on the damage parameter χ can be identified.

For low values of χ ($< 22\text{Å}^{-1}$): The mixing parameter L essentially has a linear dependence on the damage parameter χ. This is the cascade collision mixing region, where atoms are likely to be displaced from their initial positions via linear collision cascade process, and the residual energy partitioned among the atoms in the cascade volume, may not be able to form a significant thermal spike.

For relatively high values of χ ($22\text{Å}^{-1} \leq \chi < 75\text{Å}^{-1}$): Thermal spike enhanced atomic migration starts to be important. The relevant nonlinear effects of ion mixing appear, as opposed to the linear effect of the cascade collision mixing region. Basically, this thermal spike region originates from the first order of nonlinear effects, here it is referred as the Thermal Spike region I. Still, the generation of defects follows the linear cascade behavior in this region, i.e., the

Kinchin-Pease formula. However, the cooling phase of the cascade has a substantial influence on the atomic mixing via thermal spikes. The thermal spike in this case possesses a spherical shape and the ion mixing parameter is proportional to $\chi^{2.33}$.

The extremely high value of χ ($\geq 75\text{Å}^{-1}$): Nonlinear effects of thermal spike induced ion mixing are more significant. In this region, not only the residual energy (thermal spike) has great nonlinear influence on the atomic migration process, but also the creation of defects may follow nonlinear behavior. In particular, the thermal spike shape in this region is likely to evolve into a cylindrical one and the ion mixing parameter is proportional to χ^3.

Comparison of the model presented with experimental data show that, the slope of the experimental data in the extremely high density cascade region appears to be even higher than that predicted by the cylindrical thermal spike model. This is most likely due to the creation of the thermal spike related defects, as reported by Thompson and Walker in the energetic bombardment of semiconductor targets Si and Ge [19].

Heinisch [20] employed a binary collision approximation in his computer simulations of defects production in a cascade volume for the case of FCC metal elements. The cascade pictures tentatively showed that for relatively high density cascades, the cascades are isolated from each other (i.e., the spherical thermal spike case). However, for the case of extremely high density cascades, the cascade tends to become a compact line (i.e., the cylindrical thermal spike case). Thus, in a qualitative fashion the results from the thermal spike model presented here seem consistent with Heinisch's simulation.

7.5 References

[1] K. B. Winterbon, Ion Implantation Range and Energy Deposition Distributions, Vol. 2 (Plenum, New York, 1975).

[2] H. H. Andersen, Appl. Phys. 18 (1979) 131.

[3] P. Sigmund and A. Gras-Marti, Nucl. Instr. & Meth. 182/183 (1981) 25.

[4] R. Pasianot, Diana Farkas, M. Rangaswamy, and E. J. Savino, to be published.

[5] J. P. Biersack and L. G. Haggmark, Nucl. Instr. & Meth. 174 (1980) 257.

[6] S. Matteson, J. Roth and M-A. Nicolet, Radiation Effects 42 (1979) 217.

[7] S. Wen-Zhi Li, H. Kheyrandish, Z. Al-Tamimi and W. A. Grant, Nucl. Instr. & Meth. B19/20 (1987) 723.

[8] R. S. Averback, Nucl. Instr. & Meth. B15 (1986) 675.

[9] B. M. Paine and R. S. Averback, Nucl. Instr. & Meth. B7/8 (1985) 666.

[10] W. L. Johnson, Y. T. Cheng, M. Van Rossum and M-A. Nicolet, Nucl. Instr. & Meth. B7/8 (1985) 657.

[11] F. Seitz and J. S. Koehler, Solid State Physics 2 (1956) 251.

[12] G. H. Vineyard, Radiation Effects 29 (1976) 245.

[13] T. Diaz de Rubia, R. S. Averback, R. Benedek, and W. E. King, Phy. Rev. Lett. 59 (17) (1987) 1930.

[14] J. F. Ziegler, J. P. Biersack and U. Littmark, The Stopping and Range of Ion in Solids, Vol.1, 1985, p.115-116.

[15] I. A. Fenn-Tye and A. D. Marwick, Nucl. Instr. & Meth. B18 (1987) 236.

[16] J. Bottiger, S. K. Nielsen and P. T. Thorsen, Nucl. Instr. & Meth. B7/8 (1985) 707.

[17] M. Van Rossum, Y-T. Cheng, M-A. Nicolet and W. L. Johnson, Appl. Phys. Lett. 46 (6) (1985) 610.

[18] T. W. Workman, Y. T. Cheng, W. L. Johnson and M-A. Nicolet, Appl. Phys. Lett. 50 (21) (1987) 1485.

[19] D. A. Thompson and R. S. Walker, Rad. Effects 36 (1978) 91.

[20] H. L. Heinisch, J. Nucl. Mater. 103/104 (1981) 1325.

Chapter 8

Ion Mixing of Carbon Marker Layer in Amorphous Fe-Ti Alloy

8.1 Introduction

High fluence ion implantation is a widely studied surface processing technique for improving wear resistance and decreasing the friction of metal surfaces [1,2]. High fluence implantation of Ti has been found effective in reducing friction and wear in a variety of steels. In studies carried out at the Naval Research Laboratory [2-6] and Sandia National Laboratory [7-11], it has been found that most of the improvement in wear property is due to the formation of an amorphous layer at the surface. The amorphous layer was made up of a mixture of Ti, Fe and C, the C originating in the vacuum chamber environment. The mechanism by which carbon migrates into the solid (thermal diffusion, collision cascades, recoil implantation, etc)

is not better understood today than at the time when the effect was first recognized. There are two separate processes involved, the first being the pickup or adsorption of C by the surface atoms of the target and the second being the migration of C from the surface inwards. A model for the pickup of carbon atoms from the residual gases in the vacuum chamber and subsequent diffusion into the target was first described by Singer [12].

Hirvonen et. al. [13] studied the ion beam mixing of Ti/C/Ti and Fe/C/Fe tri-layers using Xe beams at room temperature without cooling the target. They found that the mixing of C with Ti was less efficient than the mixing of C with Fe by a factor of 1.5. Their experimental results demonstrated a negative correlation of mixing with the heats of mixing in the two cases in conflict with the general observation of direct correlation with the heats of mixing. Not only did the iron case show greater mixing, the Fe-C system possesses a negative heat of mixing while the Ti-C case posses a positive heat of mixing. There was however a direct correlation with diffusion. The diffusivity of C in Fe is much larger than that of C in Ti [13,14].

Nastasi et.al. [15] carried out experiments that were an extension of those in Ref. [13] at different temperatures. They found that while the mixing in the Fe-C system exceeded that in the Ti-C system by up to a factor of 3.4, at lower temperatures (below 300 K) the reverse was true and the mixing in Ti-C exceeded that in Fe-C by a factor of 1.1. The ion beam mixing at lower temperatures was also found to relatively independent of temperature.

Unpublished work [16] carried out at NRL, indicated that carbon adsorption and migration was present only when both Ti and Fe were present, and did not occur during Ti implantation into Ti or Fe implantation into Fe. The results suggest that carbon migration is greatly enhanced during the implantation due to a chemical effect involving C, Ti and Fe.

A number of mechanisms [17,18,19] could be involved in the migration of C in the Fe-Ti sample. These are (1) recoil implantation, the time duration of which is around 10^{-13}s; (2) collision cascades (ballistic mixing) occurring within 10^{-12}s; (3) thermal spike effects over a period of 10^{-11}s; (4) radiation enhanced diffusion; and (5) chemical or thermodynamic factors. Ion beam mixing has been studied widely [17,18]. However, the basic mechanisms of mixing are still not well understood. The magnitude of collision cascade mixing has been found to be proportional to the fluence and to the amount of energy deposited at the depth of interest. In certain cases thermal spike effects [19] are known to be responsible for increasing the magnitude of mixing beyond that possible by cascade mixing. Radiation enhances the thermal based diffusion by increasing the concentration of defects such as vacancies and interstitials. Finally there could be thermodynamic factors that favor the formation of stable or metastable precipitates which in turn could dictate where or how much the C would diffuse. It has been observed that during Ti implantation into Fe, when both C and O are present in the vacuum chamber in the form of carbon monoxide only C is picked up by the target [20]. Figure 8.1 [21] shows the concentration profiles of C and Ti for different fluences and incident energies for Ti implantation into Fe. As the fluence of Ti increases Ti concentration increases at the surface. The concentration of C also increases with Ti up to a limit of 16 at.%. The total C picked up increases as C diffuses into the target in the style of temperature based diffusion. Surface chemistry at the continually sputtered surface apparently plays an important role in C adsorption. The model for adsorption of C from the vacuum chamber and subsequent migration into the target proposed by Singer [12] is illustrated in Fig. 8.2. The model explains the phenomenon by a four step process involving:

1. uncovering of implanted Ti at the surface by sputtering;

2. adsorption of carbonaceous molecules from the residual gases in the vacuum chamber by Ti freshly exposed Ti atoms;
3. formation of surface carbide species by dissociation; and
4. diffusion of C atoms inwards from the surface.

In a previous work a computational method [21] was developed that considered the diffusion-like transport processes which affect the shape of the evolving profiles during high fluence ion implantation. The formalism modelled the inward migration of carbon atoms, that were adsorbed from the vacuum system during the implantation, and yielded a high observed effective diffusion of C of $6x10^{-15}$ cm^2/sec (the thermally activated diffusion of C being 10^{-16} cm^2/sec at room temperature). However, the mechanisms responsible for carbon migration into the target have not been identified.

In the current study the process being studied is the transport of C atoms inside the target. The first attempt is then to remove the surface chemistry dependence of diffusion of carbon. This was achieved by moving the carbon source away from the surface into the sample by using a thin layer of carbon within a Fe-Ti alloy. The ion implantation conditions were maintained by ion beam mixing of the C layer by an inert gas such as Ar.

The present study will examine the migrational behavior of C in the presence of Fe and Ti by ion mixing a thin layer of C embedded in a Fe-Ti matrix using a 350 keV Ar ion beam.

8.2 Experiment

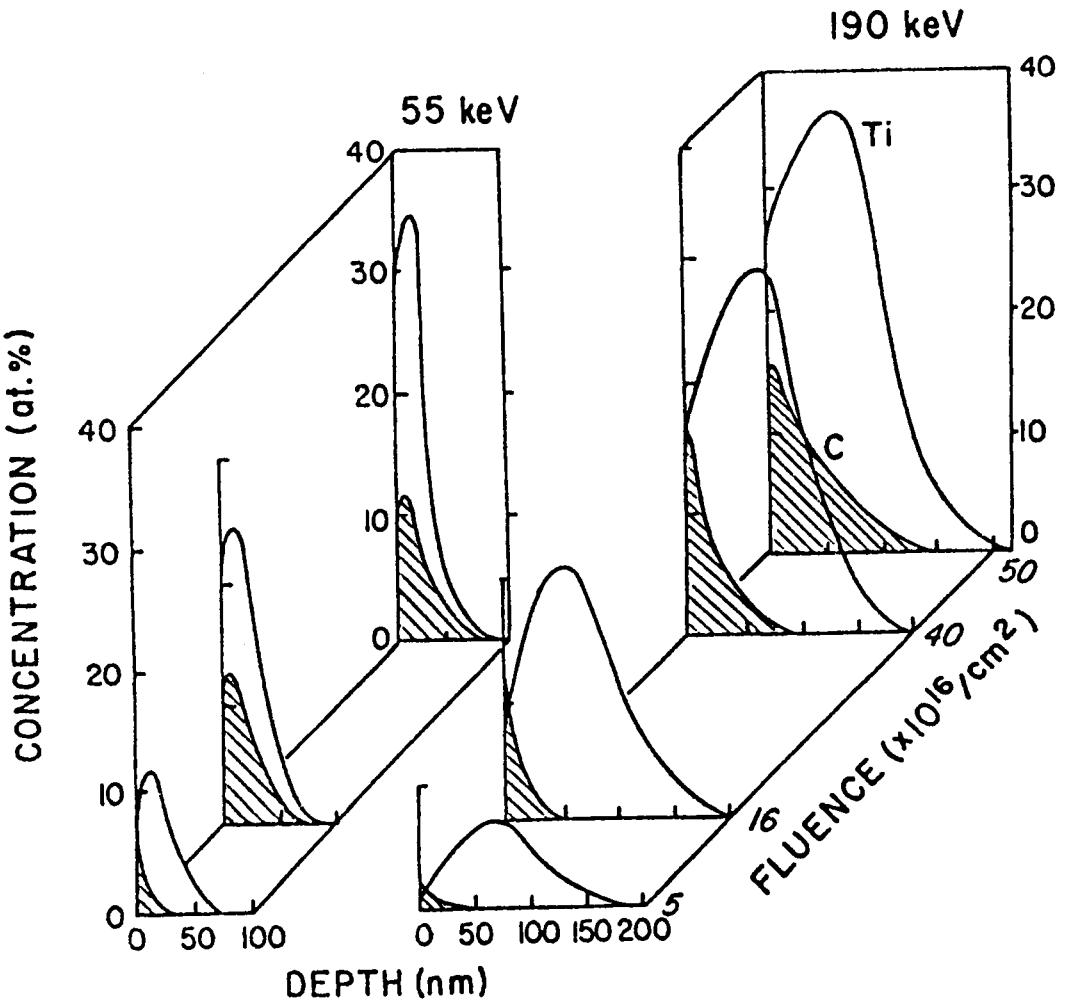

Figure 8.1. Concentration versus depth profiles for Ti and C in Ti-implanted 52100 steel at several fluences and energies, obtained by auger sputter profiling. (left) 5, 16, and 40×10^{16} Ti/cm^2 at 55 keV; (right) 5, 16, 40, and 50×10^{16} Ti/cm^2 at 190 keV. Note: bulk C concentration of steel (4 at.%) was subtracted from data. (Ref. [20])

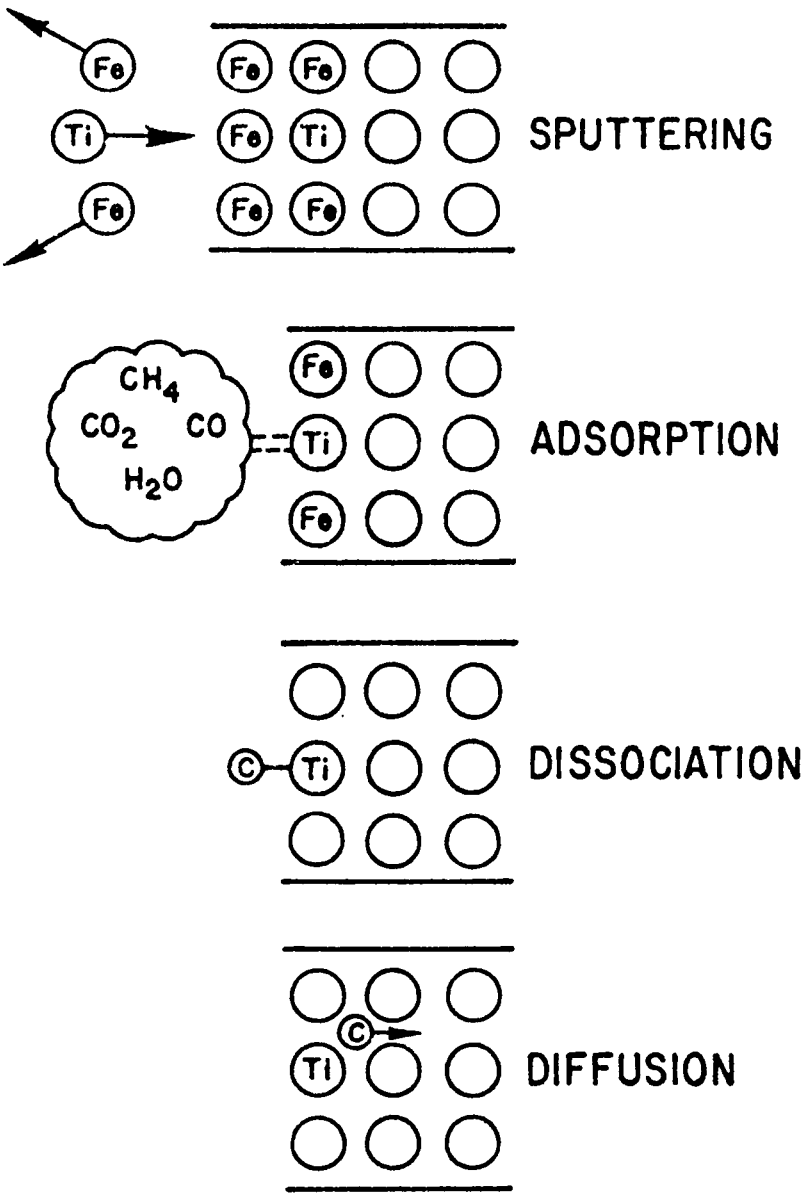

Figure 8.2. Model for vacuum carburization during implantation (Ref. [12]).

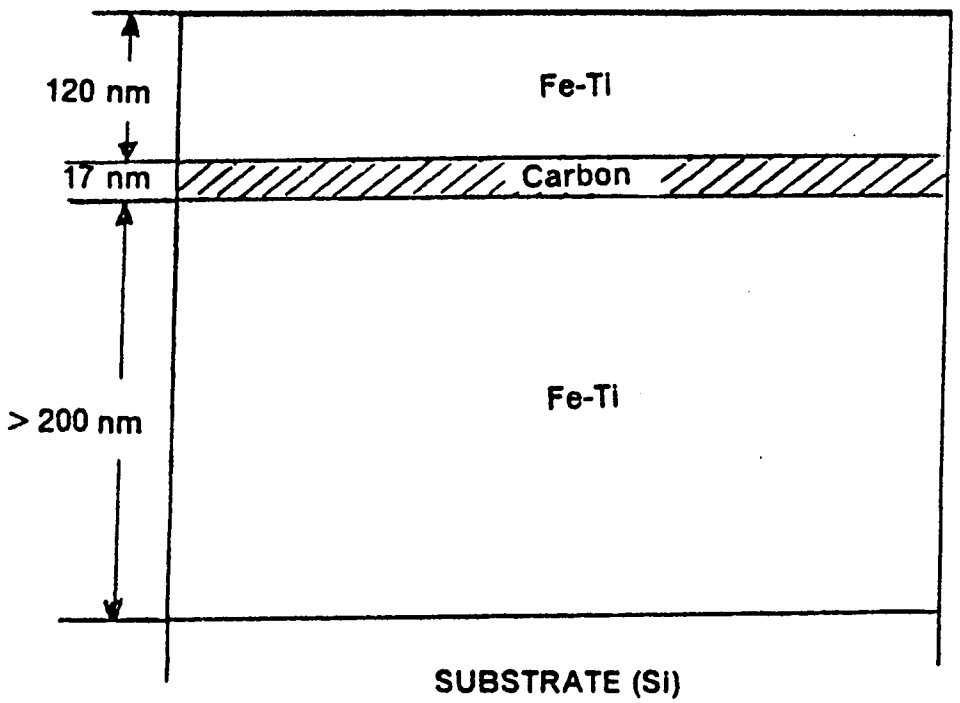

Figure 8.3. Schematic diagram of the Fe-Ti sample.

The sample configuration used was such that the C layer was away from the surface and within the Fe-Ti matrix. The basic sample configuration consisted of a thin carbon layer (approx. 17 nm) sandwiched between two layers of a Fe-Ti alloy of the composition of Fe_2Ti and is illustrated in Fig. 8.3. The outer Fe-Ti layer was about 120 nm and the inner layer around 350 nm. The Fe and Ti were sputter deposited simultaneously over a Si wafer using a magnetron sputter source. Magnetron sputter sources can isolate the plasma from the deposition surface almost completely. Magnetron sputter sources also give higher deposition rates. This reduces the extent of contamination of the film by impurity atoms from the vacuum chamber. The uniformity of deposition is also generally good. The sputter rates were adjusted by using a target consisting of plates of Fe and Ti with their exposed surface areas adjusted to give a Fe to Ti ratio of 2 to 1.

First, a 350 nm thick layer of Fe-Ti was deposited over the Si wafer. The purpose of a thicker bottom layer of Fe-Ti is to reduce the amount of contaminants from the vacuum chamber such as C and O to very low levels at the sandwiched C layer region. The impurities show a maximum concentration at the Si surface and drop to almost zero as more and more Fe-Ti is deposited. A negative bias of 200 V was applied at the substrate to obtain a denser film as well as to reduce the amount of impurities adsorbed on the film during deposition.

The carbon layer (17 nm) was deposited by vaporizing a carbon filament over the inner Fe-Ti layer by resistance heating. The carbon layer was at a depth such that the damage energy deposition due to implanted Ar in its immediate vicinity was essentially constant (115 eV/Å). The damage energy deposited and its distribution was obtained from the Monte-Carlo simulation code TRIM [22] and the code EDEP1 [23] and is illustrated in Fig. 8.4.

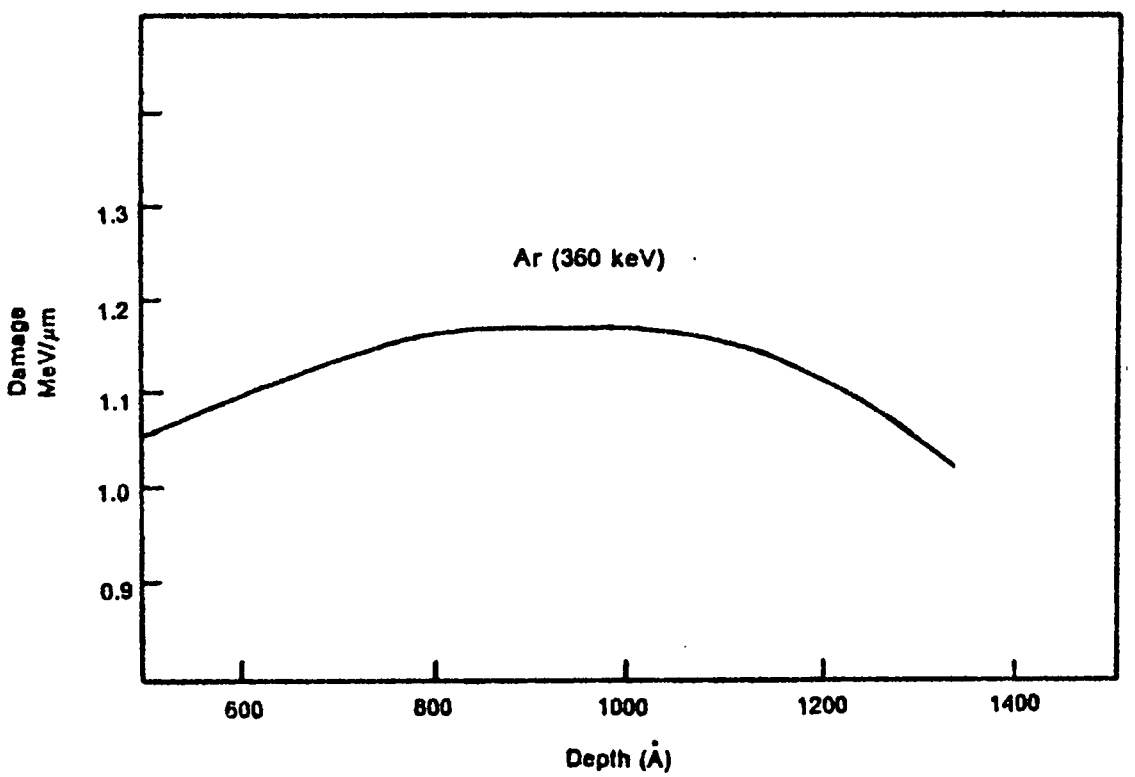

Figure 8.4. Damage energy distributions for 350 KeV Ar implanted into Fe-Ti.

The ion beam mixing was carried out at N.R.L. in a in a UHV chamber attached to the modified model 200-20A2F Varian/Extrion ion implanter. A 350 keV Ar beam was used to ion mix the samples to different fluences of 3, 7, 10 and $13x10^{16}/cm^2$. The composition profiles of the as deposited and ion mixed samples were obtained by auger electron spectroscopy using the Perkin-Elmer (PHI) model 545 Auger microprobe in the UHV chamber and by RBS.

8.3 Results and Discussion

The composition of the Fe-Ti layers was found to be similar to that of Fe_2Ti. The samples were analyzed using x-ray diffraction to determine the structure of the fe-Ti films. The structure was found to be essentially amorphous with no precipitation of the Fe_2Ti phase. The magnitude of mixing was monitored by measuring the broadening of the gaussian-like profile of C as given by the changes in the "fwhm" (full width half maximum of the gaussian profile). The change in the value of $(fwhm)^2$ has been denoted Δ^2 and is related to the diffusion length '2Dt' by [19]:

$$2Dt = \frac{\Delta^2}{8 \ln 2}. \qquad [8.1]$$

The efficiency of mixing was then obtained using the definition [24]

$$Q_1 = \left(\frac{N}{0.07}\right)\left(\frac{Dt}{F_D \Phi}\right), \qquad [8.2]$$

where N is the atomic density of the target and Φ is the fluence. Figure 8.5 shows the measured change in the Δ^2 of the C layer, divided by F_D, as a function of ion fluence.

From the slope of this plot the efficiency of mixing, Q, is directly obtained. Using an atomic density of the target given by a mixture of Fe and Ti in the composition of Fe_2Ti, a Q_1 value of 14 is obtained. This is about double the value given for the mixing efficiency of Ar in Ref. [18] for mixing in Pd. It is clear that there is a large effect other than that of collisional mixing occurring. This is attributed to chemical or thermodynamic effects on the migration of C in C-Fe-Ti.

During the deposition of C and the top Fe-Ti layer a lot of oxygen was picked up and this resulted in the formation of an oxygen peak 14 nm from the C peak towards the surface. Figure 8.6 illustrates the concentration profiles of the as deposited sample. Figure 8.7 illustrates the concentration profiles of the same sample after 350 keV Ar implantation to $13x10^{16}/cm^2$. While the carbon profile has broadened the oxygen profile shows no broadening but only a decrease in the peak height.

Chemical effects have been found to be important to explain the intermixing in some cases [25,26]. It was observed that the amount of mixing scaled with the chemical affinity between the two atoms being mixed, i.e. the heat of mixing ΔH_m. Van Rossum et.al. [27] found that a better thermodynamic model of ion beam mixing could be formed by also including the cohesive energy of the system, ΔH_{coh}. Their model of ion mixing in the presence of chemical driving forces is explained by the following equation:

$$Q_2 = 4Dt/\Phi = \frac{k_1 F_D^2}{N^{5/3}\Delta H_{coh}^2}\left[1 + \frac{k_2 \Delta H_m}{\Delta H_{coh}}\right] \qquad [8.3]$$

where (Dt/Φ) is the ion beam mixing parameter, and K_1 and K_2 are two least square fitting constants with K_1 = 0.0037 nm and K_2 = 27. The cohesive energy is calculated for a binary system using [27]:

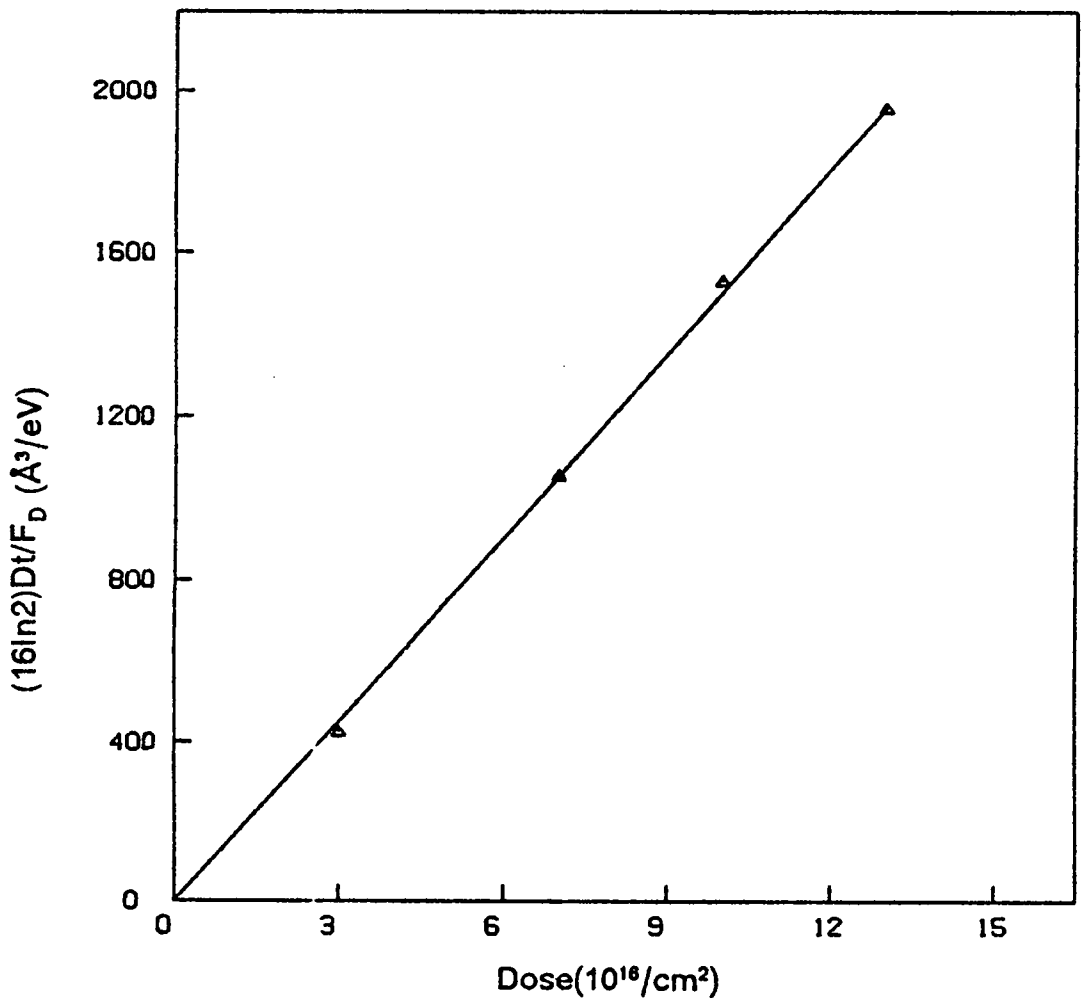

Figure 8.5. Mixing produced per unit of energy deposited per ion at the C layer as a function of fluence.

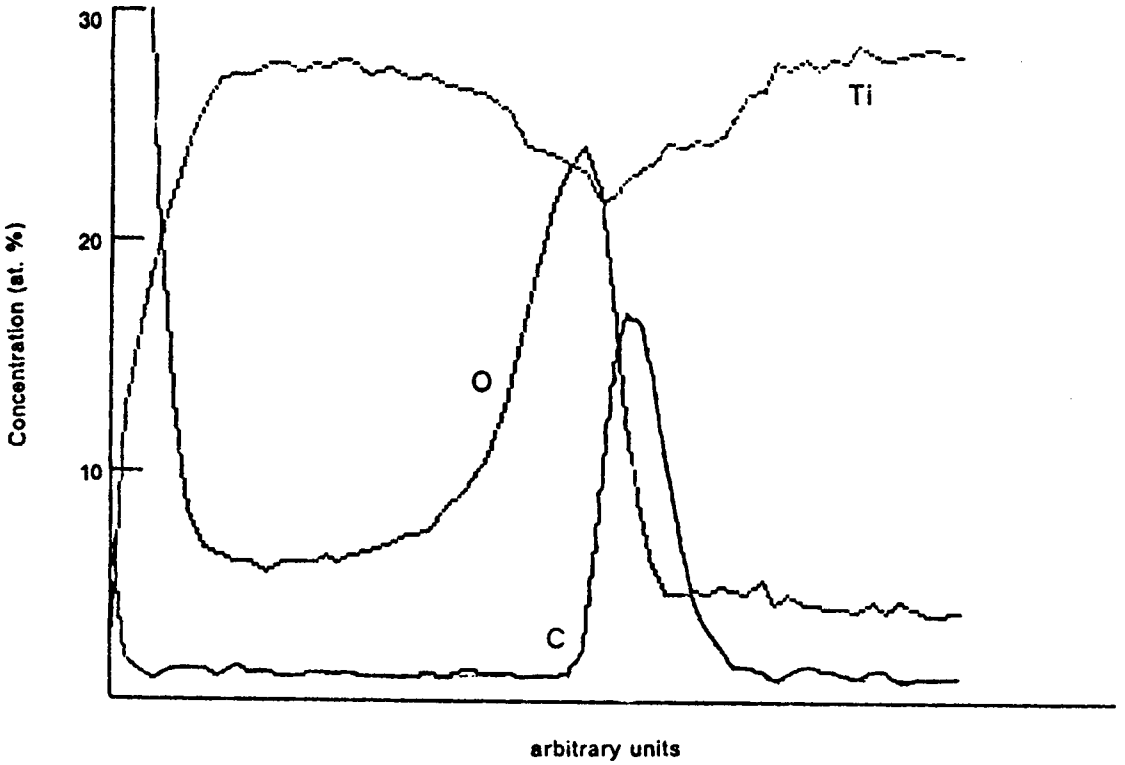

Figure 8.6. Auger concentration profile of the 'as deposited' Fe-Ti sample.

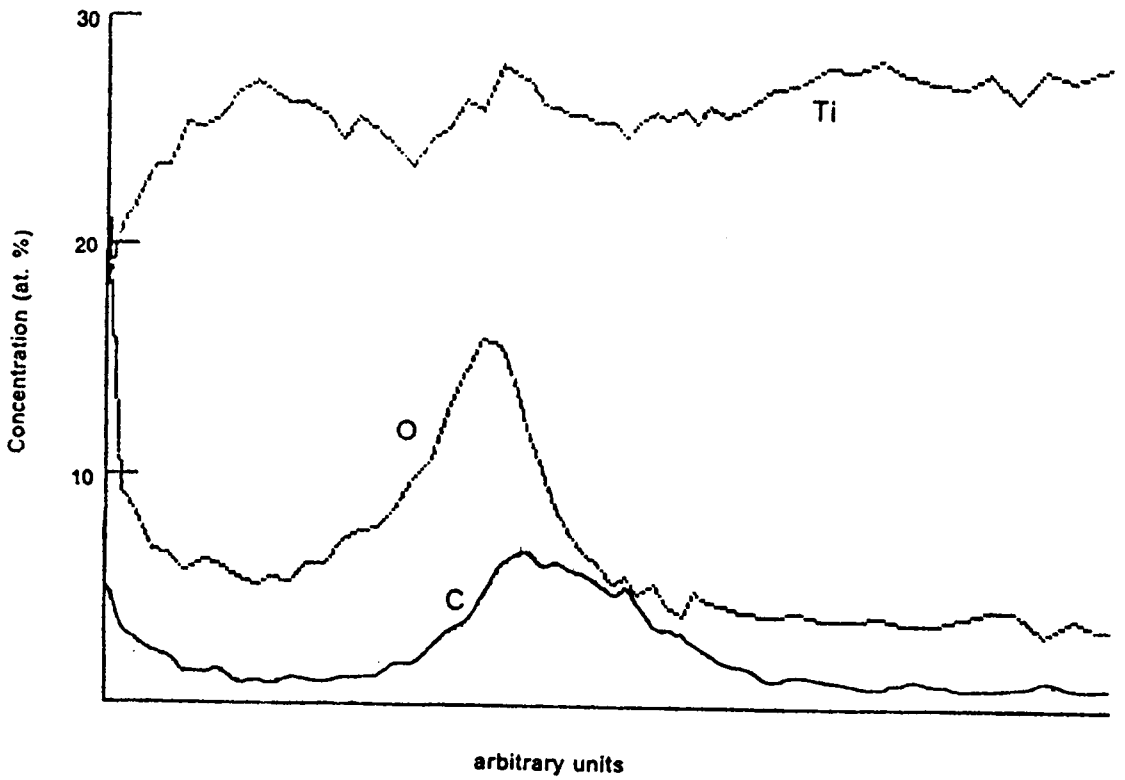

Figure 8.7. Auger concentration profile of the Fe-Ti sample after ion beam mixing with 350 keV Ar to a dose of $13 \times 10^{16}/cm^2$.

$$\Delta H_{coh} = \frac{\Delta H_A^0 + \Delta H_B^0}{2} + \Delta H_m^{pure} \qquad [8.4]$$

where ΔH_A^0 and ΔH_B^0 are the cohesive energies of pure A and B and ΔH_m^{pure} is the heat of mixing starting with pure A and B.

In the case of Fe-Ti-C the phases that are found in equilibrium are the Fe_2Ti Laves phase, Ti-carbide TiC_ν (ν between 0.5 and 1), and $(Fe,Ti)_3C$ [28]. In the case of binary Ti-C system the free energy of formation of TiC is negative whereas that of Fe_3C in the binary Fe-C system is positive. If a similar trend be assumed for the ternary system, the formation of TiC_ν is most likely to form. The driving force for the formation of TiC_ν will determine the chemical effect in the mixing of C in Fe-Ti-C.

The Q_2 (= $4Dt/\Phi$) value obtained from the slope in Fig. 8.5 is found to be 0.6244 nm^4. This is much larger than the values of 0.29 and 0.2 nm^4 obtained by Nastasi et.al. [15] for the mixing in Fe-C and Ti-C samples. This could mean that the chemical effect in the Fe-Ti-C system is much larger.

Uhrenius [29] has evaluated the Gibbs energy of formation of stoichiometric TiC in Fe-Ti-C from graphite and hcp Ti as -184640 + 11T J/mol. (= 183.54 kJ/mol. at 100 K). The corresponding Gibbs free energy of formation of TiC from graphite and hcp Ti in the Ti-C system is given as 90500 J/mol [30,31]. Using the value of the free energy of formation of TiC in the Fe-Ti-C system, and the starting points to be amorphous (liquid) Ti and amorphous (liquid) C, the difference in free energy between the as-deposited and intermetallic compound state is 2.59 eV/atom. The calculations were made using thermodynamic values from Ref. [30]. Substituting this value for the ΔH_m in Eq. (8.3) and using the ΔH_{Ti}^0, ΔH_C^0 and ΔH_m^{pure} values from Ref. [15], we get $Q_2 = 4Dt/\Phi = 0.8286$ nm^4 This is higher than the value of 0.6244 nm^4

obtained from experiment. The discrepancy could be due to the assumption that only TiC_y forms, while in reality both $(Ti,Fe)_3C$ and TiC_y will form.

8.4 References

[1] N.E.W. Hartley, in Ion Implantation, edited by J. K. Hirvonen (Academic Press, New York, 1980), p.321.

[2] G.K. Hubler, in "Metastable Materials Formation by Ion Implantation", S. T. Picraux and W. J. Choyke, eds. (Elsevier 1982), p. 35.

[3] I.L. Singer, in "Ion Implantation and Ion Beam Processing of Materials", G.K. Hubler, O.W. Holland, C.R. Clayton, C.W. White, eds. (North-Holland, New York, 1984) p. 585.

[4] I.L. Singer, R.N. Bolster, and C.A. Carosella, Thin Solid Films 73 283 (1980).

[5] I.L. Singer, Applications Surface Sci. 18 (1984) 28.

[6] C.A. Carosella, I.L. Singer, R.C. Bowers, and C.R. Gosset, "Ion Implantation Metallurgy",C.M. Preece and J.K. Hirvonen, eds., (TMS-AIME, Warrendale, Pa, 1980) p. 103.

[7] F.G. Yost, S.T. Picraux, D.M. Follstaedt, L.E. Pope, and J.A. Knapp, Thin Solid Films 107 (1983) 287.

[8] L.E. Pope, F.G. Yost, D.M. Follstaedt, S.T. Picraux, and J.A. Knapp, in "Ion Implantation and Ion Beam Processing of Materials", G.K. Hubler, O.W. Holland, C.R. Clayton, C.W. White, eds. (North-Holland, New York, 1984) p. 661.

[9] D.M. Follstaedt, F.G. Yost, L.E. Pope, S.T. Picraux, and J.A. Knapp, Appl. Phys. Lett. 43 (1983) 358.

[10] D.M. Follstaedt, F.G. Yost, L.E. Pope, in "Ion Implantation and Ion Beam Processing of Materials", G.K. Hubler, O.W. Holland, C.R. Clayton, C.W. White, eds. (North-Holland, New York, 1984) p. 655.

[11] L.E. Pope, F.G. Yost, D.M. Follstaedt, J.A. Knapp, and S.T. Picraux, in "Wear of Materials", K.C. Ludema, ed., (ASME, New York, 1983) p. 280.

[12] I.L. Singer, J. Vac. Sci. Technology. A 1 (1983) 419.

[13] J.P. Hirvonen, M. Nastasi and J.W. Mayer, Nucl. Instr. and Meth. B13 (1986) 479.

[14] D. Bergner, in Proc. Int. Conf. on Diffusion in Metals and Alloys, eds., F.J. Kedves and D.L. Beke (Trans. Tech., SA, 1084) p. 223.

[15] M. Nastasi, J. R. Tesmer, and J.-P. Hirvonen, Mat. Res. Soc. Symp. Proc. 93, (1987) 215.

[16] K.L. Grabowski and B. D. Sartwell, private communication.

[17] B.M. Paine and R.S. Averback, Nucl. Instr. and Meth. B7/8 (1985) 666.

[18] R.S. Averback, Nucl. Instr. and Meth. B15 (1986) 675.

[19] I.A. Fenn-Tye and A.D. Marwick, Nucl. Instr. and Meth. B18 (1987) 236.

[20] I.L. Singer and T.M. Barlak, Appl. Phys. Lett. 43, (1983) 457.

[21] D. Farkas, I.L. Singer, and M. Rangaswamy, J. Appl. Phys. 57, (1985) 1114.

[22] J. P. Biersack, L. G. Haggmark, Nucl. Inst. Meth. 174 (1980) 257.

[23] I. Manning and G.P. Mueller, Comp. Phys. Comm. 7 (1974) 85.

[24] G. J. Clark, A.D. Marwick and D.B. Poker, Nucl. Instr. and Meth. 209/210 (1983) 107.

[25] Y-T. Cheng, M. Van Rossum, M. A. Nicolet, and W. L. Johnson, Appl. Phys. Lett. 45 (1984) 185.

[26] M. Nastasi, J-P. Hirvonen, M. Caro, E. Rimini, and J. W. Mayer, Appl. Phys. Lett. 50 (1987) 177.

[27] M. Van Rossum, Y-T. Cheng, M. A. Nicolet, and W. L. Johnson, Appl. Phys. Lett. 46 (1985) 610.

[28] H. Ohtani, T. Tanaka, M. Hasebe, and T. Nishizawa, CALPHAD 12 (1988) 225.

[29] B. Uhrenius, CALPHAD 8 (1984) 101.

[30] L. Kaufman and H. Nesor, CALPHAD 2 (1978) 295.

[31] R. Hultgren, P. D. Desai, D. T. Hawkins, M. Gleiserand, K. K. Kelley, Selected Values of the Thermodynamic Properties of Metals (and Binary Alloys), ASM Metals Park, Ohio (1973).

Chapter 9

Conclusions

A variety of techniques can be employed to understand the processes involved in ion beam surface modification of metals. From the results of Chapters 2 to 5, it can be seen that simple phenomenological models can be used successfully to understand and predict effects of ion beam surface modification. In different implant atom-target atom combinations, different processes can dominate. The results from this study have shown that it is necessary to have some understanding of the processes involved either through experiment or through results from systems similar to the one under study before applying any of the simulation models.

In cases where preferential sputtering is important such as in the case of Ta implanted into Fe, the evolution of the concentration profiles is strongly affected and when diffusion is also present the effects of preferential sputtering can extend well into the target. Since Ta sputters much less than Fe , a larger retained dose of Ta could be maintained. The higher the diffusivities that are operating, the greater are the effects of preferential sputtering, causing an increase in the retained dose as well

as the time taken to reach steady state. The model for preferential sputtering could successfully model the implantation of Ta into Fe. The model can also be applied to analyze the compositional effects that occur during sputter profiling in surface analysis techniques such as SIMS or Auger Electron Spectroscopy.

The simple phenomenological model for radiation-damage induced migration that uses only one parameter to account for coupling of solute and defect fluxes could successfully calculate the implanted atom concentration profiles in a semi-quantitative manner. From the results obtained for Sn implantation into Fe and Ti implantation into Fe, it appears that the magnitude of the effect depends on the relative positions of the distributions of the implanted species and damage and also the surface. In the case of Sn implanted into Fe, radiation induced segregation effects were shown to be significant. The positive sign of the solute-defect coupling parameter suggests that a vacancy mechanism was not dominant. In the case of Ti implantation into Fe there were no significant effects.

In the case of N implantation into Fe the model for RDIM could explain the formation of the two peak structure through interstitial diffusion of N down the defect gradient. The activation energy under irradiation obtained (32 kJ) from the Arrhenius plot in Chapter 4 was much lower than the thermal activation energy (77 kJ) for the diffusion of N in Fe.

From the results of calculations using the second phase precipitation model for N implantation into Nb it is seen that the precipitation of second phases can have an effect on the actual shape of the implantation profiles. This was particularly so for the deeper region of the profile. Second phase precipitation however did not affect the total retained dose of the implanted species very much since the precipitated region was away from the surface and the loss due to sputtering was not modified. The effects became more significant when the implanted species were highly mobile

during the implantation process. For relatively low doses, where the amount of precipitate was negligible or none at all which in the present case was below 14x $10^{16}N/cm^2$, the effects on the profile shape were not significant. The precipitated amount can be calculated using the present formalism if the solubility limits under irradiation are known. The solubility limits will have to be determined from experiment by using methods such as X-ray diffraction.

The Monte Carlo simulation code TRAL was used to calculate the mixing effect in the case of two bilayer samples, namely Sn-Fe and C-Fe the mixing being by argon and Ti ion beams respectively. From the results of the simulation a greater mixing effect was found in the C-Fe case than in the Sn-Fe case. This is probably due to a higher diffusivity for the smaller atom, i.e. carbon. Comparison with error function type profiles indicate a 1.5 to 2 times greater diffusivity in the inner layer compared to the surface layer. This corresponds very well to the larger damage energy deposition in the inner layers. The diffusivity values obtained for the cascade collision mixing were of the order of $10^{16}cm^2/s$ and were in agreement with the results obtained using the Kinchin-Pease relationship.

By applying the thermal spike model to experimental data involving different levels of damage deposition, three distinct regions dependent on the damage parameter χ can be identified. For low values of χ ($< 22Å^{-1}$), the mixing parameter L essentially has a linear dependence on the damage parameter χ. This is described as the linear cascade collision mixing region. For relatively high values of χ ($22Å^{-1} \leq \chi < 75Å^{-1}$), thermal spike enhanced atomic migration starts to be important and the nonlinear effects of ion mixing appear. The thermal spike in this case is described as a spherical thermal spike and the ion mixing parameter is proportional to $\chi^{2.33}$. For extremely high value of χ ($\geq 75Å^{-1}$), nonlinear effects of thermal spike induced ion mixing are more significant. The thermal spike shape in

this region is described as cylindrical and the ion mixing parameter is proportional to χ^3. The thermal spike effects could explain the greater mixing seen compared to that predicted by binary collision approximation.

The results of the experiment of ion beam mixing of the C marker layer in Fe-Ti indicate that the broadening is a lot more than that predicted by cascade collision mixing. This can be explained only by a very negative heat of mixing for C in a matrix containing Fe and Ti, biasing the diffusion towards interdiffusion.

Appendix A

Program Listings

A.1 SPUTEFF Fortran Code

Given below is the listing of the program 'sputeff' that was used to generate the implantation concentration profiles for the preferential sputtering case.

```
C                                                              C
C--5 -FROM IMPDIF1A--BUT WITH DIFFERENT SPUTTER  MODEL-----C
C     SPUTTERS OFF 1/3 BIN, CALCULATES  DELT FROM TIME     C
C     REQD TO SPUTTER 1/3 BIN. EXCESS ATOMS IF ANY ARE     C
C     ADDED TO NEW 1ST BIN.                                C
C                                                          C
C  4  CREATED FROM SPUTEFF5 ON 2/21/89  WITH DIFFERENT     C
C     ATOMIC VOLUMES, OUTPUT CHOICE   OF AT/CM2 OR NM,     C
C     AND  VOLUME CHANGE IN BINS FOR DIFNT ATOM FLUXES     C
C     ALSO HAS A BILAYER INPUT FORMAT WITH A TOP LAYER     C
C     THICKNESS OF PLTH.                                   C
C                                                          C
C  3  CREATED FROM SPUTEFF2 INTRODUCING VARIABLE DENSITIES C
C     AND VAR LATTICE DILATION (DILK).                     C
C                                                          C
```

```
C  2  CREATED FROM TIMEFF AND SPUTDI ON 5-23-84                C
C                                                              C
C  1  FROM IMPLAN WITH CHANGES IN D AND LATTICE DILATION       C
C                                                              C
C--------------------------------------------------------------C
C
C     THIS   PROGRAM  CALCULATES THE  CONCENTRATION PROFILES
C     OF THE  IMPLANTED ION & CARBON ( WHICH  IS  PICKED  UP
C     DURING IMPLANTATION) CONSIDERING PREFERENTIAL SPUTTER-
C     ING OF THE DIFFERENT ELEMENTS PRESENT.
C
C     THE LANGUAGE USED IS FORTRAN-77.
C
C     TO  RUN THE  PROGRAM, AN  INPUT FILE IS REQUIRED WHICH
C     GIVES THE FOLLOWING DATA.:-
C     LINE  1) NUMBER OF (A) IMPLANT  ENERGIES, (B) FLUENCES,
C              (C)  FLUXES,  (D) SPUTTERING YIELD PAIRS   AND
C              (E) LATTICE DILATION VARIABLE.
C     LINE  2) IMPLANT ATOM  AND  TARGET ATOM  SYMBOLS  USING
C              THE FORMAT(1X,4A1,4A1)
C     LINE  3) ENERGY, MAX IMPLANT. DEPTH , RANGE, STRAGGLING
C              (-----------------DO ----------------------)
C              TO AS MANY LINES AS THERE ARE IMPLANT ENERGIES
C     LINE  4) TIME IN  HOURS  CORRESPONDING TO THE DIFFERENT
C              FLUENCES IN INCREASING ORDER.
C     LINE  5) THE CORRESPONDING FLUENCES.
C     LINE  6) THE DIFFERENT FLUX VALUES USED IN AT/CM2/SEC.
C     LINE  7) SPUT YIELD-1, SPUT YIELD-2, SPUT YIELD-3
C              (-----------------DO ----------------------)
C              TO AS MANY LINES AS THERE ARE PAIRS.
C     LINE  8) THE  DIFFUSIVITIES  D11, D22, D33 IN  UNITS OF
C              CM**2/SEC.
C     LINE  9) THE  INITIAL BULK  CONCENTRATION VALUES OF C1,
C              C2, C3, NAMELY  C1P0, C2P0, AND  C3P0   (FIRST
C              LAYER)  AND  C10, C20, AND C30  (SECOND LAYER)
C              IN AT. FRAC.
C     LINE 10) THE  ATOMIC DENSITIES OF ATOMS  1, 2  AND 3 IN
C              UNITS OF ATOMS/CM**3.
C     LINE 11) THE  INCREMENT OF TIME IN SECONDS, SPACE STEPS
C              AND THE TOP LAYER THICKNESS IN CM.
C     LINE 12) ALTERNATE INPUT OF INITIAL COMNPOSITION
C              0=NO ALT INPUT; 1=INPUT FROM FILE
C     THE  CALCULATED VALUES GO INTO AN  OUTPUT FILE. ASSIGN
C     STATEMENTS  HAVE TO  BE USED  DESIGNATE  THE INPUT AND
C     OUTPUT FILE.  FILE  5 IS FOR THE INPUT AND FILE  6 FOR
C     THE OUTPUT.
C
C     THE PROGRAM  MAKES USE OF  TWO  SUBROUTINES VMULFF AND
C     LINV1F WHICH ARE AVAILABLE IN THE IMSL (MATH) LIBRARY.
C
C     THE PROGRAM HAD BEEN CHANGED TO INCLUDE  THE EFFECT ON
```

```
C     CARBON  PICKUP DUE TO  ELEMENTS  OTHER THAN  THE  IMP-
C     LANTED IONS AND TO CONSIDER  SATURATION  OF  CARBON AT
C     SURFACE. THE CHANGES AND THE CORRESPONDING  STATEMENTS
C     ARE PRESENT AS COMMENT CARDS.
C
C     THE FOLL IS AN EXAMPLE OF AN INPUT FILE.:-
C     L 1)         2,4,1,3,1.0
C     L 2)          TA  FE
C     L 3)         145.0,2.0E-5,2.020E-6,0.700E-6
C                  55.0,1.0E-5,2.0E-6,.86E-6
C     L 4)         0.1875,0.375,0.75,1.5
C     L 5)         5.,10.,20.,40.
C     L 6)         2.41E+13
C     L 7)         3.0,6.0,5.0
C                  4.0,4.0,4.0
C                  4.0,5.0,3.0
C     L 8)         0.6E-14,0.60E-14,0.60E-14
C     L 9)         1.0,.0,.0, .50,.0,.50
C     L 10)        8.487E22, 8.487E22, 8.487E22
C     L 11)        60.0, 60, 2.0E-6
C     L 12)        0
C
C     DEFINITIONS
C
      INTEGER R,S
C     COMMON /WORKSP/ RWKSP
      CHARACTER*1 IMPAT(4), TARAT(4)
      REAL*4 MATRIX(360,360), MAT(360,360)
      DIMENSION X(360), D(360), C1(180), C2(180), C3(180)
      DIMENSION  C1N(180), C2N(180), C3N(180)
      DIMENSION XD(121), X1(121), X2(121), X3(121)
      DIMENSION A(3,3), B(3,3), C(3,3), T(3,3)
C     DIMENSION WKAREA(360)
      DIMENSION EPS(180), C1P(180), C2P(180), C3P(180),
     :RHNP(180), RHNN(180), DX(180)
      DIMENSION XMAX(10), YMAX(10), TMAX(20), XP(10),
     :SPUT(20), FLU(10), FLUXX(10), FLNC(20), YP(10),
     :ENERGY(10), SIG(10), CSIG(10), TNTV(20), RHN(180)
      DIMENSION SP01(10),SP02(10),SP03(10)
C     WK(*) = N + N*(N-1)/2; IWK(*) = N ;HERE N=360
      DIMENSION WK(64980), IWK(360)
C     REAL RWKSP(65360)
C
      CALL ERRSET (208,256,-1)
C
C     CALL IWKIN (65360)
C
C     READ INPUT
C
      READ(5,*) IPV,IFV,JFV,IIV,DILK
      READ(5,51) IMPAT,TARAT
```

```
  51  FORMAT(1X,4A1,4A1)
      READ(5,*) (ENERGY(I),XMAX(I),XP(I),SIG(I),I=1,IPV)
      READ(5,*) (TMAX(I),I=1,IFV)
      READ(5,*) (FLNC(I),I=1,IFV)
      READ(5,*) (FLU(I),I=1,JFV)
C     NOTE THAT POSITIONS OF SP01 AND SP02 ARE SWITCHED IN IMPDIF1A
      READ(5,*) (SP01(I),SP02(I),SP03(I),I=1,IIV)
      READ(5,*) D11,D22,D33
      READ(5,*) C1P0,C2P0,C3P0,C10,C20,C30
      READ(5,*) RH1,RH2,RH3
      READ(5,*) DELT,NX, PLTH
      READ(5,*) INPU
C
C     GET DIFFUSIVITIES (FROM SUBROUTINE IN THE FUTURE)
C     CHANGE  PROGRAM  TO  ACCEPT  FUNCTIONS  AND  FLUXES AS
C     BOUNDARY CONDITIONS HERE
C
      WRITE(6,399) IPV,IFV,JFV,IIV,NX,DILK
 399  FORMAT(1X,5(I5,2X),F8.2)
      WRITE(6,51) IMPAT,TARAT
C
      DO 134 IP=1,IPV
      DELX=XMAX(IP)/NX
C
C     IF(IP.EQ.2)IFV=IFV-1
C
      DO 144 IWZ = 1,IFV
      TNTV(IWZ) = 3600*TMAX(IWZ)
  144 CONTINUE
      TNTVMAX = TNTV(IFV)
C
      DO 134 JF=1,JFV
C
      DO 134 II=1,IIV
C
C     FORM INITIAL CONCENTRATION VECTORS
C
      IF (INPU.EQ.1) THEN
C
C     CHECK THAT THE INPUT DATA HAS APPROPRIATE DELX UNIFORM SPACING.
C
      DO 203 I=1,NX
      READ(15,*) XD(I), C1(I), C2(I), C3(I)
      RHNI = (C1(I)/RH1) + (C2(I)/RH2) + (C3(I)/RH3)
      RHN(I) = 1.0/RHNI
203   CONTINUE
      DO 207 I=NX+1,NXDOS
      C1(I) = C1(NX)
      C2(I) = C2(NX)
      C3(I) = C3(NX)
```

```
      RHN(I) = RHN(NX)
207   CONTINUE
C
      ELSE
C
      IPLTH=PLTH/DELX
      NXDOS=3*NX/2
      DO 201 I=1,IPLTH
      C1(I) = C1P0
      C2(I) = C2P0
      C3(I) = C3P0
      RHNI = (C1(I)/RH1) + (C2(I)/RH2) + (C3(I)/RH3)
      RHN(I) = 1.0/RHNI
201   CONTINUE
      DO 202 I=IPLTH+1,NXDOS
      C1(I) = C10
      C2(I) = C20
      C3(I) = C30
      RHNI = (C1(I)/RH1) + (C2(I)/RH2) + (C3(I)/RH3)
      RHN(I) = 1.0/RHNI
202   CONTINUE
C
      END IF
C
C     START LOOP
C
      INC=1
      DELT=0
      TDELT=0
C
C     CONTINUE THE LOOP TILL TDELT REACHES EACH FLUENCE VALUE
C
 1342 CONTINUE
C
C     SPUTTERING
C
      SPUT(II) = C1(1)*SP01(II)*RHN(1)/RH1 + C2(1)*SP02(II)*RHN(1)/RH2
     ' + C3(1)*SP03(II)*RHN(1)/RH3
      SS1 = SPUT(II)*FLU(JF)
C     SPUTTER OFF 1/3 OF THE BIN
      SS2 = RHN(1)*DELX/3.0
      DELT = SS2/SS1
      TDELT = TDELT + DELT
C
      DO 225 I=1,NXDOS,1
      DC2=(FLU(JF)*DELT*DELX/(2.507*SIG(IP)))*EXP(-(((I-0.5)*DELX-
     :XP(IP))**2)/(2*SIG(IP)**2))
      DDC1 =  (RHN(I)*DELX*C1(I))        /( DELX + (DC2*DILK/RH2) )
      DDC2 =( (RHN(I)*DELX*C2(I)) + DC2 )/( DELX + (DC2*DILK/RH2) )
      DDC3 =  (RHN(I)*DELX*C3(I))        /( DELX + (DC2*DILK/RH2) )
      RHN(I) =( (RHN(I)*DELX) + DC2 )/( DELX + (DC2*DILK/RH2) )
```

```
      C1(I) = DDC1/RHN(I)
      C2(I) = DDC2/RHN(I)
      C3(I) = DDC3/RHN(I)
  225 CONTINUE
C
C     CIIN1 ARE THE ATOMS OF I IN BIN 1
      C1IN1 = RHN(1)*C1(1)*DELX/3.0
      C2IN1 = RHN(1)*C2(1)*DELX/3.0
      C3IN1 = RHN(1)*C3(1)*DELX/3.0
C     CISPOF ARE THE ATOMS OF I SPUTTERED OFF
      C1SPOF = C1(1)*SP01(II)*RHN(1)/RH1*FLU(JF)*DELT
      C2SPOF = C2(1)*SP02(II)*RHN(1)/RH2*FLU(JF)*DELT
      C3SPOF = C3(1)*SP03(II)*RHN(1)/RH3*FLU(JF)*DELT
C     EXCI ARE THE EXCESS (+ OR -) ATOMS OF I DUMPED INTO FIRST BIN
      EXC1 = C1IN1 -C1SPOF
      EXC2 = C2IN1 -C2SPOF
      EXC3 = C3IN1 -C3SPOF
C     EXTRR IS THE EXTRA VOL ADDED TO BIN 1 BY EXCI ATOMS AFTER SPUTTER
      EXTRR = EXC1/RH1 + EXC2/RH2 + EXC3/RH3
C     SPVOL IS THE SPUTTERED VOL / UNIT AREA IE THE SPUT THICKNESS
      SPVOL = C1SPOF/RH1 +C2SPOF/RH2 + C3SPOF/RH3
      SPIU = SPVOL/DELX
      IKE = INT(SPIU)
      SPIKE = SPIU-IKE
C
C     SHIFT COORDINATES FOR SPUTTERING
C
      DO 379 IQ=1,NXDOS-IKE-1
      C1(IQ)=C1(IKE+IQ)+((C1(IKE+IQ+1)-C1(IKE+IQ))*SPIKE)
      C2(IQ)=C2(IKE+IQ)+((C2(IKE+IQ+1)-C2(IKE+IQ))*SPIKE)
      C3(IQ)=C3(IKE+IQ)+((C3(IKE+IQ+1)-C3(IKE+IQ))*SPIKE)
      RHNI = (C1(IQ)/RH1) + (C2(IQ)/RH2) + (C3(IQ)/RH3)
      RHN(IQ) = 1.0/RHNI
  379 CONTINUE
C
C     CHANGE THE CONCENTRATION IN BIN 1 BY EXCESS ATOMS
C
      DDC1 =( (RHN(1)*DELX*C1(1)) + EXC1 ) /( DELX + EXTRR )
      DDC2 =( (RHN(1)*DELX*C2(1)) + EXC2 ) /( DELX + EXTRR )
      DDC3 =( (RHN(1)*DELX*C3(1)) + EXC3 ) /( DELX + EXTRR )
      RHN(1) =( (RHN(1)*DELX) + EXC1 + EXC2 + EXC3 ) / ( DELX + EXTRR )
      C1(1) = DDC1/RHN(1)
      C2(1) = DDC2/RHN(1)
      C3(1) = DDC3/RHN(1)
C
C     DX(1) = BY IMPLANTED ATOMS + EXCI ATOMS
      DX(1)=DELX*(FLU(JF)/RH2*DELT/(2.507*SIG(IP)))*
     :EXP(-(((0.5)*DELX-XP(IP))**2)/(2*SIG(IP)**2))
      DX(1) = DX(1)*DILK + EXTRR
      DO 226 I=2,NXDOS,1
      DX(I)=DELX*(FLU(JF)/RH2*DELT/(2.507*SIG(IP)))*
```

```
     :EXP(-(((I-0.5)*DELX-XP(IP))**2)/(2*SIG(IP)**2))
 226  CONTINUE
      EPS(1) = DX(1)
      DO 228 I=2,NXDOS,1
      EPS(I)=EPS(I-1) + (DX(I)*DILK)
 228  CONTINUE
C
C     LATTICE DILATION
C
      NTK = 2
      DO 255 I=2,NXDOS
      DELIM1 = (I-1)*DELX
      DO 256 J=NTK,NXDOS
      IF((EPS(J-1)+(J-1)*DELX).GE.DELIM1) THEN
      NTK = J
      DOX = (EPS(J-1)+(J-1)*DELX) - DELIM1
      GO TO 257
      END IF
 256  CONTINUE
 257  CONTINUE
      C1P(I) = ( (C1(NTK-1)-C1(NTK))*DOX/(DELX+DX(NTK-1)) ) +
     :C1(NTK)
      C2P(I) = ( (C2(NTK-1)-C2(NTK))*DOX/(DELX+DX(NTK-1)) ) +
     :C2(NTK)
      C3P(I) = ( (C3(NTK-1)-C3(NTK))*DOX/(DELX+DX(NTK-1)) ) +
     :C3(NTK)
      RHNI = (C1P(I)/RH1) + (C2P(I)/RH2) + (C3P(I)/RH3)
      RHNP(I) = 1.0/RHNI
 255  CONTINUE
C
      DO 275 I=2,NXDOS,1
      C1(I)=C1P(I)
      C2(I)=C2P(I)
      C3(I)=C3P(I)
      RHN(I)=RHNP(I)
      EPS(I)=0
 275  CONTINUE
C
C
C     FORM MATRIX
C
C     FIRST A,B,C MATRICES
C
      D12 = 0.0
      D13 = 0.0
      A(1,1) = DELT*D11/(2*DELX**2)
      A(1,2) = DELT*D12/(2*DELX**2)
      A(1,3) = DELT*D13/(2*DELX**2)
      A(2,3) = 0
      A(2,1) = 0
      A(3,1) = 0
```

```
      A(3,2) = 0
      A(2,2) = DELT*D22/(2*DELX**2)
      A(3,3) = DELT*D33/(2*DELX**2)
      B(1,1) = -2*A(1,1) -1
      B(2,2) = -2*A(2,2) -1
      B(3,3) = -2*A(3,3) -1
      B(1,2) = -2*A(1,2)
      B(1,3) = -2*A(1,3)
      B(2,1) = 0
      B(2,3) = 0
      B(3,1) = 0
      B(3,2) = 0
      DO 460 R=1,3,1
      DO 460 S=1,3,1
      C(R,S)=A(R,S)
460   CONTINUE
C
C     NOW FORM THE TRIDIAGONAL MATRIX OF A  B, AND C
C
C     CONSIDER THE SURFACE FIRST
C
      DO 200 IH=1,NX,1
      IF (IH.EQ.1)   THEN
      DO 571 R=1,3,1
      DO 571 S=1,3,1
      T(R,S)=B(R,S) + A(R,S)
571   CONTINUE
      GO TO 301
      END IF
      IF (IH.EQ.2) THEN
      DO 591 R=1,3,1
      DO 591 S=1,3,1
      T(R,S)=C(R,S)
591   CONTINUE
      GO TO 301
      END IF
      DO 450 I=1,3,1
      DO 450 J=1,3,1
      T(I,J) = 0
450   CONTINUE
 301  CONTINUE
      DO 101 I=1,3,1
      DO 101 J=1,3,1
      M = I
      N = 3*(IH-1)+J
      MATRIX(M,N) = T(I,J)
101   CONTINUE
 200  CONTINUE
C
C    CONSIDER THE OTHER LAYERS
C
```

```
      DO 100 L=2,NX,1
      DO 100 IH=1,NX,1
      IF (IH.EQ.L-1) GO TO 50
      IF (IH.EQ.L)   GO TO 60
      IF (IH.EQ.L+1) GO TO 70
      DO 45 I=1,3,1
      DO 45 J=1,3,1
      T(I,J) = 0
45    CONTINUE
      GO TO 80
50    CONTINUE
      DO 550 R=1,3,1
      DO 550 S=1,3,1
      T(R,S)=A(R,S)
550   CONTINUE
      GO TO 80
60    CONTINUE
      DO 570 R=1,3,1
      DO 570 S=1,3,1
      T(R,S)=B(R,S)
570   CONTINUE
      GO TO 80
70    CONTINUE
      DO 590 R=1,3,1
      DO 590 S=1,3,1
      T(R,S)=C(R,S)
590   CONTINUE
80    CONTINUE
      DO 100 I=1,3,1
      DO 100 J=1,3,1
      M = 3*(L-1)+I
      N = 3*(IH-1)+J
      MATRIX(M,N) = T(I,J)
100   CONTINUE
C
C     INVERT MATRIX
C
      LNVF2=3*NX
      LNVF3=360
      LNVF5=0
C     CALL LINV1F(MATRIX,LNVF2,LNVF3,MAT,LNVF5,WKAREA,IER)
C     CALL LINRG(LNVF2,MATRIX,LNVF3,MAT,LNVF3)
      CALL L2NRG(LNVF2,MATRIX,LNVF3,MAT,LNVF3,WK,IWK)
C
C     FORM D
C
      D21 = 0.0
      D23 = 0.0
      D31 = 0.0
      D32 = 0.0
C
```

```
C     CNS AND CN(NX+1) ARE PSEUDO-POINTS OUTSIDE THE CURRENT
C     F-D GRID.  CNS ARE  GIVEN A VALUE EQUAL TO THAT AT THE
C     SURFACE  SINCE  THERE ARE NO ATOMS  DIFFUSING OUT FROM
C     THE SURFACE. CN(NX+1) ARE  KNOWN  FROM  THE  EXTENDED
C     SPACE GRID USED (I.E. 90 INSTEAD OF 60 GRID POINTS)
C
      C1S = C1(1)
      C2S = C2(1)
      C3S = C3(1)
C
      D(1) = (DELT*D11/(2*DELX**2))*(2*C1(1)-C1(2)-C1S)-
     :C1(1)
      D(2) = (DELT*D22/(2*DELX**2))*(2*C2(1)-C2(2)-C2S)-
     :C2(1)
      D(3) = (DELT*D33/(2*DELX**2))*(2*C3(1)-C3(2)-C3S)-
     :C3(1)
      DO 300 I=2,NX-1,1
      D(3*I-2) = (DELT*D11/(2*DELX**2))*(2*C1(I)-C1(I+1)-
     :C1(I-1))-C1(I)
      D(3*I-1) = (DELT*D22/(2*DELX**2))*(2*C2(I)-C2(I+1)-
     :C2(I-1))-C2(I)
      D(3*I) = (DELT*D33/(2*DELX**2))*(2*C3(I)-C3(I+1)-
     :C3(I-1))-C3(I)
300   CONTINUE
      D(3*NX-2)=(DELT*D11/(2*DELX**2))*
     :(2*C1(NX)-2*C1(NX+1)-C1(NX-1))-C1(NX)
      D(3*NX-1)=(DELT*D22/(2*DELX**2))*
     :(2*C2(NX)-2*C2(NX+1)-C2(NX-1))-C2(NX)
      D(3*NX)=(DELT*D33/(2*DELX**2))*
     :(2*C3(NX)-2*C3(NX+1)-C3(NX-1))-C3(NX)
C
C     SOLVE SYSTEM OF EQUATIONS
C
      JVMLF3=3*NX
      JVMLF4=3*NX
      JVMLF5=1
      JVMLF6=360
      JVMLF7=360
      JVMLF9=360
      IPATH= 1
C     CALL VMULFF(MAT,D,JVMLF3,JVMLF4,JVMLF5,JVMLF6,JVMLF7,
C    :X,JVMLF9,IERR)
C     CALL MRRRR(JVMLF3,JVMLF4,MAT,JVMLF6,JVMLF4,JVMLF5,D,JVMLF7,
C    :JVMLF3,JVMLF5,X,JVMLF9)
      CALL MURRV(JVMLF3,JVMLF4,MAT,JVMLF6,JVMLF4,D,IPATH,JVMLF3,X)
C
C     FROM X FORM CONCENTRATION VECTORS
C
      DO 404 I=1,NX,1
      C1N(I) = X(3*I-2)
      C2N(I) = X(3*I-1)
```

```
      C3N(I) = X(3*I)
  404 CONTINUE
      C2NI1I = C2N(1)
      C2NI2I = C2N(2)
      DO 400 I=1,NX,1
      CTOTAL=C1N(I)+C2N(I)+C3N(I)
      C1N(I)=C1N(I)/CTOTAL
      C2N(I)=C2N(2)/CTOTAL
      C3N(I)=C3N(I)/CTOTAL
      RHNI = (C1N(I)/RH1) + (C2N(I)/RH2) + (C3N(I)/RH3)
      RHNN(I) = 1.0/RHNI
      DRHN = ( RHN(I)/RHNN(I) ) - 1
      DX(I+1) = DELX*DRHN
      EPS(I+1) = EPS(I) + DX(I+1)
  400 CONTINUE
C     GIVE VALUES FOR CIN'S BEYOND NX
      DO 405 I=NX+1,NXDOS,1
      C1N(I) = C1(I)
      C2N(I) = C2(I)
      C3N(I) = C3(I)
 405  CONTINUE
      C2NI11 = C2N(1)
      C2NI21 = C2N(2)
C
C ---- BIN DIMN CHANGE DUE TO FLOW OF ATOMS OF DIFF VOL
C
      RHN(1) = RHNN(1)
      C1(1) = C1N(1)
      C2(1) = C2N(1)
      C3(1) = C3N(1)
      NTK = 2
      DO 355 I=2,NX
      DELIM1 = (I-1)*DELX
      DO 356 J=NTK,NXDOS
      IF((EPS(J)+(J-1)*DELX).GE.DELIM1) THEN
      NTK = J
      DOX = (EPS(J)+(J-1)*DELX) - DELIM1
      GO TO 357
      END IF
 356  CONTINUE
 357  CONTINUE
      C1P(I) = ( (C1N(NTK-1)-C1N(NTK))*DOX/(DELX+DX(NTK)) ) +
     :C1N(NTK)
      C2P(I) = ( (C2N(NTK-1)-C2N(NTK))*DOX/(DELX+DX(NTK)) ) +
     :C2N(NTK)
      C3P(I) = ( (C3N(NTK-1)-C3N(NTK))*DOX/(DELX+DX(NTK)) ) +
     :C3N(NTK)
      RHNI = (C1P(I)/RH1) + (C2P(I)/RH2) + (C3P(I)/RH3)
      RHNP(I) = 1.0/RHNI
 355  CONTINUE
C
```

```
C     GIVE VALUES FOR CIN'S BEYOND NX
C
      DO 406 I=NX+1,NXDOS,1
      C1P(I) = C1(I)
      C2P(I) = C2(I)
      C3P(I) = C3(I)
 406  CONTINUE
C
      DO 375 I=2,NXDOS,1
      C1(I)=C1P(I)
      C2(I)=C2P(I)
      C3(I)=C3P(I)
      RHN(I)=RHNP(I)
      EPS(I)=0
 375  CONTINUE
C
C     WRITE( 27,*) C2NI1I, C2NI11, C2(1)
C     WRITE( 27,*) C2NI2I, C2NI21, C2(2)
C     WRITE( 27,*) C1N(2), C2N(2), C3N(2)
C     WRITE( 27,*) C1(1), C2(1), C3(1)
C     WRITE( 27,*) '     '
C
      IF (TDELT.LT.TNTV(INC)) GO TO 1341
C
      RHOUT = 0.0
      ARN1 = 0.0
      ARN2 = 0.0
      DO 600 I=1,NX+1,1
      XD(I)=(I-1)*DELX*1.E7
      X1(I)=C1(I)*100.0
      X2(I)=C2(I)*100.0
      X3(I)=C3(I)*100.0
C
      IF(I.EQ.NX+1)GO TO 1112
      ARN1 = ARN1 + C1(I)*DELX*RHN(I)
     '+ 0.5 * ( C1(I+1)*RHN(I+1) - C1(I)*RHN(I) ) * DELX
      ARN2 = ARN2 + C2(I)*DELX*RHN(I)
     '+ 0.5 * ( C2(I+1)*RHN(I+1) - C2(I)*RHN(I) ) * DELX
 1112 CONTINUE
C
      WRITE(6,114) XD(I),RHOUT,X1(I),X2(I),X3(I)
114   FORMAT(1X,F8.3,2X,E10.3,2X,F8.3,2X,F8.3,2X,F8.3,2X)
      RHOUT = RHOUT + RHN(I)*DELX/1.0E+16
600   CONTINUE
C
      WRITE(66,727) D11,D22,FLNC(INC),TMAX(INC)
 727  FORMAT (1X,'D11 = ',E10.3,'  D22 = ',E10.3,/,
     :1X,'FLUENCE = ',F8.3,'  TIME (HOURS) = ',F8.5,/)
      WRITE(66,726) ARN1, ARN2
 726  FORMAT (1X,'ARN1 = ',E10.3,'  ARN2 = ',E10.3,/)
      YMAX(IP)=XMAX(IP)*10000000.0
```

```
      YP(IP)=XP(IP)*10000000.0
      CSIG(IP)=SIG(IP)*10000000.0
      FLUXX(JF)=FLU(JF)*1.0E9/RH2
      WRITE(6,66)
      WRITE(6,67)
      WRITE(6,68)
 66   FORMAT (1X,'IMPLANT   MAX   FLUENCE  RANGE  SIGMA  SPUT Y',
     :'IELD   FLUX              ')
 67   FORMAT (1X,'ENERGY   DEPTH  (10**16)                    FE',
     :'   TA     (10**-9)       ')
 68   FORMAT (1X,' (KEV)   (NM)   (/SQ.CM) (NM)    (NM)
     :                          ')
      WRITE(6,69) ENERGY(IP),YMAX(IP),FLNC(INC),YP(IP),CSIG(IP),
     :SP01(II),SP02(II),FLUXX(JF)
 69   FORMAT (1X,F7.2,3X,F7.2,2X,F7.2,3X,F7.2,3X,F6.2,2X,F5.1,2X,
     : F5.1,3X,F7.2,6X)
      WRITE(6,666)
 666  FORMAT (1X,'DIFFUSIVITIES (SQ.CM/SEC)  ')
      WRITE(6,63)
 63   FORMAT (1X,'   D11          D12          D13        ',
     :'  D22          D33         ')
      WRITE(6,64) D11,D12,D13,D22,D33
 64   FORMAT (1X,5(E10.3,3X),7X)
      INC = INC + 1
1341  CONTINUE
      IF(TDELT.LT.TNTVMAX) GO TO 1342
134   CONTINUE
      STOP
      END
```

A.2 RISTRAN Fortran Code

Given below is the listing of the program 'Ristran' that was used to generate the implantation concentration profiles using the second phase precipitation model and the solute flux-defect coupling model.

```
C
C     THIS   PROGRAM  CALCULATES THE  CONCENTRATION PROFILES
C     OF THE  IMPLANTED ION & PRECIPITATES.
C
C     THE LANGUAGE USED IS FORTRAN-77.
C
C     TO  RUN THE  PROGRAM, AN  INPUT FILE IS REQUIRED WHICH
C     GIVES THE FOLLOWING DATA.:-
C     LINE  1) TITLE
C     LINE  2) GRID DIVISIONS, TIME INTERVAL
C     LINE  3) MAXIMUM DEPTH, OPTIMUM DIFFUSION COEFFICIENT
C     LINE  4) 1) NO. OF IMPLANTED ELEMENTS,
C              2) NO. OF PRODUCTS FORMED BY EACH ELEMENT,
C              3) NO. OF IMPLANTATION  SETS.
C     LINE  5) NO. OF INTERMEDIATE VALUES
C     LINE  6) THE INTERMEDIATE TIME IN HOURS
C     LINE  7) BLANK --- DIFFUSIVITIES
C     LINE  8) THE  DIFFUSIVITIES  D11, D12, D13 IN CM2/SEC.
C     LINE  9) THE  DIFFUSIVITIES  D21, D22, D23 IN CM2/SEC.
C     LINE 10) THE  DIFFUSIVITIES  D31, D32, D33 IN CM2/SEC.
C     LINE 11) BLANK --- DATA FOR SPECIES-1
C     LINE 12) INITIAL CONCENTRATION OF ELEMENT 1
C     LINE 13) ATOMIC DENSITY OF ELEMENT 1
C     LINE 14) ACTIVITY COEFFICIENT, GAMMA-0 OF ELEMENT 1
C     LINE 15) WAGNER INTERACTION PARAMETERS,E11,E12,E13
C     LINE 16) THE EQUILIBRIUM CONSTANT EK FOR ELEMENT 1 TO
C              FORM PRODUCT 1, FACTOR FACT (=M/N)
C     LINE 17) THE EQUILIBRIUM CONSTANT EK FOR ELEMENT 1 TO
C              FORM PRODUCT 2, FACTOR FACT (=M/N)
C     LINE 18) THE EQUILIBRIUM CONSTANT EK FOR ELEMENT 1 TO
C              FORM PRODUCT 3, FACTOR FACT (=M/N)
C     LINE 19) BLANK --- DATA FOR SPECIES-2
C     LINE 20) INITIAL CONCENTRATION OF ELEMENT 2
C     LINE 21) ATOMIC DENSITY OF ELEMENT 2
C     LINE 22) ACTIVITY COEFFICIENT, GAMMA-0 OF ELEMENT 2
C     LINE 23) WAGNER INTERACTION PARAMETERS,E21,E22,E23
```

```
C     LINE 24) THE EQUILIBRIUM CONSTANT EK FOR ELEMENT 2 TO
C              FORM PRODUCT 1, FACTOR FACT (=M/N)
C     LINE 25) THE EQUILIBRIUM CONSTANT EK FOR ELEMENT 2 TO
C              FORM PRODUCT 2, FACTOR FACT (=M/N)
C     LINE 26) THE EQUILIBRIUM CONSTANT EK FOR ELEMENT 2 TO
C              FORM PRODUCT 3, FACTOR FACT (=M/N)
C     LINE 27) BLANK --- DATA FOR SPECIES-3
C     LINE 28) INITIAL CONCENTRATION OF ELEMENT 3
C     LINE 29) ATOMIC DENSITY OF ELEMENT 3
C     LINE 30) ACTIVITY COEFFICIENT, GAMMA-0 OF ELEMENT 3
C     LINE 31) WAGNER INTERACTION PARAMETERS,E31,E32,E33
C     LINE 32) THE EQUILIBRIUM CONSTANT EK FOR ELEMENT 3 TO
C              FORM PRODUCT 1, FACTOR FACT (=M/N)
C     LINE 33) THE EQUILIBRIUM CONSTANT EK FOR ELEMENT 3 TO
C              FORM PRODUCT 2, FACTOR FACT (=M/N)
C     LINE 34) THE EQUILIBRIUM CONSTANT EK FOR ELEMENT 3 TO
C              FORM PRODUCT 3, FACTOR FACT (=M/N)
C     LINE 35) BLANK  --- IMPLANTATION PARAMETERS (1)
C     LINE 36) ELEMENT TYPE (1, 2, OR 3)
C     LINE 37) ENERGY, RANGE, STRAGGLING, SKEW, KURT, FOR SET 1
C     LINE 38) TIME IN  HOURS BEGIN AND END, THE CORRESPONDING
C              FLUENCE.
C     LINE 39) THE FLUX VALUE USED IN CM/SEC, LATTICE DILATION
C              FACTOR.
C     LINE 40) THE SPUTTERING YIELD USED.
C     LINE 41) BLANK  --- IMPLANTATION PARAMETERS (2)
C     LINE 42) ELEMENT TYPE (1, 2, OR 3)
C     LINE 43) ENERGY, RANGE, STRAGGLING, SKEW, KURT, FOR SET 2
C     LINE 44) TIME IN  HOURS BEGIN AND END, THE CORRESPONDING
C              FLUENCE.
C     LINE 45) THE FLUX VALUE USED IN CM/SEC, LATTICE DILATION
C              FACTOR.
C     LINE 46) THE SPUTTERING YIELD USED.
C     LINE 47) BLANK  --- IMPLANTATION PARAMETERS (3)
C     LINE 48) ELEMENT TYPE (1, 2, OR 3)
C     LINE 49) ENERGY, RANGE, STRAGGLING, SKEW, KURT, FOR SET 3
C     LINE 50) TIME IN  HOURS BEGIN AND END, THE CORRESPONDING
C             FLUENCE.
C     LINE 51) THE FLUX VALUE USED IN CM/SEC, LATTICE DILATION
C             FACTOR.
C     LINE 52) THE SPUTTERING YIELD USED.
C     LINE 53) ATOMIC DENSITY OF TARGET ELEMENT
C
C     NOTE: CAREFULLY CHOOSE WHAT'S TO BE ELEMENT-1, -2, OR
C     -3, ESPECIALLY WHEN THERE'S SIMULTANEOUS IMPLANTATION
C     OF MORE THAN ONE ELEMENT. THE PROGRAM WILL CONSIDER
C     ONLY ONE ELEMENT AT A TIME. ELEMENT-1 WILL COME FIRST.
C
C     THE  CALCULATED VALUES GO INTO AN  OUTPUT FILE. ASSIGN
C     STATEMENTS  HAVE TO  BE USED  DESIGNATE  THE INPUT AND
C     OUTPUT FILE.  FILE 5 IS FOR THE INPUT AND FILE 26 FOR
```

```
C     THE OUTPUT.
C
C     THE PROGRAM  MAKES USE OF  TWO  SUBROUTINES VMULFF AND
C     LINV1F WHICH ARE AVAILABLE IN THE IMSL (MATH) LIBRARY.
C
C     THE PROGRAM HAD BEEN CHANGED TO INCLUDE  THE EFFECT ON
C     CARBON  PICKUP DUE TO  ELEMENTS  OTHER THAN  THE  IMP-
C     LANTED IONS AND TO CONSIDER  SATURATION  OF  CARBON AT
C     SURFACE. THE CHANGES AND THE CORRESPONDING  STATEMENTS
C     ARE PRESENT AS COMMENT CARDS.
C
C     THE FOLL IS AN EXAMPLE OF AN INPUT FILE.:-
C     L   1)      60 N INTO TI/TRIM
C     L   2)    60,30.0
C     L   3)    4.0E-5
C     L   4)    3,3,3
C     L   5)    1
C     L   6)    8.889
C     L   7)      DIFFUSION COEFFICIENTS
C     L   8)    0.000E-16, 0.000E-15, 0.000E-15
C     L   9)    0.000E-15, 0.000E-15, 0.000E-15
C     L  10)    0.000E-15, 0.000E-15, 0.000E-15
C     L  11)      DATA FOR SPECIES-1
C     L  12)    0.0
C     L  13)    5.0E22
C     L  14)    1.0
C     L  15)    0.0,0.0,0.0
C     L  16)    0.0E6,1.0
C     L  17)    0.0E2,3.0
C     L  18)    0.0,1.0
C     L  19)      DATA FOR SPECIES-2
C     L  20)    0.0
C     L  21)    8.2E22
C     L  22)    1.0
C     L  23)    0.0,0.0,0.0
C     L  24)    0.0E3,2.0
C     L  25)    0.0,0.0
C     L  26)    0.0,0.0
C     L  27)      DATA FOR SPECIES-3
C     L  28)    0.0
C     L  29)    6.22E22
C     L  30)    1.0
C     L  31)    0.0,0.0,0.0
C     L  32)    0.0,1.0
C     L  33)    0.0,1.0
C     L  34)    0.0,1.0
C     L  35)      IMPLANTATION PARAMETERS (1)
C     L  36)    1
C     L  37)    60.0,10.29E-6,3.99E-6,-0.170,-0.42
C     L  38)    0.0,8.889,100.0
C     L  39)    2.42E13,0.8
```

```
C     L  40)    0.00
C     L  41)      IMPLANTATION PARAMETERS (2)
C     L  42)    2
C     L  43)    60.0,7.16E-6,4.00E-6,-0.00,0.000
C     L  44)    0.00,8.889,100.0
C     L  45)    5.59E13,0.0
C     L  46)    0.0
C     L  47)      IMPLANTATION PARAMETERS (3)
C     L  48)    3
C     L  49)    200.0,3.6E-6,1.1E-6,0.0,0.0
C     L  50)    0.00,0.00,00.0
C     L  51)    0.00E13,1.
C     L  52)    0.0
C     L  53)    8.42E22
C
      INTEGER R,S,H
      REAL*4 MATRIX(360,360), KUR(10), MAT(360,360)
      DIMENSION CAR(3,3,180),ASY(10),TIMBIT(10),NITV(10)
      DIMENSION CA(3,3,121), RHOUT(122)
      DIMENSION X(360), D(360), CN(3,180), CFE(180)
      DIMENSION XD(121), XN(3,180), XFE(121)
      DIMENSION A(3,3), B(3,3), C(3,3), T(3,3)
      DIMENSION DX(180), WKAREA(361)
      DIMENSION EPS(0:180), CP(3,180)
C
      DIMENSION  TIMAX(10), XP(10), TIMIN(10), DILK(10),
     'SPUT(10), FLU(10), FLNC(10), IATOM(10),
     'ENERGY(10), SIG(10), NTVI(10), NTVO(10)
C
      DIMENSION E(3,3), GAMO(3), GAMMA(3), CMAX(3,3), JATOM(3),
     'FACT(3,3), CNO(3), EK(3,3), CS(3), ARN(3), ARC(3,3)
      DIMENSION PROLAB(10), SPACE(1)
C
      DIMENSION RH(3), RHNP(180), RHN(180),CFEP(180)
C
      CALL ERRSET (208,256,-1)
C
C     READ CONDITIONS
C
C     XMAX / THE MAXIMUM DEPTH THAT WE ARE INTERESTED IN.
C
C     ICV (MAXIMUM = 3) IS THE NUMBER OF DIFFERENT CARBIDES
C     OR NITRIDES.
C     IMPV (MAXIMUM = 3) IS THE NUMBER OF DIFFERENT SPECIES
C     THAT ARE IMPLANTED.
C     ITV (MAXIMUM = 10) IS THE NUMBER OF TIMES THE
C     CONCENTRATION PROFILES ARE NEEDED DURING IMPLANTATION.
C     NIMP (MAXIMUM =10) IS THE NUMBER OF DIFFERENT IMPLANTATION
C     CONDITIONS.
C     TIMBIT (MAXIMUM = 10) ARE THE CORRESPONDING TIMES (HR)
C     OPEN (UNIT=5,STATUS='OLD',FILE='UNIMP.IND')
```

```
C     OPEN (UNIT=26,FILE='UNIMP.TUO')
C     OPEN (UNIT=25,FILE='UNIMP.OUT')
C     OPEN (UNIT=25,FILE=':OUTPUT')
      READ (5,1039) PROLAB
 1039 FORMAT(10A4)
  551 FORMAT(A4)
      READ (5,*)  NX, DELT
      READ (5,*)  XMAX
      READ (5,*)  IMPV, ICV, NIMP
      READ (5,*)  ITV
      READ (5,*)  (TIMBIT(I),I=1,ITV)
      READ (5,551) SPACE
      READ (5,*)  D11, D12, D13
      READ (5,*)  D21, D22, D23
      READ (5,*)  D31, D32, D33
C     Enn are the Wagner interaction parameters. These are
C     used to evaluate GAMx, where X is the implanted
C     species, reacting with FE. GAMx is evaluated from :
C          ln GAMx = ln GAMx0 + E11*C1 + E12*C2 + E13*C3
C
C     NOTE : ALL CONCENTRATIONS ARE IN ATOM FRACTIONS.
C
C     LET A REPRESENTATIVE REACTION BE :
C
C         m.FE + n.X  -->  FEmXn          (Delta-G = DELG)
C
C     Obtain DELG so that n = 1. Then, the equilibrium
C     constant, EK, is obtained from :
C         EK = exp(-DELG/RT)
C         EK = 1/[Ax] = 1/(GAMx * CMAXx)
C     Thus CMAXx is obtained from EK and GAMx.
C     FACT = M/N .... / THE NUMBER OF ATOMS OF IRON THAT
C                       ATTACH TO ONE ATOM OF X
C
      DO 811 I1 = 1,IMPV
      READ (5,551) SPACE
      READ (5,*)  CN0(I1)
      READ (5,*)  RH(I1)
      READ (5,*)  GAM0(I1)
      READ (5,*)  (E(I1,I2),I2 = 1,IMPV)
      DO 811 I = 1,ICV
      READ(5,*) EK(I1,I), FACT(I1,I)
 811  CONTINUE
C
      DO 810 IT = 1,NIMP
      READ (5,551) SPACE
      READ(5,*) IATOM(IT)
      READ(5,*) ENERGY(IT),XP(IT),SIG(IT),ASY(IT),KUR(IT)
      READ(5,*) TIMIN(IT), TIMAX(IT), FLNC(IT)
      READ(5,*) FLU(IT), DILK(IT)
      READ(5,*) SPUT(IT)
```

```
 810  CONTINUE
C
      READ(5,*) RHFE
C
      DELX = XMAX/NX
C
C     NQ IS THE TOTAL NUMBER OF TIME CYCLES
C     NTVI(I) IS THE TIME CYCLE IN WHICH THE IMPLANTATION I
C     BEGINS.
C     NTVO(I) IS THE TIME CYCLE IN WHICH THE IMPLANTATION I
C     ENDS.
C
      NQ = 1
      TMAX = 0.0
      DO 199 I = 1,NIMP,1
      IF(TIMAX(I).GT.TMAX)TMAX=TIMAX(I)
      NTVI(I) = 3600*TIMIN(I)/DELT
      NTVO(I) = 3600*TIMAX(I)/DELT
 199  CONTINUE
      NQ=3600*TMAX/DELT
C
      DO 299 IDD = 1,ITV,1
      NITV(IDD) = 3600*TIMBIT(IDD)/DELT
 299  CONTINUE
C
C     INITIAL CONDITIONS
C
C     INITIALIZE CONCENTRATIONS
C     THE GRID IS EXTENDED TO 1.5 TIMES THE REQUIRED DEPTH
C     TO ACCOUNT FOR TRANSLATION  DUE TO SPUTTERING AND
C     LATTICE DILATION; AND ALSO TO OBTAIN A BETTER TAIL.
C
      NXDOS = 3*NX/2
C
      DO 205 IMP=1,IMPV
      DO 205 I=1,NX,1
      XN(IMP,I) = 0.0
      DO 205 ICV1=1,ICV
      CA(IMP,ICV1,I) = 0.0
  205 CONTINUE
      DO 203 I=1,NXDOS,1
      CFE(I) = 1.0
      DO 200 IMP=1,IMPV
      CN(IMP,I) = CN0(IMP)
      CFE(I) = CFE(I) - CN0(IMP)
C
C     INITIALIZE CONCENTRATION OF PRODUCTS TO 0.0
C
      DO 200 ICV1=1,ICV
      CAR(IMP,ICV1,I) = 0.0
 200  CONTINUE
```

```
 203  CONTINUE
C
      DO 201 I=1,NXDOS,1
C     RHN(I) = RHFE
      RHNI = (CN(1,I)/RH(1)) + ((1-CN(1,I))/RHFE)
      RHN(I) = 1.0/RHNI
 201  CONTINUE
C
C     CONSIDER INITIAL REACTIONS
      DO 206 I=1,NXDOS,1
C
      DO 211 IMP = 1,IMPV
C
C     DETERMINATION OF GAMMA
C
      ALOGAM = ALOG(GAMO(IMP))
      DO 911 IRY = 1,IMPV
      ALOGAM = ALOGAM + E(IMP,IRY)*CN(IRY,I)
 911  CONTINUE
      GAMMA(IMP) = EXP(ALOGAM)
      CMINC = 100.0
C
      DO 130 IA = 1,ICV
      CMAX(IMP,IA)=100.0
         IF (EK(IMP,IA).EQ.0.0) GO TO 5526
CCC           CMAX(IMP,IA) = 100.0
               CMAX(IMP,IA) = 1.0/(GAMMA(IMP)*EK(IMP,IA))
              IF(CMAX(IMP,IA).GT.CMINC)GO TO 5526
                   CMINC = CMAX(IMP,IA)
                   IMINC = IA
 5526 CONTINUE
 130  CONTINUE
      IF (CN(IMP,I).LT.CMINC) GO TO 211
      QT=FACT(IMP,IMINC)*(CN(IMP,I)-CMINC)
      IF(QT.LT.CFE(I)) GO TO 140
      CAR(IMP,IMINC,I) = CAR(IMP,IMINC,I) + CFE(I)/
     'FACT(IMP,IMINC)
      CN(IMP,I) = CN(IMP,I) - CFE(I)/FACT(IMP,IMINC)
      CFE(I)=0.0
      GO TO 211
 140  CONTINUE
      CAR(IMP,IMINC,I) = CAR(IMP,IMINC,I) + CN(IMP,I)-CMINC
      CFE(I) = CFE(I)-FACT(IMP,IMINC)*(CN(IMP,I)-CMINC)
      CN(IMP,I) = CMINC
 211  CONTINUE
 206  CONTINUE
C
C  ..............  FOLL STATEMENTS HERE IF DIFF WITHIN LOOP
C     ITINC = 1
C     DO 134 NT=1,NQ
C     SPIU = 0.0
```

```
C     DO 146 NA=1,IMPV,1
C     JATOM(NA) = 0
C146  CONTINUE
C  ............... END ABOVE STATEMENTS.
C     FORM MATRIX
C
C     FIRST A,B,C MATRICES
      A(1,1) = DELT*D11/(2*DELX**2)
      A(1,2) = DELT*D12/(2*DELX**2)
      A(1,3) = DELT*D13/(2*DELX**2)
      A(2,1) = DELT*D21/(2*DELX**2)
      A(2,2) = DELT*D22/(2*DELX**2)
      A(2,3) = DELT*D23/(2*DELX**2)
      A(3,1) = DELT*D31/(2*DELX**2)
      A(3,2) = DELT*D32/(2*DELX**2)
      A(3,3) = DELT*D33/(2*DELX**2)
      B(1,1) = -2*A(1,1) -1
      B(2,2) = -2*A(2,2) -1
      B(3,3) = -2*A(3,3) -1
      B(1,2) = -2*A(1,2)
      B(1,3) = -2*A(1,3)
      B(2,1) = -2*A(2,1)
      B(2,3) = -2*A(2,3)
      B(3,1) = -2*A(3,1)
      B(3,2) = -2*A(3,2)
      DO 460 R=1,3,1
      DO 460 S=1,3,1
      C(R,S)=A(R,S)
460   CONTINUE
      DO 100 L=1,NX,1
      DO 100 H=1,NX,1
      IF (H.EQ.L-1) GO TO 50
      IF (H.EQ.L)   GO TO 60
      IF (H.EQ.L+1) GO TO 70
      DO 45 I=1,3,1
      DO 45 J=1,3,1
      T(I,J) = 0
45    CONTINUE
      GO TO 80
50    CONTINUE
      DO 550 R=1,3,1
      DO 550 S=1,3,1
      T(R,S)=A(R,S)
550   CONTINUE
      GO TO 80
60    CONTINUE
      DO 570 R=1,3,1
      DO 570 S=1,3,1
      T(R,S)=B(R,S)
570   CONTINUE
```

```
      GO TO 80
70    CONTINUE
      DO 590 R=1,3,1
      DO 590 S=1,3,1
      T(R,S)=C(R,S)
590   CONTINUE
80    CONTINUE
      DO 100 I=1,3,1
      DO 100 J=1,3,1
      M = 3*(L-1)+I
      N = 3*(H-1)+J
      MATRIX(M,N) = T(I,J)
100   CONTINUE
C
C     INVERT MATRIX
C
C
      LNVF2 = 3*NX
      LNVF3 = 360
      LNVF5 = 0
      CALL LINV1F (MATRIX,LNVF2,LNVF3,MAT,LNVF5,WKAREA,IER)
C     IFINV1 = 3*NX
C     CALL PFINV (IFINV1,MATRIX,WKAREA,MAT,IER)
C
C     END MATRIX SETUP
C
C     START LOOP
C     INC DETERMINES WHICH ELEMENT IS BEING IMPLANTED
C
      ITINC = 1
      DO 134 NT=1,NQ
      SPIU = 0.0
      DO 146 NA=1,IMPV,1
      JATOM(NA) = 0
 146  CONTINUE
      DO 147 NA=1,NXDOS,1
      DX(NA) = 0.0
      EPS(NA) = 0.0
 147  CONTINUE
      EPS(0) = 0.0
C  XN(*,*) IS USED AS A TEMPOR. VARIABLE AS WELL AS FOR O/P CONC.
      DO 144 NA=1,IMPV
      DO 144 I=1,NXDOS,1
      XN(NA,I) = 0.0
  144 CONTINUE
C
C-----BEGIN IMPLANTATION + LATTICE DILATION
C
      DO 135 NINC=1,NIMP,1
      IF(NTVI(NINC).EQ.NTVO(NINC))GO TO 135
      IF(NT.LT.NTVI(NINC).OR.NT.GT.NTVO(NINC))GO TO 135
```

```
      INC = IATOM(NINC)
      JATOM(INC) = 1
C
C     IMPLANTATION AT EACH GRID POINT
C
      DO 225 I=1,NXDOS,1
      DCINC = (FLU(NINC)*DELT*DELX/(2.507*SIG(NINC)))*EXP(-(((I-0.5)*
     'DELX-XP(NINC))**2)/(2*SIG(NINC)**2))
      ASYM=ASY(NINC)/6.
      KURT=KUR(NINC)/24.
      PSI= ((I-0.5)*DELX-XP(NINC))/SIG(NINC)
      DCINC=DCINC*(1-ASYM*(3*PSI-PSI**3)+KURT*(3-6*PSI**2+
     'PSI**4))
C     DX IS THE INCREASE IN THICKNESS OF LAYER IN ONE TIME INCREMENT
      DX(I) = DX(I) + ( DCINC*DILK(NINC)/RH(INC) )
C     XN HERE IS THE INCREASE IN ATOMS OF SPECIES INC IN A TIME INCREMENT
      XN(INC,I) = XN(INC,I) +  DCINC
 225  CONTINUE
C
 135  CONTINUE
C
C     BEGIN LATTICE DILATION
C     EPS AND DX ARE RELATED TO LATTICE DILATION
C
C
      DO 237 I = 1,NXDOS
      EPS(I)=EPS(I-1) +DX(I)
 237  CONTINUE
C
      DO 258 I = 1,NXDOS
      DCINC = 0.0
      DO 259 ICQ = 1,IMPV
C     CALCULATION OF DAMAGE AS SPECIES COUNT FOR RHN(I) IS SUPPRESSED
      IF(ICQ.EQ.2)GOTO 259
      DCINC = DCINC + XN(ICQ,I)
 259  CONTINUE
      DVOL =  DELX + DX(I)
      DO 260 ICQ = 1,IMPV
      CN(ICQ,I) = ( (RHN(I)*DELX*CN(ICQ,I)) + XN(ICQ,I) ) / DVOL
 260  CONTINUE
      RHN(I) = ( (RHN(I)*DELX) + DCINC )/DVOL
      DO 261 ICQ = 1,IMPV
      CN(ICQ,I) = CN(ICQ,I)/RHN(I)
 261  CONTINUE
      IF(CN(2,I).GT.DAMSAT)CN(2,I)=DAMSAT
 258  CONTINUE
C
      NTK = 2
      DO 255 I=2,NXDOS
      DELIM1 = (I-1)*DELX
      DO 256 J=NTK,NXDOS
```

```
      IF((EPS(J)+(J-1)*DELX).LT.DELIM1) GO TO 256
      NTK = J
      DOX = (EPS(J)+(J-1)*DELX) - DELIM1
      GO TO 257
 256  CONTINUE
 257  RHNP(I) = ( (RHN(NTK-1)-RHN(NTK))*DOX/(DELX+
     'DX(NTK)) ) + RHN(NTK)
      CFEP(I) = ( (CFE(NTK-1)-CFE(NTK))*DOX/(DELX+
     'DX(NTK)) ) + CFE(NTK)
      DO 255 ICQ = 1,IMPV
      CP(ICQ,I) = ( (CN(ICQ,NTK-1)-CN(ICQ,NTK))*DOX/(DELX+
     'DX(NTK)) ) + CN(ICQ,NTK)
 255  CONTINUE
C
      DO 275 I=2,NXDOS,1
      RHN(I)=RHNP(I)
      CFE(I)=CFEP(I)
      DO 275 J=1,IMPV
      CN(J,I)=CP(J,I)
 275  CONTINUE
C
C------LATTICE DILATION ENDS
C
C     SPUTTERING CONSIDERATION (SPIU = SPUTTERED LAYER IN
C     UNITS OF DELX).
C
      DO 148 INC = 1,NIMP,1
      IF(NTVI(INC).EQ.NTVO(INC))GO TO 148
      IF(NT.LT.NTVI(INC).OR.NT.GT.NTVO(INC))GO TO 148
C
      SPIU = SPIU + (FLU(INC)/RHN(1)*DELT*SPUT(INC))/DELX
C
 148  CONTINUE
C
C     DETERMINE THICKNESS OF SPUTTERED LAYER FROM SPIU.
C
      IKE = INT(SPIU)
      SPIKE = SPIU-IKE
      NXIKE = NXDOS-IKE-1
      DO 379 IQ=1,NXIKE
      DO 3791 IQC =1,IMPV
      CN(IQC,IQ)=CN(IQC,IKE+IQ)+((CN(IQC,IKE+IQ+1)-
     'CN(IQC,IKE+IQ))*SPIKE)
      DO 3791 IQD =1,ICV
      CAR(IQC,IQD,IQ)=CAR(IQC,IQD,IKE+IQ)+((CAR(IQC,IQD,IKE+
     'IQ+1)-CAR(IQC,IQD,IKE+IQ))*SPIKE)
 3791 CONTINUE
      CFE(IQ)=CFE(IKE+IQ)+((CFE(IKE+IQ+1)-
     'CFE(IKE+IQ))*SPIKE)
      RHN(IQ)=RHN(IKE+IQ)+((RHN(IKE+IQ+1)-
     'RHN(IKE+IQ))*SPIKE)
```

```
 379  CONTINUE
C
C     END SPUTTERING
C
C------END OF IMPLANTATION + SPUTTERING + LATTICE DILATION
C
C*****//CHANGE PROGRAM TO INCLUDE C INCREASE DUE TO CR//*****
C     C3(1)=.18*(100.-C2(1))
C     C1(1)=C10+C2(1)+C3(1)
C**************************************************************************
C
C     C1(1)=C10+C2(1)
C
C*****//CHANGE PROG TO CONSIDER SATURATION OF DAMAGE AT SURFACE//
C     IF (C1(1).GE.0.16) THEN
C     CN(2,1)=0.0
C**************************************************************************
C
C     FORM D
C
C     CS(I) AND CN(I,NX+1) ARE PSEODO-POINTS OUTSIDE THE CURRENT
C     F-D GRID.  CS(I) ARE  GIVEN A VALUE EQUAL TO THAT AT THE
C     SURFACE  SINCE  THERE ARE NO ATOMS  DIFFUSING OUT FROM
C     THE SURFACE. CN(I,NX+1) ARE ALREADY KNOWN FROM THE EXTEND-
C     ED SPACE GRID USED (I.E. 1.5*NX INSTEAD OF NX GRID POINTS)
C
      DO 231 J = 1,IMPV
      CS(J) = CN(J,1)
 231  CONTINUE
C
      D(1) = (DELT*D11/(2*DELX**2))*(2*CN(1,1)-CN(1,2)-2*CS(1))-
     'CN(1,1)+(DELT*D12/(2*DELX**2))*(2*CN(2,1)-CN(2,2)-2*CS(2))
     '+(DELT*D13/(2*DELX**2))*(2*CN(3,1)-CN(3,2)-2*CS(3))
      D(2) = (DELT*D22/(2*DELX**2))*(2*CN(2,1)-CN(2,2)-2*CS(2))-
     'CN(2,1)+(DELT*D23/(2*DELX**2))*(2*CN(3,1)-CN(3,2)-2*CS(3))
     '+(DELT*D21/(2*DELX**2))*(2*CN(1,1)-CN(1,2)-2*CS(1))
      D(3) = (DELT*D33/(2*DELX**2))*(2*CN(3,1)-CN(3,2)-2*CS(3))-
     'CN(3,1)+(DELT*D32/(2*DELX**2))*(2*CN(2,1)-CN(2,2)-2*CS(2))
     '+(DELT*D31/(2*DELX**2))*(2*CN(1,1)-CN(1,2)-2*CS(1))
      NXM1 =NX-1
      DO 300 I=2,NXM1,1
      D(3*I-2) = (DELT*D11/(2*DELX**2))*(2*CN(1,I)-CN(1,I+1)-
     'CN(1,I-1))-CN(1,I)+(DELT*D12/(2*DELX**2))*(2*CN(2,I)-
     'CN(2,I-1)-CN(2,I+1))+(DELT*D13/(2*DELX**2))*(2*CN(3,I)-
     'CN(3,I-1)-CN(3,I+1))
      D(3*I-1) = (DELT*D22/(2*DELX**2))*(2*CN(2,I)-CN(2,I+1)-
     'CN(2,I-1))-CN(2,I)+(DELT*D23/(2*DELX**2))*(2*CN(3,I)-
     'CN(3,I-1)-CN(3,I+1))+(DELT*D21/(2*DELX**2))*(2*CN(1,I)-
     'CN(1,I-1)-CN(1,I+1))
      D(3*I) = (DELT*D33/(2*DELX**2))*(2*CN(3,I)-CN(3,I+1)-
     'CN(3,I-1))-CN(3,I)+(DELT*D32/(2*DELX**2))*(2*CN(2,I)-
```

```
     'CN(2,I-1)-CN(2,I+1))+(DELT*D31/(2*DELX**2))*(2*CN(1,I)-
     'CN(1,I-1)-CN(1,I+1))
300   CONTINUE
      D(3*NX-2)=(DELT*D11/(2*DELX**2))*
     '(2*CN(1,NX)-2*CN(1,NX+1)-CN(1,NX-1))-CN(1,NX)
     '+(DELT*D12/(2*DELX**2))*
     '(2*CN(2,NX)-2*CN(2,NX+1)-CN(2,NX-1))
     '+(DELT*D13/(2*DELX**2))*
     '(2*CN(3,NX)-2*CN(3,NX+1)-CN(3,NX-1))
      D(3*NX-1)=(DELT*D22/(2*DELX**2))*
     '(2*CN(2,NX)-2*CN(2,NX+1)-CN(2,NX-1))-CN(2,NX)
     '+(DELT*D23/(2*DELX**2))*
     '(2*CN(3,NX)-2*CN(3,NX+1)-CN(3,NX-1))
     '+(DELT*D21/(2*DELX**2))*
     '(2*CN(1,NX)-2*CN(1,NX+1)-CN(1,NX-1))
      D(3*NX)=(DELT*D33/(2*DELX**2))*
     '(2*CN(3,NX)-2*CN(3,NX+1)-CN(3,NX-1))-CN(3,NX)
     '+(DELT*D32/(2*DELX**2))*
     '(2*CN(2,NX)-2*CN(2,NX+1)-CN(2,NX-1))
     '+(DELT*D31/(2*DELX**2))*
     '(2*CN(1,NX)-2*CN(1,NX+1)-CN(1,NX-1))
C
C       SOLVE SYSTEM OF EQUATIONS
C
      JVMLF3=3*NX
      JVMLF4=3*NX
      JVMLF5=1
      JVMLF6=360
      JVMLF7=360
      JVMLF9=360
      CALL VMULFF(MAT,D,JVMLF3,JVMLF4,JVMLF5,JVMLF6,JVMLF7,
     'X,JVMLF9,IERR)
C     IMMMV4=3*NX
C     IMMMV5=1
C     IMMMV6=3*NX
C     CALL FMMMV(MAT,D,X,IMMMV4,IMMMV5,IMMMV6)
C
C     FROM X FORM CONCENTRATION VECTORS
C
      DO 401 I = 1,NX,1
      CN(1,I) = X(3*I-2)
      CN(2,I) = X(3*I-1)
      CN(3,I) = X(3*I)
 401  CONTINUE
C
C***** BEGIN PRECIPITATION ************************************
C
      DO 136 INC = 1,IMPV,1
      IF(JATOM(INC).EQ.0)GO TO 136
```

```
      DO 400 I = 1,NXDOS,1
C     I = SPACE INCREMENT
C
      CMINC = 100.0
C
      ALOGAM = ALOG(GAMO(INC))
      DO 912 IRY = 1,IMPV
      ALOGAM = ALOGAM + E(INC,IRY)*CN(IRY,I)
 912  CONTINUE
      GAMMA(INC) = EXP(ALOGAM)
C
      DO 131 IA = 1,ICV
            CMAX(INC,IA) = 100.0
         IF (EK(INC,IA).EQ.0.0) GO TO 6299
             CMAX(INC,IA) = 1.0/(GAMMA(INC)*EK(INC,IA))
            IF(CMAX(INC,IA).GT.CMINC)GO TO 6299
                 CMINC = CMAX(INC,IA)
                 IMINC = IA
 6299      CONTINUE
 131  CONTINUE
      IF (CN(INC,I).LT.CMINC) GO TO 212
      QT=FACT(INC,IMINC)*(CN(INC,I)-CMINC)
      IF(QT.LT.CFE(I)) GO TO 141
      CAR(INC,IMINC,I) = CAR(INC,IMINC,I) + CFE(I)/
     'FACT(INC,IMINC)
      CN(INC,I) = CN(INC,I) - CFE(I)/FACT(INC,IMINC)
      CFE(I)=0
      GO TO 212
 141  CONTINUE
      CAR(INC,IMINC,I) = CAR(INC,IMINC,I) + CN(INC,I)-CMINC
      CFE(I) = CFE(I)-FACT(INC,IMINC)*(CN(INC,I)-CMINC)
      CN(INC,I) = CMINC
 212  CONTINUE
C
 400  CONTINUE
 136  CONTINUE
C
C     CHECK IF OUTPUT IS REQUIRED.
C
      IF (NT.NE.NITV(ITINC).AND.NT.NE.NQ) GO TO 134
C
      NXS1 =NX+1
      RHOUT(1) = 0.0
      DO 601 I=1,NXS1,1
      XD(I)=(I-1)*DELX*1.E7
      RHOUT(I+1)=RHOUT(I) + RHN(I)*DELX/1.0E16
      DO 600 ID = 1,IMPV
      XN(ID,I)=CN(ID,I)*100.0
      DO 600 IE = 1,ICV
      CA(ID,IE,I) = CAR(ID,IE,I)*100.0
      XN(ID,I)=XN(ID,I)+CA(ID,IE,I)
```

```
 600  CONTINUE
 601  CONTINUE
      DO 1112 J = 1,IMPV
      ARN(J) = 0.0
      DO 1112 K = 1,ICV
      ARC(J,K) = 0.0
 1112 CONTINUE
      DO 1111 I=1,NX
      DO 1111 J=1,IMPV
      ARN(J) = ARN(J)+CN(J,I)*DELX*RHN(I)+.5*(CN(J,I+1)*RHN(I+1)
     ,-CN(J,I)*RHN(I))*DELX
C
      DO 1111 K=1,ICV
      ARC(J,K)=ARC(J,K)+CAR(J,K,I)*DELX*RHN(I)+
     ,.5*(CAR(J,K,I+1)*RHN(I+1)-CAR(J,K,I)*RHN(I))*DELX
 1111 CONTINUE
C
      DO 1113 J = 1,IMPV
      WRITE (26,103) J,TIMBIT(ITINC)
 103  FORMAT(//,1X,'ELEMENT = ',I2,5X,'TIME = ',F10.3,1X,'HOURS',
     '//,1X,5X,'XD',10X,'RHOUT',5X,10X,'XN',
     '9X,'CAR1',8X,'CAR2',8X,'CAR3',/)
      DO 1114 I = 1,NXS1
      WRITE (26,14) XD(I),RHOUT(I),XN(J,I),(CA(J,K,I),K=1,ICV)
 1114 CONTINUE
  14  FORMAT(1X,E10.3,2X,E10.3,2X,E10.3,2X,E10.3,2X,E10.3,2X,E10.3)
1499  FORMAT(5(E10.3,2X))
      WRITE (26,104)
 104  FORMAT(//,1X,'AREA UNDER THE CURVE',//,1X,5X,'XN',9X,
     ''CAR1',8X,'CAR2',8X,'CAR3',/)
      WRITE(26,14) ARN(J),(ARC(J,I),I=1,ICV)
 1113 CONTINUE
      WRITE (25,1038) NX,PROLAB
 1038 FORMAT(1X,I3/1X,10A4)
      TIMOTH = NT*DELT/3600
      WRITE (25,1037) ITINC, TIMBIT(ITINC),TIMOTH,DELT,
     'NT,D11,D12,D22
 1037 FORMAT(1X,I3,5X,2F10.3,3X,F10.3,5X,I3,
     '/,' D11 = ',E10.3,'  D12 =',E10.3,'  D22 =',E10.3)
      DO 1198 I=1,NXS1
      WRITE (25,1499) XD(I),RHOUT(I),(XN(J,I),J=1,IMPV)
1198  CONTINUE
C
      ITINC = ITINC + 1
      IF(ITINC.GT.ITV)TIMBIT(ITINC)=TMAX
 134  CONTINUE
C
      WRITE (26,114)
 114  FORMAT(//,1X,'INPUT VALUES',//)
      WRITE(26,1051)  NX, DELT
 1051 FORMAT(1X,'# GRID POINTS = ',I3,4X,'DELTA T USED = ',
```

```
     'F10.3)
      WRITE(26,105)  XMAX
 105  FORMAT(1X,'XMAX = ',E10.3)
      WRITE(26,106)  IMPV, ICV, NIMP
 106  FORMAT(1X,'IMPV = ',I5,5X,'ICV = ',I5,5X,'NIMP = ',I5)
      WRITE(26,63) D11, D12, D13
      WRITE(26,64) D21, D22, D23
      WRITE(26,65) D31, D32, D33
 63   FORMAT (1X,' D11 = ',E10.3,' D12 = ',E10.3,' D13 = ',
     'E10.3)
 64   FORMAT (1X,' D21 = ',E10.3,' D22 = ',E10.3,' D23 = ',
     'E10.3)
 65   FORMAT (1X,' D31 = ',E10.3,' D32 = ',E10.3,' D33 = ',
     'E10.3)
C     WRITE(26,107)
C107  FORMAT(/,1X,'WAGNER INTERACTION PARAMETERS',/)
      DO 8100 IT = 1,IMPV
      WRITE(26,115)  IT
 115  FORMAT(//,1X,'ELEMENT = ',I2,/)
      WRITE(26,109)  GAM0(IT),CN0(IT)
 109  FORMAT(1X,'GAM0 = ',F10.3,5X,'CN0 = ',F10.3)
      WRITE(26,108)  (IT,I2,E(IT,I2),I2 = 1,IMPV)
 108  FORMAT(1X,'E',2I1,' = ',F10.3,2X,
     ''E',2I1,' = ',F10.3,2X,'E',2I1,' = ',F10.3,2X)
      DO 8100 I = 1,ICV
      WRITE(26,113) I, EK(IT,I), I, FACT(IT,I)
 113  FORMAT(1X,'EK',I2,' = ',E10.3,5X,'FACT',I2,' = ',F10.3)
 8100 CONTINUE
      DO 8101 IT = 1,NIMP
      WRITE(26,116)  IT, IATOM(IT)
 116  FORMAT(//,1X,'IMPLANT CYCLE # ',I2,' USING ELEMENT # ',I2,/)
      WRITE(26,110) ENERGY(IT), XP(IT), SIG(IT)
 110  FORMAT(1X,'ENERGY = ',F10.3,5X,'RANGE = ',E10.3,5X,
     ''STRAGGLING = ',E10.3)
      WRITE(26,111) TIMIN(IT), TIMAX(IT), FLNC(IT)
 111  FORMAT(1X,'TIME IN = ',F10.3,5X,'TIME OUT = ',F10.3,
     '5X,'FLUENCE = ',F10.3)
      WRITE(26,112) FLU(IT), SPUT(IT), DILK(IT)
 112  FORMAT(1X,'FLUX = ',E10.3,5X,'SPUTTERING YIELD = ',F10.3,
     '5X,'DILAT = ',F10.3)
 8101 CONTINUE
      STOP
      END
```

A.3 TRAL Fortran Code

Given below is the listing of the program 'TRAL' that was used for the dynamic Monte Carlo simulation.

```
C
C     PROGRAM TRALL - MONTE CARLO SIMULATION OF ION IMPLANTATION
C     USES 100 OR LESS TARGET LAYERS AND MAXIMUM 3 COMPONENTS,
C     THE FIRST BEING THE ION.
C     USES UNIVERSAL SCREEN. LENGTH & POTENTIAL / ZIEGLER ELECTR.
C     STOPPING (NOVEMBER 1985).
C
C     INCLUDED IRAND IN THE WRITE STATEMENT 2/22/89
C
C
C     INPUT:
C                  FILE 4
C          TABLES FOR RSTOP SUBROUTINE
C                  FILE 5
C       1  EOKEV,DOSTEP,NT
C       2  XO,ALFA,BE,SBE,ED,EF,IRAND
C       3  NH,ICLMIT,CRTCNC (NH SHOULD BE A MULTIPLE OF 50)
C       4  CWMAX,CWMIN (MAXIMUN AND MINIMUN BIN LENGTH)
C       5  IZ(1),.....,IZ(*) (1, ION  2,3,4...:TARGET)
C       6  M(1,.......,M(*)  MASSES
C       7  SV(1),.....,SV(*) SPECIFIC VOLUMES
C       8  XX(L+1),T(L,I)
C       9  0.0 - END OF DATA FOR XX(L+1)
C      10  ICL,OUTPUT(1,..,ICL)
C      11  BEGINING DOSE, DOSACM - USEFUL WHEN SPLITTING LONG RUNS
C
C
      LOGICAL MRKVAC(50),MARKMG,MRKMGR
      LOGICAL IDEATH(7000),MRKI1(7000)
      LOGICAL IDETH2(7000)
      REAL M,M2,LS,LM,ION,MY,MU
      REAL*8 XSUM,X2SUM,X3SUM,X4SUM,Y2SUM
      REAL*8 SIGMAX,SIGMAY
      REAL*8 AVEX,VARI,SIGMA,V,V2,GAMMA,BETA,YH
      DIMENSION LL(50),LS(50),LM(100)
     ,,X1(50),P(50),PHI(50)
     ,,X(50),Y(50),ZET(50),PL(50),COSIN(50),SINE(50),COSY(50),COSZ(50)
```

```
     ,,SELECT(100,4),IESP(50),S2(50),TAU(50),DEN(50)
     ,,E(50),IBIN(50),SV2(100)
      DIMENSION COSXR(7000),COSYR(7000),COSZR(7000),SINXR(7000)
     ,,XR(7000),YR(7000),ZR(7000),INDC(7000)
      DIMENSION COSXRR(7000),COSYRR(7000),COSZRR(7000),SINXRR(7000)
     ,,ENR(7000),RLS(7000),IESPR(7000),LLR(7000)
     ,,PR(7000),PHIR(7000),XRR(7000),YRR(7000),ZRR(7000)
     ,,LLRR(7000),IESPRR(7000)
     ,,ENRR(7000),RLSR(7000)
      DIMENSION CW(100)
      DIMENSION RHO(100),T(100,3)
      DIMENSION SE(100,100,3)
      DIMENSION H(100),XX(101),M2(100),Z2(100)
     ,,PMAX(100)
      DIMENSION Z(3),EREC(3),AR(3),EC(3,3),A(3,3)
     ,,MY(3,3),MU(3,3),F(3,3)
      DIMENSION DMG(100),ION(100),ESP(3),IRP(100)
      DIMENSION DELC(100,3),SV(3),CONC1(100,3)
     ,,UX(100),OUTPUT(20)
      DIMENSION IVAC(100,3),ISTL(100,3),IMID(50)
      DIMENSION IDEAD(50),MRKSTP(50),IMARK(50),ILIVE(50)
      COMMON/RAN1/RA1(50),RA2(50),RA3(50)
      COMMON/RAN2/IRAND,INUM,RN1(7000),RN2(7000),RN3(7000)
      COMMON/MAG/MARKMG(50),EPS(50),B(50),C2(50),AUX1(50),AUX2(50)
      COMMON/MAG2/ITREE,MRKMGR(7000),EPSR(7000),BR(7000),CR(7000)
     ,,AUX1R(7000),AUX2R(7000)
      COMMON/COEF/SCOEF(8,92),RCOEF(5,92)
      COMMON/RSTP/N,E0KEV,IZ(3),M(3),SE1(100,3,3)
      DATA DMG/100*0./,AVEX/0./,ION/100*0./,IRP/100*0/,SV2/100*0./
      DATA PI/3.1415926/,IB/0/,XSUM/0./,IT/0/,EB/0./,ET/0./
      DATA ISPUT/0/,ESPUT/0./,ESP/3*0./
      DATA X3SUM/0./,X4SUM/0./,Y2SUM/0./,X2SUM/0./
      DATA IVAC/300*0/,ISTL/300*0/
      DATA H/100*0./,SE/30000*0./,ITTR/0/,IC/1/,DOSACM/0./,IDOSAC/0/
      DATA NVAC/0/,NISTL/0/,BT/0./,TTT/0./,SPUTT/0./
      DATA M2/100*0./,Z2/100*0./,XSURF/0./
      DATA PL/50*0./,TAU/50*0./,LS/50*0./,SELECT/400*0./
      DATA MAXLIV/0/,TIME/0./
      DATA MRKVAC/50*.FALSE./,MRKSTP/50*0/
      DATA IMARK/50*0/,IESP/50*1/,PHI/50*0./,P/50*0./
      DATA IDEATH/7000*.FALSE./,MRKI1/7000*.FALSE./
      DATA IDETH2/7000*.FALSE./
      DO1I=1,50
    1 MARKMG(I)=.FALSE.
      DO2I=1,7000
    2 MRKMGR(I)=.FALSE.
      SQPI=SQRT(PI)
      READ(4,*)RCOEF,SCOEF
      READ(5,*)E0KEV,DOSTEP,NT
      READ(5,*)X0,ALFA,BE,SBE,ED,EF,IRAND
      READ(5,*)NH,ICLMIT,CRTCNC
```

```
      READ(5,*)CWMAX,CWMIN
      IF(IRAND.EQ.0)IRAND=65549
      E0=E0KEV*1000
      N=NT+1
      N1=N+1
      IF(ED.EQ.0.) ED=25.
      IF(BE.EQ.0.) BE=2.
      IF(SBE.EQ.0.) SBE=5.
      IF(EF.EQ.0.) EF=ED
      ALPHA=ALFA*PI/180.
      COSINA=COS(ALPHA)
      SINEA=SQRT(1.-COSINA*COSINA)
      READ(5,*)IZ
      READ(5,*)M
      READ(5,*)SV
C
      Z(1)=IZ(1)
      Z(2)=IZ(2)
      Z(3)=IZ(3)
      XX(1)=0.
      DO 77 L=1,100
      READ(5,*)XX(L+1),(T(L,I),I=1,N)
      IF(XX(L+1).EQ.0.)GOTO 80
   77 CONTINUE
      L=101
   80 L=L-1
      L1=L+1
      DO 90 I=1,L
   90 CW(I)=XX(I+1)-XX(I)
      TT=XX(L+1)
      READ(5,*)ICL,OUTPUT
      READ(5,*)DOSACM
      DOSACM0=DOSACM
      DO 160 J=1,N
      DO 160 I=1,N
      MY(J,I)=M(J)/M(I)
      MU(J,I)=1./MY(J,I)
      EC(J,I)=4.*MY(J,I)/(1.+MY(J,I))**2
      A(J,I)=.5292*.8853/(Z(J)**.23 + Z(I)**.23)
      F(J,I)=A(J,I)/(Z(J)*Z(I)*14.41*(1.+MY(J,I)))
  160 CONTINUE
C
C                   GET ELECTRONIC STOPPING CROSS SECTIONS
      CALL RSTOP
C
C
C          START NEW DOSE STEP
C
 6666 CONTINUE
C                        AVERAGE MASS AND ATOMIC NUMBER
      DO 110 LI=1,L
```

```
      H(LI)=0.
      M2(LI)=0.
  110 Z2(LI)=0.
      DO 111 I=1,N
      DO 111 LI=1,L
  111 H(LI)=H(LI)+T(LI,I)
      DO 120 I=1,N
      DO 120 LI=1,L
      T(LI,I)=T(LI,I)/H(LI)
      M2(LI)=M2(LI)+T(LI,I)*M(I)
      SV2(LI)=SV2(LI)+T(LI,I)*SV(I)
  120 Z2(LI)=Z2(LI)+T(LI,I)*Z(I)
C             AVERAGE ELECTRONIC STOPPING FOR EACH LAYER
      IF(IDOSAC.NE.0)GOTO142
      DO150LI=1,L
  150 RHO(LI)=1./SV2(LI)
      DO143J=1,N
      DO143LI=1,L
  143 CONC1(LI,J)=RHO(LI)*T(LI,J)
  142 DO141LI=1,L
      LM(LI)=RHO(LI)**(-1./3.)
  141 PMAX(LI)=LM(LI)/SQPI
      DO 140 LI=1,L
      DO 140 I=1,100
      DO 140 J=1,N
      SE(LI,I,J)=0.
      DO 140 NN=1,N
  140 SE(LI,I,J)=SE(LI,I,J)+SE1(I,J,NN)*CONC1(LI,NN)
C            SPECIES SELECTION VECTOR ,SELECT(LI,1)=0.
      DO147I=2,N1
      DO147LI=1,L
      TLI1=T(LI,I-1)
      IF(TLI1.LT.CRTCNC)TLI1=0
  147 SELECT(LI,I)=SELECT(LI,I-1)+TLI1
C          SELECTION RENORMALIZATION
      DO148I=2,N1
      DO148LI=1,L
  148 SELECT(LI,I)=SELECT(LI,I)/SELECT(LI,N1)
C
      III=NH/50
      IF(III*50.LT.NH)III=III+1
      DO666IO=1,III
      DO619J=1,50
  619 IDEAD(J)=0
      IEND=0
C                     RANDOM NUMBERS
C
C
      CALL RANDU
C                           NEW ION HISTORY
      DO 620 J=1,50
```

```
      E(J)=E0
      COSIN(J)=COSINA
      SINE(J)=SINEA
      COSY(J)=SINEA
      COSZ(J)=0.
      X(J)=X0+LM(1)*COSIN(J)*RA1(J)
      Y(J)=LM(1)*COSY(J)*RA1(J)
      ZET(J)=0.
  620 PL(J)=0.
C                              CYCLING IONS
C     *ICLIMT' IS A DATA THAT TELLS HOW MANY TIMES ONE ION
C     COLLIDES BEFORE  STARTING THE (AT MOST) 50*ICLIMT
C     CASCADES SIMULTANEOUSLY
C
C     AFTER CASCADES RETURN TO LABEL 5555
C
 5555 ITREE=0
      DO5000II=1,ICLMIT
C
C     RANDOM NUMBERS FIRST
C
      CALL RANDU
C
      DO328I=1,L
      DO328J=1,50
      IF(IDEAD(J).EQ.1)GOTO328
C      GET THE LLAYER WHERE THE ION IS MOVING
      IF(X(J).LT.XX(I))GOTO328
      IF(X(J).GE.XX(I+1))GOTO328
      LL(J)=I
      LS(J)=LM(I)
C
C      FIRST CALCULATE ELECTRONIC LOSSES AND STORE
C
      IE=E(J)/E0KEV/10.+.5
      IF(IE.LE.0)THEN
                 DEE=0
      ELSE
      DEE=LS(J)*SE(I,IE,1)
      END IF
      E(J)=E(J)-DEE
      ION(I)=ION(I)+DEE
C
      IF(E(J).LT.EF)THEN
                    MRKSTP(J)=1
                    IDEAD(J)=1
                    LS(J)=0.
                    Y2SUM=Y2SUM+Y(J)*Y(J)
                    XSUM=XSUM+X(J)
                    X2SUM=X2SUM+X(J)*X(J)
                    X3SUM=X3SUM+X(J)*X(J)*X(J)
```

```
                    X4SUM=X4SUM+X(J)*X(J)*X(J)*X(J)
      ELSE
C          IMPACT PARAMETER, AZIMUTH ANGLE AND TARGET LOCATION X1
      PHI(J)=2.*PI*RA1(J)
      P(J)=SQRT(RA2(J))*PMAX(I)
      X1(J)=X(J)-P(J)*COS(PHI(J))*SINE(J)
      IF(X1(J).GT.PMAX(I)) GOTO328
      P(J)=P(J)+PMAX(I)
      PHI(J)=PHI(J)+PI
      X1(J)=X(J)-P(J)*COS(PHI(J))*SINE(J)
      IF(X1(J).GE.PMAX(I)) GOTO328
C                      IMARK(J)=1 MEANS NO COLLISION
      IMARK(J)=1
      END IF
  328 CONTINUE
C        TARGET SPECIES #IESP(J), EPSILON AND B VALUES
      DO239J=1,50
      IBIN(J)=0
      IF(IMARK(J).EQ.1.OR.IDEAD(J).EQ.1)GOTO239
      IF(X1(J).GE.XX(LL(J)+1))THEN
                             IBIN(J)=1
      ELSE
      IF(X1(J).LT.XX(LL(J)))IBIN(J)=-1
      END IF
  239 CONTINUE
      DO240I=2,N1
      DO240J=1,50
      IF(IMARK(J).EQ.1.OR.IDEAD(J).EQ.1)GOTO240
      IF(RA3(J).LE.SELECT(LL(J)+IBIN(J),I-1))GOTO240
      IF(RA3(J).GT.SELECT(LL(J)+IBIN(J),I))GOTO240
      IESP(J)=I-1
  240 CONTINUE
      DO247J=1,50
      IMID(J)=(1-IMARK(J))*(1-IDEAD(J))
      EPS(J)=IMID(J)*E(J)*F(1,IESP(J))
      B(J)=IMID(J)*P(J)*(1./A(1,IESP(J)))
      MARKMG(J)=.TRUE.
      IF(IMID(J).EQ.0)MARKMG(J)=.FALSE.
      IF(EPS(J).GE.10.)THEN
                      S2(J)=1./(1.+(2.*EPS(J)*B(J))**2)
                      C2(J)=1.-S2(J)
                      TAU(J)=0.
                      MARKMG(J)=.FALSE.
C              MARKMG(J)=.TRUE. MEANS ION 'J' CALLS MAGIC
                      END IF
  247 CONTINUE
C                   RESOLVE THE COLLISION
C
c     TIM1=ZA01AS(DUMMY)
      CALL MAGIC
c     TIM2=ZA01AS(DUMMY)
```

```
c     TIME=TIME+TIM2-TIM1
C
C
      DO241J=1,50
      C2(J)=IMID(J)*(C2(J)-1)+1
      P(J)=IMID(J)*P(J)
      IESP(J)=IMID(J)*(IESP(J)-1)+1
      PHI(J)=IMID(J)*PHI(J)
      C2(J)=C2(J)*C2(J)
      IF(C2(J).GT.1.)C2(J)=1.
      S2(J)=1.-C2(J)
      DEN(J)=EC(1,IESP(J))*S2(J)*E(J)
  241 CONTINUE
      DO562J=1,50
C                              STORE DAMAGE
      DMG(LL(J))=DMG(LL(J))+DEN(J)
C
C     IF THE RECOIL ENERGY IS NOT ENOUGH TO START THE
C     CASCADE CONTINUE FOLLOWING ION,OTHERWISE PREPARE
C     CASCADE SUPERVECTORS...(THEY ARE REALY HUGE)
C
      IF(IMID(J).EQ.0.OR.((X1(J).GT.2.*LM(1).AND.DEN(J).LT.ED).OR.
     ,(X1(J).LE.2.*LM(1).AND.DEN(J).LT.SBE)))THEN
                                                 INDC(J)=7000
      ELSE
      MRKVAC(J)=.TRUE.
      ITREE=ITREE+1
      INDC(J)=ITREE
      END IF
  562 CONTINUE
      DO280J=1,50
      TAU(J)=P(J)*SQRT(S2(J)/C2(J))
      X(J)=X(J)-TAU(J)*COSIN(J)
      Y(J)=Y(J)-TAU(J)*COSY(J)
      ZET(J)=ZET(J)-TAU(J)*COSZ(J)
      PL(J)=PL(J)+LS(J)-TAU(J)
      E(J)=E(J)-DEN(J)
      PSI=ATAN(SQRT(1.-(2.*C2(J)-1)*(2.*C2(J)-1.))/
     ,(2.*C2(J)-1.+MY(1,IESP(J))+1.E-7))
      IF(PSI.LT.0.) PSI=PSI+PI
C
C       FIND NEW DIRECTIONS (CX2,CY2,CZ2) GIVEN THE OLD ONES
C       (COSIN,COSY,COSZ) C AND AZIMUTAL AND POLAR ANGLES (PHI,PSI).
C       THIS IS SUBROUTINE COSINS ONLINE
C
      CPHI=COS(PHI(J))
      SPHI=SIN(PHI(J))
      CPSI=COS(PSI)
      SPSI=SQRT(1.-CPSI*CPSI)
      SRAT=SPSI/(SINE(J)+1.E-7)
      CX22=CPSI*COSIN(J)+SRAT*SINE(J)*SINE(J)*CPHI
```

```
      CY22=CPSI*COSY(J)-SRAT*(COSY(J)*COSIN(J)*CPHI-COSZ(J)*SPHI)
      CZ22=CPSI*COSZ(J)-SRAT*(COSZ(J)*COSIN(J)*CPHI+COSY(J)*SPHI)
      IF(SINE(J).EQ.0.)THEN
                       CX22= CPSI
                       CY22=-SPSI*CPHI
                       CZ22=-SPSI*SPHI
                       END IF
C      COSINES RENORMALIZATION
      AUXI=SQRT(CX22*CX22+CY22*CY22+CZ22*CZ22)
      CX2=CX22/AUXI
      CY2=CY22/AUXI
      CZ2=CZ22/AUXI
      SINE(J)=SQRT(1.-CX2*CX2)
C
C      NOW FILL CASCADE VECTORS....AND UPDATE ION COSINES AND POSITION
C
      IESPR(INDC(J))=IESP(J)
      RLS(INDC(J))=LM(LL(J)+IBIN(J))
      LLR(INDC(J))=LL(J)+IBIN(J)
      ENR(INDC(J))=DEN(J)-BE
C
C      CALCULATES TARGET DIRECTION USING MOMENTUM CONSERVATION
C
      RATIO=SQRT(E(J)/(E(J)+DEN(J)))
C     WRITE(36,*)RATIO
      IF(RATIO.NE.1.)THEN
      RMODL=SQRT(1.00001-2.*RATIO*(COSIN(J)*CX2+COSY(J)*CY2+
     ,COSZ(J)*CZ2)+RATIO*RATIO)
      IF(RMODL.LE.1.E-3)     WRITE(6,*)RATIO, RMODL
      COSXR2=(COSIN(J)-RATIO*CX2)/RMODL
      COSYR2=(COSY(J)-RATIO*CY2)/RMODL
      COSZR2=(COSZ(J)-RATIO*CZ2)/RMODL
      AUXL=SQRT(COSXR2*COSXR2+COSYR2*COSYR2+COSZR2*COSZR2)
      COSXR(INDC(J))=COSXR2/AUXL
      COSYR(INDC(J))=COSYR2/AUXL
      COSZR(INDC(J))=COSZR2/AUXL
      SINXR(INDC(J))=SQRT(1.-COSXR2*COSXR2/AUXL/AUXL)
      XR(INDC(J))=X1(J)
      YR(INDC(J))=Y(J)-P(J)*(SPHI*COSZ(J)-CPHI*COSY(J)*COSIN(J))
     ,/(SINE(J)+1.E-7)
      ZR(INDC(J))=ZET(J)-P(J)*(SPHI*COSY(J)+CPHI*COSZ(J)*COSIN(J))
     ,/(SINE(J)+1.E-7)
                       END IF
      COSIN(J)=CX2
      COSY(J)=CY2
      COSZ(J)=CZ2
      X(J)=X(J)+LS(J)*CX2
      Y(J)=Y(J)+LS(J)*CY2
      ZET(J)=ZET(J)+LS(J)*CZ2
C
C                          STOPPED
```

```
      ITEF=(1-(E(J)-EF)/ABS(E(J)-EF))/2
      IXLTO=(1-X(J)/ABS(X(J)))/2
      IXGTT=(1+(X(J)-TT)/ABS(X(J)-TT))/2
      ILIVE(J)=1-IDEAD(J)
      Y2SUM=Y2SUM+Y(J)*Y(J)*ITEF*ILIVE(J)
      XSUM=XSUM+X(J)*ITEF*ILIVE(J)
      X2SUM=X2SUM+X(J)*X(J)*ITEF*ILIVE(J)
      X3SUM=X3SUM+X(J)*X(J)*X(J)*ITEF*ILIVE(J)
      X4SUM=X4SUM+X(J)*X(J)*X(J)*X(J)*ITEF*ILIVE(J)
      MRKSTP(J)=ITEF*ILIVE(J)
      IDEAD(J)=IDEAD(J)+ITEF-IDEAD(J)*ITEF
      ILIVE(J)=1-IDEAD(J)
C                              BACKSCATTERED
      IB=IB+IXLTO*ILIVE(J)
      EB=EB+E(J)*IXLTO*ILIVE(J)
      IDEAD(J)=IXLTO+IDEAD(J)-IDEAD(J)*IXLTO
      ILIVE(J)=1-IDEAD(J)
C                               TRANSMITED
      IT=IT+IXGTT*ILIVE(J)
      ET=ET+E(J)*IXGTT*ILIVE(J)
      IDEAD(J)=IXGTT+IDEAD(J)-IXGTT*IDEAD(J)
      LS(J)=LS(J)*(1-IDEAD(J))
  280 CONTINUE
      IEND=0
      DO563J=1,50
      IF(.NOT.MRKVAC(J))GOTO467
      IVAC(LL(J)+IBIN(J),IESP(J))=IVAC(LL(J)+IBIN(J),IESP(J))+1
      NVAC=NVAC+1
      MRKVAC(J)=.FALSE.
  467 IF(MRKSTP(J).EQ.1)IRP(LL(J))=IRP(LL(J))+1
      MRKSTP(J)=0
      IMARK(J)=0
      MARKMG(J)=.FALSE.
      IF(IDEAD(J).EQ.1)IEND=IEND+1
  563 CONTINUE
 5000 CONTINUE
      IF(ITREE.EQ.0)THEN
                    ITREE=1
                    ENR(1)=.001
      END IF
C
C                        END OF CYCLING IONS
C                        CASCADE BEGUINS
C
 1111 INUM=ITREE
C
C     RANDOM NUMBERS  FOR CASCADES
C
      CALL RANDUC
C
      DO317J=1,ITREE
```

```
      XR(J)=XR(J)+RLS(J)*COSXR(J)
      YR(J)=YR(J)+RLS(J)*COSYR(J)
      ZR(J)=ZR(J)+RLS(J)*COSZR(J)
C
C  FIRST CALCULATE ELECTRONIC LOSSES ,CASE (0) (BEFORE UPDATE ION LAYER)
C
      IE=ENR(J)/EOKEV/10+.5
      IF(IE.LE.0)THEN
                 DEER=0
      ELSE
      DEER=RLS(J)*SE(LLR(J),IE,IESPR(J))
      END IF
      IF(XR(J).GE.XX(LLR(J)+1))THEN
                                LLR(J)=LLR(J)+1
      ELSE
      IF(XR(J).LT.XX(LLR(J)))LLR(J)=LLR(J)-1
      END IF
      IF(LLR(J).EQ.0)LLR(J)=1
      RLS(J)=LM(LLR(J))
      ENR(J)=ENR(J)-DEER
      IF(ENR(J).LT.EF)THEN
                      IDEATH(J)=.TRUE.
                      IDETH2(J)=.TRUE.
                      IF(ENR(J).EQ..001)GOTO317
                      MRKI1(J)=.TRUE.
                      GOTO317
      ELSE
      IF(XR(J).GT.0.)GOTO460
C
C    IN CASES 1,2,3,4 THERE ARE NO COLLISION PARTNERS; SO WE HAVE
C      TO KILL IT.
C      PUTTING IDETH2(J)=.TRUE. IN ORDER TO GET UNIFORM OPERATIONS
C      WHEN COMPACTING SUPERVECTORS AT CASCADE END
C
C                     COLLISION WITH THE SURFACE (1)
      IF(ENR(J)*COSXR(J)*COSXR(J).LT.SBE)THEN
                                         XR(J)=-XR(J)
                                         LLR(J)=1
                                         RLS(J)=LM(1)
                                         COSXR(J)=-COSXR(J)
                                         GOTO460
      ELSE
C                           SPUTTERING (2)
      ISPUT=ISPUT+1
      ENR(J)=ENR(J)-SBE
      ESPUT=ESPUT+ENR(J)
      IDEATH(J)=.TRUE.
      IDETH2(J)=.TRUE.
      GOTO317
      END IF
```

```
  460 IF(XR(J).GT.TT)THEN
C                          TRANSMITION (3)
                       ITTR=ITTR+1
                       IDEATH(J)=.TRUE.
                       IDETH2(J)=.TRUE.
      ELSE
      PHIR(J)=2.*PI*RN1(J)
      PR(J)=SQRT(RN2(J))*RLS(J)/SQPI
      XRR(J)=XR(J)-PR(J)*COS(PHIR(J))*SINXR(J)
      IF(XRR(J).GT.RLS(J)/SQPI)THEN
                                 MRKMGR(J)=.TRUE.
      ELSE
      PR(J)=PR(J)+RLS(J)/SQPI
      PHIR(J)=PHIR(J)+PI
      XRR(J)=XR(J)-PR(J)*COS(PHIR(J))*SINXR(J)
      IF(XRR(J).GT.RLS(J)/SQPI)THEN
                                 MRKMGR(J)=.TRUE.
      ELSE
C  THIS IS THE RARE CASE OF NO COLLISION AT ALL (4)
C  CANDIDATE FOR SPUTTERING NEXT CYCLE
      IDETH2(J)=.TRUE.
      END IF
      END IF
      END IF
      END IF
  317 CONTINUE
      DO327I=1,L
      DO327J=1,ITREE
      IF(.NOT.MRKMGR(J))GOTO327
      IF(XRR(J).LT.XX(I))GOTO327
      IF(XRR(J).GE.XX(I+1))GOTO327
      LLRR(J)=I
      RLSR(J)=LM(I)
  327 CONTINUE
C          SPECIES SELECTION,EPS AND B VALUES
      DO360I=2,N1
      DO360J=1,ITREE
      IF(.NOT.MRKMGR(J))GOTO360
      IF(RN3(J).LE.SELECT(LLRR(J),I-1))GOTO360
      IF(RN3(J).GT.SELECT(LLRR(J),I))GOTO360
      IESPRR(J)=I-1
      EPSR(J)=ENR(J)*F(IESPR(J),I-1)
      BR(J)=PR(J)*(1./A(IESPR(J),I-1))
  360 CONTINUE
C      IN CASCADES PARTICLES ALLWAYS GO THROUGH MAGIC
C
C
c     TIM1=ZA01AS(DUMMY)
      CALL MAGIC2
c     TIM2=ZA01AS(DUMMY)
c     TIME=TIME+TIM2-TIM1
```

```
C
C
      DO361J=1,ITREE
      IF(.NOT.MRKMGR(J))THEN
                        CR(J)=1.
                        IESPRR(J)=1
                        PR(J)=0.
                        PHIR(J)=0.
                        END IF
      CR(J)=CR(J)*CR(J)
      IF(CR(J).GE.1.)CR(J)=1.
      S1=1.-CR(J)
      TAUR=PR(J)*SQRT(S1/CR(J))
      XR(J)=XR(J)-TAUR*COSXR(J)
      YR(J)=YR(J)-TAUR*COSYR(J)
      ZR(J)=ZR(J)-TAUR*COSZR(J)
      PSIR=ATAN(SQRT(1.-(2.*CR(J)-1.)*(2.*CR(J)-1.))/
     ,(2.*CR(J)-1.+MY(IESPR(J),IESPRR(J))+1.E-7))
      IF(PSIR.LT.0.) PSIR=PSIR+PI
      CPSI=COS(PSIR)
      SPSI=SQRT(1.-CPSI*CPSI)
      CPHI=COS(PHIR(J))
      SPHI=SIN(PHIR(J))
      YRR(J)=YR(J)-PR(J)*(SPHI*COSZR(J)
     ,-CPHI*COSYR(J)*COSXR(J))/(SINXR(J)+1.0E-7)
      ZRR(J)=ZR(J)+PR(J)*(SPHI*COSYR(J)
     ,+CPHI*COSXR(J)*COSZR(J))/(SINXR(J)+1.0E-7)
C                CALCULATE DIRECTIONS
      SRAT=SPSI/(SINXR(J)+1.E-7)
      CX22=CPSI*COSXR(J)+SRAT*SINXR(J)*SINXR(J)*CPHI
      CY22=CPSI*COSYR(J)-SRAT*(COSYR(J)*COSXR(J)*CPHI-COSZR(J)*SPHI)
      CZ22=CPSI*COSZR(J)-SRAT*(COSZR(J)*COSXR(J)*CPHI+COSYR(J)*SPHI)
      IF(SINXR(J).LT.1.0E-7)THEN
                        CX22= CPSI
                        CY22=-SPSI*CPHI
                        CZ22=-SPSI*SPHI
                        END IF
C
C      COSINES RENORMALIZATION. ( ROUNDOFF ERRORS )
C
      RMDULE=SQRT(CX22*CX22+CY22*CY22+CZ22*CZ22)
      CX2=CX22/RMDULE
      CY2=CY22/RMDULE
      CZ2=CZ22/RMDULE
C
      ENRR(J)=ENR(J)*S1*EC(IESPR(J),IESPRR(J))
      ENR(J)=ENR(J)-ENRR(J)
C
C      CALCULATES TARGET DIRECTION USING MOMENTUM CONSERVATION
C      UNLESS ENERGY IS NOT ENOUGH TO START CASCADE
C
```

```
      IF(MRKMGR(J).AND.(ENRR(J).LT.ED.AND.XRR(J).GT.2.*LM(1)).OR.
     ,(ENRR(J).LT.SBE.AND.XRR(J).LE.2.*LM(1)))IDETH2(J)=.TRUE.
      RATIO=SQRT(ENR(J)/(ENR(J)+ENRR(J)))
      IF(RATIO.NE.1.)THEN
      RMODL=SQRT(-2.*RATIO*(COSXR(J)*CX2+COSYR(J)*CY2+COSZR(J)*CZ2)+
     ,RATIO*RATIO+1)
      IF(RMODL.LE.1.E-3)     WRITE(6,*)RATIO, RMODL
      COSXR2=(COSXR(J)-RATIO*CX2)/RMODL
      COSYR2=(COSYR(J)-RATIO*CY2)/RMODL
      COSZR2=(COSZR(J)-RATIO*CZ2)/RMODL
C
C      COSINES  RENORMALIZATION
C
      AUXI=SQRT(COSXR2*COSXR2+COSYR2*COSYR2+COSZR2*COSZR2)
      COSXRR(J)=COSXR2/AUXI
      COSYRR(J)=COSYR2/AUXI
      COSZRR(J)=COSZR2/AUXI
C
      SINXRR(J)=SQRT(1.-COSXR2*COSXR2/AUXI/AUXI)
                    END IF
      SINXR(J)=SQRT(1.-CX2*CX2)
      COSXR(J)=CX2
      COSYR(J)=CY2
      COSZR(J)=CZ2
      IF(ENR(J).LT.EF.AND.MRKMGR(J))THEN
                                    MRKI1(J)=.TRUE.
                                    IDEATH(J)=.TRUE.
                                    END IF
  361 CONTINUE
C
C      NOW STORE CASCADE VACANCIES,INTERSTITIALS AND
C      COMPACT SUPERVECTOR
C
      ICC=0
      DO362J=1,ITREE
      IF(.NOT.MRKI1(J))GOTO370
      ISTL(LLR(J),IESPR(J))=ISTL(LLR(J),IESPR(J))+1
      NISTL=NISTL+1
      GOTO362
  370 IF(IDEATH(J))GOTO362
      ICC=ICC+1
      COSXR(ICC)=COSXR(J)
      COSYR(ICC)=COSYR(J)
      COSZR(ICC)=COSZR(J)
      SINXR(ICC)=SINXR(J)
      XR(ICC)=XR(J)
      YR(ICC)=YR(J)
      ZR(ICC)=ZR(J)
      ENR(ICC)=ENR(J)
      IESPR(ICC)=IESPR(J)
      LLR(ICC)=LLR(J)
```

```
      RLS(ICC)=RLS(J)
  362 CONTINUE
      DO173J=1,ITREE
      IF(IDETH2(J))THEN
                  INDC(J)=7000
      ELSE
      IVAC(LLRR(J),IESPRR(J))=IVAC(LLRR(J),IESPRR(J))+1
      NVAC=NVAC+1
      ICC=ICC+1
      INDC(J)=ICC
      END IF
  173 CONTINUE
      DO371J=1,ITREE
      COSXR(INDC(J))=COSXRR(J)
      COSYR(INDC(J))=COSYRR(J)
      COSZR(INDC(J))=COSZRR(J)
      SINXR(INDC(J))=SINXRR(J)
      XR(INDC(J))=XRR(J)
      YR(INDC(J))=YRR(J)
      ZR(INDC(J))=ZRR(J)
      ENR(INDC(J))=ENRR(J)-BE
      IESPR(INDC(J))=IESPRR(J)
      LLR(INDC(J))=LLRR(J)
      RLS(INDC(J))=RLSR(J)
  371 CONTINUE
      DO363J=1,7000
      MRKMGR(J)=.FALSE.
      IDEATH(J)=.FALSE.
      IDETH2(J)=.FALSE.
  363 MRKI1(J)=.FALSE.
C
C      THIS IS A CHECK TO OPTIMIZE MEMORY REQUIREMENTS,MAXLIV
C      KEEPS THE MAXIMUN NUMBER OF SIMULTANEOUS LIVING ATOMS OVER
C      ALL CASCADES
C
      IF(MAXLIV.LT.ICC)MAXLIV=ICC
C
C      IF ICC.NE.0 THERE STILL ARE LIVING CASCADE ATOMS,SO CONTINUE
C      THE CASCADE;OTHERWISE ASK IF THERE ARE STILL LIVING IONS,IF
C      SO,COME BACK TO FOLLOW THEM,IF NOT SO ALL THE PROCESS IS OVER
C      AND GO  TO NEXT STEP (OR START ANOTHER 50 IONS)
C
      IF(ICC.NE.0)THEN
                  ITREE=ICC
                  GOTO1111
      ELSE
      IF(IEND.NE.50)GOTO5555
      END IF
  666 CONTINUE
C
C
```

```
C       STEP FINISHED,NOW MESH RELAXATION AND SO
C
C       BUT FIRST,CURVE FITTING TO IVAC,ISTL AND IRP MAY BE NEEDED
C
C
      DO2001I=1,L
 2001 ISTL(I,1)=ISTL(I,1)+IRP(I)
C               THE ANGSTROM IS TAKEN AS UNIT LENGTH
      ESC=DOSTEP/NH
      DO1004I=1,L
 1004 UX(I)=0
      DO1002J=1,N
      DO1002I=1,L
      DELC(I,J)=(ISTL(I,J)-IVAC(I,J))*ESC/CW(I)/1.E16
 1002 UX(I)=UX(I)+SV(J)*DELC(I,J)
      DO1033I=1,L
 1033 CW(I)=CW(I)*(1+UX(I))
      DO1003J=1,N
      DO1003I=1,L
 1003 CONC1(I,J)=(CONC1(I,J)+DELC(I,J))/(1+UX(I))
C
C       ALGORITHM TO CONTROL MESH WIDTH
C
      IK=1
3005  IF(CW(IK).LT.CWMAX)GOTO3007
      L=L+1
      DO3001I=1,L-IK
      CW(L-I+1)=CW(L-I)
      DO3001J=1,N
 3001 CONC1(L-I+1,J)=CONC1(L-I,J)
      CW(IK)=CW(IK)/2
      CW(IK+1)=CW(IK)
      GOTO3004
 3007 IF(CW(IK).GT.CWMIN)GOTO3004
      L=L-1
      DO3003J=1,N
 3003 CONC1(IK,J)=(CW(IK)*CONC1(IK,J)+CW(IK+1)*CONC1(IK+1,J))/
     *(CW(IK)+CW(IK+1))
      CW(IK)=CW(IK)+CW(IK+1)
      DO3002I=IK+1,L
      CW(I)=CW(I+1)
      DO3002J=1,N
 3002 CONC1(I,J)=CONC1(I+1,J)
      GOTO3005
 3004 IK=IK+1
      IF(IK.LE.L)GOTO3005
      XX(1)=0.
      DO1114I=1,L
      XX(I+1)=XX(I)+CW(I)
 1114 CONTINUE
      XSURF=XSURF+TT-XX(L+1)
```

```
      TT=XX(L+1)
      DOSACM=DOSACM+DOSTEP
      IDOSAC=IDOSAC + 1
C WHAT IS IDISCON IN TRAL1 USED FOR?
      BT=IB*ESC+BT
      TTT=IT*ESC+TTT
      SPUTT=ISPUT*ESC+SPUTT
      IF(DOSACM.LT.OUTPUT(IC)*.999)GOTO1012
C
C             STEP OUTPUT
C
C
C
C
      WRITE(16,*)MAXLIV,TIME ,IRAND
C
      YH=NH-IB-IT
      AVEX = XSUM/YH
      SIGMAX=DSQRT(X2SUM/YH-AVEX**2)
      SIGMAY=DSQRT(Y2SUM/YH)
      V=AVEX/SIGMAX
      V2=V**2
      GAMMA=X3SUM/(YH*SIGMAX**3) -V*(3.+V2)
      BETA=X4SUM/YH/SIGMAX**4- 4.*V*GAMMA-V2*(6.+V2)
      DO2000I=1,L
      DMG(I)=DMG(I)/NH
 2000 ION(I)=ION(I)/NH
      WRITE(16,888)DOSACM , DOSACM0
  888 FORMAT(10X,' DOSE : ',E10.4,' AT/CM**2','   (START AT ',E10.4,')')
C
C      WRITE RANGE STRAGGLING AND SO
C
  799 WRITE(16,800)AVEX,SIGMAX
  800 FORMAT(//5X,'  AVERAGE  DEPTH =',F8.2/6X,
     1'STANDARD DEVIAT.=',F8.2)
      WRITE(16,810) GAMMA,BETA,SIGMAY
  810 FORMAT(5X,'  LONG. SKEWNESS =',F8.2/5X,'  LONG. KURTOSIS =',F8.2
     1,4X,' LATERAL STRAGGLING=',F8.2//)
C
C    THIS OUTPUT MAY BE OF INTEREST SOMETIMES
C
C     WRITE(16,52)
C  52 FORMAT(10X,'DAMAGE AND PRIMARY IONIZ. ENERGY DISTRIBUTIOS'/,
C    ,10X,'IN EV/PARTICLE IN THE CORRESPONDING BIN'//)
C     WRITE(16,62)(DMG(I),ION(I),I=1,L)
C  62 FORMAT(10X,2E15.4)
      WRITE(16,57)BT,TTT,SPUTT
   57 FORMAT(//10X,'BACKSCATTERED PART./ CM**2 = ',E10.4/,10X,'TRANSMITE
     ,D PART./ CM**2 = ',E10.4/,10X,'SPUTTERED PART. / CM**2 = ',E10.4/)
C
      WRITE(16,58)XSURF
```

```
   58 FORMAT(//10X,E15.6,'  ...SURFACE POSITION ...'//)
      WRITE(16,52)
   52 FORMAT(//10X,'   FRACTIONAL CONCENTRATIONS        '//,5X,'DEPTH',
     ,20X,'CONC(1)',13X,'CONC(2)',13X,'CONC(3)',13X,'TOTAL IN AT/A3 '//)
      DO405J=1,L
      TOTAL=CONC1(J,1)+CONC1(J,2)+CONC1(J,3)
      T1=CONC1(J,1)/TOTAL
      T2=CONC1(J,2)/TOTAL
      T3=CONC1(J,3)/TOTAL
  405 WRITE(16,44)XX(J+1),T1,T2,T3,TOTAL
      WRITE(16,531)
  531 FORMAT(1X,'-9999 -9999 0 0 0 ... END OF DATA LINE')
   44 FORMAT(5(10X,E10.4))
      IC=IC+1
      IF(IC.GT.ICL)GOTO960
 1012 CONTINUE
      DO2021I=1,L
      RHO(I)=0
      IRP(I)=0
      DMG(I)=0
 2021 ION(I)=0
      DO2022J=1,N
      DO2022I=1,L
      IVAC(I,J)=0
      ISTL(I,J)=0
      T(I,J)=CONC1(I,J)
 2022 RHO(I)=CONC1(I,J)+RHO(I)
      DO2003I=1,3
 2003 ESP(I)=0
      IB=0
      EB=0
      IT=0
      ET=0
      ISPUT=0
      ESPUT=0
      XSUM=0
      X2SUM=0
      X3SUM=0
      X4SUM=0
      Y2SUM=0
      AVEX=0
      NVAC=0
      NISTL=0
C                          GOTO NEXT DOSE STEP
      GOTO6666
  960 STOP
      END
C
      BLOCK DATA
      COMMON/SPLINE/XINT(18),HHH(4,18)
      DATA XINT/ 0.,.46875,.9375,1.40625,1.875,2.8125,3.75,4.6875,5.625
```

```
     *,7.5,9.375,11.25,13.125,15.,18.75,22.5,26.25,30./
      DATA HHH/ 0.           ,0.         ,0.       ,0.        ,
     *0.1000070E+01,-.4746000E+00,0.1094497E+00,-.8910771E-02,
     *0.6260086E+00,-.2824327E+00,0.1465768E+00,-.5494863E-01,
     *0.4352041E+00,-.1541250E+00,0.5424936E-01,-.1757129E-01,
     *0.3177572E+00,-.9834009E-01,0.2784677E-01,-.8740980E-02,
     *0.2385229E+00,-.1377390E+00,0.6093091E-01,-.1946777E-01,
     *0.1422470E+00,-.7428044E-01,0.3308070E-01,-.1108593E-01,
     *0.8996135E-01,-.4137687E-01,0.1600022E-01,-.5091108E-02,
     *0.5949359E-01,-.2464975E-01,0.8755356E-02,-.2936527E-02,
     *0.4066267E-01,-.3189724E-01,0.1765303E-01,-.6122939E-02,
     *0.2029552E-01,-.1496000E-01,0.8439105E-02,-.3031716E-02,
     *0.1074291E-01,-.7176932E-02,0.3613627E-02,-.1237954E-02,
     *0.5941652E-02,-.3663541E-02,0.1703159E-02,-.5654371E-03,
     *0.3415832E-02,-.1953535E-02,0.8916634E-03,-.3193661E-03,
     *0.2034594E-02,-.2256613E-02,0.1628702E-02,-.6169835E-03,
     *0.7896987E-03,-.8501606E-03,0.6544397E-03,-.2597077E-03,
     *0.3342701E-03,-.3204043E-03,0.2177436E-03,-.8271659E-04,
     *0.1488928E-03,-.1330670E-03,0.6572084E-04,-.1341460E-04/
      END
C
C*******************************************************************************
      SUBROUTINE MAGIC
C*******************************************************************************
      LOGICAL MARKMG,MRKMGR
      COMMON/MAG/MARKMG(50),EPS(50),B(50),C2(50),AUX1(50),AUX2(50)
      COMMON/MAG2/ITREE,MRKMGR(7000),EPSR(7000),BR(7000),CR(7000)
     ,,AUX1R(7000),AUX2R(7000)
      COMMON/SPLINE/XINT(18),HHH(4,18)
      DO20J=1,50
      IF(.NOT.MARKMG(J))GOTO20
      R=B(J)
      IF(R.GE.XINT(18))GOTO18
      DO22K=2,18
      IF(R.LT.XINT(K))GOTO25
 22   CONTINUE
 25   RXN=XINT(K)-XINT(K-1)
 23   RS=(R-XINT(K-1))/RXN
      FR=R-(HHH(1,K)+RS*(HHH(2,K)+RS*(HHH(3,K)+RS*HHH(4,K))))/
     ,EPS(J)-B(J)*B(J)/R
      FR1=1.+B(J)*B(J)/R/R-(HHH(2,K)+RS*(2.*HHH(3,K)+3.*RS*HHH(4,K)))
     ,/RXN/EPS(J)
      Q=FR/FR1
      R=R-Q
      IF(R.GE.XINT(K))THEN
                      IF(K.EQ.18)GOTO18
                      K=K+1
                      GOTO25
      ELSE
      IF(ABS(Q/R).LT..001)GOTO19
      GOTO23
```

```
      END IF
   18 XP=EXP(-.2016*R)/EPS(J)
      FR=R-.02817*XP-B(J)*B(J)/R
      FR1=1.+B(J)*B(J)/R/R+5.679E-03*XP
      Q=FR/FR1
      R=R-Q
      IF(ABS(Q/R).LT..001)GOTO19
      GOTO18
   19 ROC=1./(R*FR1/B(J)/B(J)/2.-1./R)
      AUX1(J)=R
      AUX2(J)=ROC
   20 CONTINUE
C
C
      DO21J=1,50
      IF(.NOT.MARKMG(J))GOTO21
      SQE=SQRT(EPS(J))
      CC=(.01185+SQE)/(.0068338+SQE)
      AA=2.*EPS(J)*(1.+(.80061/SQE))*B(J)**CC
      FF=(SQRT(AA**2+1.)-AA)*((10.855+EPS(J))/(16.883+EPS(J)))
      DELTA=(AUX1(J)-B(J))*AA*FF/(FF+1.)
      C2(J)=(B(J)+DELTA+AUX2(J))/(AUX1(J)+AUX2(J))
   21 CONTINUE
      RETURN
      ENTRY MAGIC2
      DO27J=1,ITREE
      IF(.NOT.MRKMGR(J))GOTO27
      R=BR(J)
      IF(R.GE.XINT(18))GOTO180
      DO220K=2,18
      IF(R.LT.XINT(K))GOTO250
  220 CONTINUE
  250 RXN=XINT(K)-XINT(K-1)
  230 RS=(R-XINT(K-1))/RXN
      FR=R-(HHH(1,K)+RS*(HHH(2,K)+RS*(HHH(3,K)+RS*HHH(4,K))))/
     ,EPSR(J)-BR(J)*BR(J)/R
      FR1=1.+BR(J)*BR(J)/R/R-(HHH(2,K)+RS*(2.*HHH(3,K)+RS*3.*HHH(4,K)))
     ,/RXN/EPSR(J)
      Q=FR/FR1
      R=R-Q
      IF(R.GE.XINT(K))THEN
                      IF(K.EQ.18)GOTO180
                      K=K+1
                      GOTO250
      ELSE
      IF(ABS(Q/R).LT..001)GOTO190
      GOTO230
      END IF
  180 XP=EXP(-.2016*R)/EPSR(J)
      FR=R-.02817*XP-BR(J)*BR(J)/R
      FR1=1.+BR(J)*BR(J)/R/R+5.679E-03*XP
```

```
      Q=FR/FR1
      R=R-Q
      IF(ABS(Q/R).GT..001)GOTO180
  190 ROC=1./(R*FR1/BR(J)/BR(J)/2.-1./R)
      AUX1R(J)=R
      AUX2R(J)=ROC
   27 CONTINUE
C
C
      DO210J=1,ITREE
      IF(.NOT.MRKMGR(J))GOTO210
      SQE=SQRT(EPSR(J))
      CC=(.01185+SQE)/(.0068338+SQE)
      AA=2.*EPSR(J)*(1.+(.80061/SQE))*BR(J)**CC
      FF=(SQRT(AA**2+1.)-AA)*((10.855+EPSR(J))/(16.883+EPSR(J)))
      DELTA=(AUX1R(J)-BR(J))*AA*FF/(FF+1.)
      CR(J)=(BR(J)+DELTA+AUX2R(J))/(AUX1R(J)+AUX2R(J))
  210 CONTINUE
      RETURN
      END
C*************************************************************
      SUBROUTINE RSTOP
C*************************************************************************
C*********     UNIVERSAL STOPPING POWER SUBROUTINE          *********
C*********     (OUTPUT IS 100* VALUES OF SE (EV*ANG.**2/ATOM))********
C
C            Z1 = ION ATOMIC NUMBER
C            M1 = ION ATOMIC WEIGHT (AMU)
C            Z2 = TARGET ATOMIC NUMBER
C            E0KEV = ION ENERGY (KEV)
C            ATRHO=TARGET DENSITY (ATOMS/CM3)
C            VFERMI = (FERMI VELOCITY OF SOLID) / V0
C            LFCTR = LAMBDA SCREENING FACTOR FOR IONS
C            PCOEF = STOPPING COEFFICIENTS FOR PROTONS
C            SE = CALCULATED ELECTRONIC STOPPING CROSS SECTION
C                 IN EV*A**2/ATOM
C            TABLE 1 :RCOEF(5,92)
C            TABLE 2 :SCOEF(8,92)
C
      IMPLICIT REAL*4(A-Z)
      LOGICAL MARK(100)
      INTEGER Z1,Z2,I,J
      INTEGER IZ,K1,K2,N
      DIMENSION E(100),EEE(100),ZETA(100),HE(100),HEH(100)
      COMMON/RSTP/N,E0KEV,IZ(3),M(3),SE1(100,3,3)
      COMMON/COEF/SCOEF(8,92),RCOEF(5,92)
      COMMON/PCSE/PCOEF(8),SE(100)
      DO999K1=1,N
      DO999K2=1,N
      Z1=IZ(K1)
      Z2=IZ(K2)
```

```
      M1=M(K1)
      LFCTR=RCOEF(5,Z1)
      VFERMI=RCOEF(4,Z2)
      DO 88 J=1,8
   88 PCOEF(J)=SCOEF(J,Z2)
      E0=.01*E0KEV/M1
      DO10I=1,100
      MARK(I)=.FALSE.
    10 E(I)=E0*I
      IF (Z1-2) 100,200,300
   100 CALL RPSTOP(Z2,E)
      GOTO18
C
C      HELIUM ELECTRONIC STOPPING POWERS
C      VELOCITY PROPORTIONAL STOPPING BELOW KEV/AMU  ** HE0 **.
   200 HE0=1.
      DO15I=1,100
      HE(I)=AMAX1(HE0,E(I))
      B=ALOG(HE(I))
      A=.2865+.1266*B-.001429*B*B+.02402*B*B*B-.01135*B**4+.001475*B**5
    15 HEH(I)=1.-EXP(-AMIN1(30.,A))
      CALL RPSTOP(Z2,HE)
      DO16I=1,100
      SE(I)=SE(I)*HEH(I)*4.
      IF (E(I).GT.HE0) GO TO 16
C      CALC. HE VELOCITY PROPORTIONAL STOPPING
      SE(I)=SE(I)*SQRT(E(I)/HE0)
    16 CONTINUE
      GOTO18
C
C      HEAVY ION ELECTRONIC STOPPING POWERS
C      USE VELOCITY STOPPING FOR (YRMIN=VR/Z1**.67) .LE. 0.13
C      OR FOR VR .LE. 1.0
  300 DO17I=1,100
      YRMIN=0.13
      VRMIN=1.0
      V=SQRT(E(I)/25)/VFERMI
      IF (V.GE.1.) GO TO 302
      VR=(3*VFERMI/4)*(1+(2*V*V/3)-V**4/15)
      GO TO 303
   302 VR=V*VFERMI*(1+1/(5*V*V))
C      SET YR = MAXIMUM OF (VR/Z1**.67),(VRMIN/Z1**.67) OR YRMIN.
   303 YR=AMAX1(YRMIN,VR/Z1**.6667)
      YR=AMAX1(YR,VRMIN/Z1**.6667)
      A=-.803*YR**0.3+1.3167*YR**0.6+.38157*YR+.008983*YR*YR
      Q=AMIN1(1.,AMAX1(0.,1.-EXP(-AMIN1(A,50.))))
C      Q = IONIZATION LEVEL OF THE ION AT VELOCITY * YR *.
C      NOW WE CONVERT IONIZATION LEVEL TO EFFECTIVE CHARGE.
      B=(AMIN1(0.43,AMAX1(.32,.12+.025*Z1)))/Z1**.3333
      LO=(.8-Q*(AMIN1(1.2,0.6+Z1/30.)))/Z1**.3333
      IF (Q.LT.0.2) GO TO 307
```

```
      IF (Q.LT.(AMAX1(0.,.9-.025*Z1))) GO TO 306
      IF (Q.LT.(AMAX1(0.,1.-.025*AMIN1(16.,1.*Z1)))) GO TO 305
      L1=B*(1.-Q)/(.025*AMIN1(16.,1.*Z1))
      GO TO 308
  305 L1=B
      GO TO 308
  306 Q1=0.2
      L1=B*(Q-.2D0)/ABS(AMAX1(0.,.9-.025*Z1)-.2000001)
      GO TO 308
  307 L1=0
  308 L=AMAX1(L1,L0*LFCTR)
      ZETA(I)=Q+(1./(2.*VFERMI**2))*(1.-Q)*ALOG(1+(4*L*VFERMI/1.919)**2)
C      ADD Z1**3 EFFECT AS SHOWN IN REF. 779.
      A=-(7.6-AMAX1(0.,ALOG(E(I))))**2
      ZETA(I)=ZETA(I)*(1.+(1./Z1**2)*(.18+.0015*Z2)*EXP(A))
      IF (YR.GT.AMAX1(YRMIN,VRMIN/Z1**.6667)) THEN
                                              EEE(I)=E(I)
      ELSE
C      CALCULATE VELOCITY STOPPING FOR YR LESS THAN YRMIN.
      VRMIN=AMAX1(VRMIN,YRMIN*Z1**.6667)
      VMIN=.5*(VRMIN+SQRT(AMAX1(0.,VRMIN**2-0.8*VFERMI**2)))
      EEE(I)=25*VMIN**2
      MARK(I)=.TRUE.
      END IF
   17 CONTINUE
      CALL RPSTOP(Z2,EEE)
      DO19I=1,100
      IF(.NOT.MARK(I))THEN
                     SE(I)=SE(I)*(ZETA(I)*Z1)**2
      ELSE
      POWER=.5
      IF((Z2.EQ.6).OR.(((Z2.EQ.14).OR.(Z2.EQ.32)).AND.(Z1.LE.19)))
     # POWER=.35
      SE(I)=(SE(I)*(ZETA(I)*Z1)**2)*(E(I)/EEE(I))**.5
      END IF
C      SPECIAL CORRECTION FOR LOW ENERGY IONS IN CARBON
      IF(Z2.EQ.6)SE(I)=SE(I)*((E(I)/EEE(I))**(.75*.5))/(E(I)/EEE(I))**.5
   19 CONTINUE
   18 DO999I=1,100
  999 SE1(I,K1,K2)=SE(I)*10.
      RETURN
      END
C
C      PROTON ELECTRONIC STOPPING POWERS

      SUBROUTINE RPSTOP(Z2,E)
      IMPLICIT REAL*4(A-H,M-Z)
      INTEGER Z2
      COMMON/PCSE/PCOEF(8),SE(100)
      DIMENSION E(100)
C      VELOCITY PROPORTIONAL STOPPING BELOW VELOCITY ** PEO **.
```

```
      PE0=25.
      DO10I=1,100
      PE=AMAX1(PE0,E(I))
      SL=(PCOEF(1)*PE**PCOEF(2))+PCOEF(3)*PE**PCOEF(4)
      SH=PCOEF(5)/PE**PCOEF(6)*ALOG((PCOEF(7)/PE)+PCOEF(8)*PE)
      SE(I)=SL*SH/(SL+SH)
      IF (E(I).GT.PE0) GO TO 10
C      VELPWR IS THE POWER OF VELOCITY STOPPING BELOW PE0.
      VELPWR=0.45
      IF (Z2.LE.6) VELPWR=0.25
      SE(I)=SE(I)*(E(I)/PE0)**VELPWR
   10 CONTINUE
      RETURN
      END
C
      SUBROUTINE RANDU
      COMMON/RAN2/IRAND,INUM,RN1(7000),RN2(7000),RN3(7000)
      COMMON/RAN1/RA1(50),RA2(50),RA3(50)
      DO618J=1,50
      IRAND=IRAND*65539
      IF(IRAND.LT.0)IRAND=IRAND+2147483647+1
      RA1(J)=IRAND*4.656613E-10
      IRAND=IRAND*65539
      IF(IRAND.LT.0)IRAND=IRAND+2147483647+1
      RA2(J)=IRAND*4.656613E-10
      IRAND=IRAND*65539
      IF(IRAND.LT.0)IRAND=IRAND+2147483647+1
  618 RA3(J)=IRAND*4.656613E-10
      RETURN
C
      ENTRY RANDUC
      DO418J=1,INUM
      IRAND=IRAND*65539
      IF(IRAND.LT.0)IRAND=IRAND+2147483647+1
      RN1(J)=IRAND*4.656613E-10
      IRAND=IRAND*65539
      IF(IRAND.LT.0)IRAND=IRAND+2147483647+1
      RN2(J)=IRAND*4.656613E-10
      IRAND=IRAND*65539
      IF(IRAND.LT.0)IRAND=IRAND+2147483647+1
  418 RN3(J)=IRAND*4.656613E-10
      RETURN
      END
```

The vita has been removed from the scanned document